Student Theses and Dissertations

2019

Sensory Coding and Olfactory Integration in Caenorhabditis Elegans

May Dobosiewicz

SENSORY CODING AND OLFACTORY INTEGRATION IN

CAENORHABDITIS ELEGANS

A Thesis Presented to the Faculty of

The Rockefeller University

in Partial Fulfillment of the Requirements for

the degree of Doctor of Philosophy

by

May Dobosiewicz

June 2019

SENSORY CODING AND OLFACTORY INTEGRATION IN

CAENORHABDITIS ELEGANS

May Dobosiewicz, Ph.D.

The Rockefeller University 2019

Animals must sense their external environments to guide meaningful behavior. The nematode *Caenorhabditis elegans*, for example, uses volatile cues to navigate toward food from a distance. How does an animal integrate the olfactory information from its environment? Here, I ask how multiple sensory neurons drive and shape one interneuron's activity.

C. elegans senses several odors, including the bacterial metabolite diacetyl, using the AWA sensory neurons. AWA forms chemical and electrical synapses onto several interconnected interneurons, which contribute to chemotaxis toward attractive odors like diacetyl. One AWA target is the interneuron AIA, which is connected to AWA via a putative electrical synapse. Both AWA and AIA are robustly activated by diacetyl, but the reliability of their responses decreases at low concentrations. AIA relies on AWA for its reliable response to diacetyl. However, directly activating AWA is not sufficient to evoke reliable AIA responses. Instead, AIA responses to optogenetic AWA stimulation had high and variable latencies and low probabilities. AIA responses, when they did occur, had stereotyped on-dynamics to all concentrations of diacetyl tested, to AWA optogenetic

stimulation, and to several additional attractive odors, suggesting all-or-none AIA activation to sensory input.

In animals lacking chemical synaptic transmission, AIA responses to direct AWA optogenetic stimulation were fast and reliable, resembling those evoked by diacetyl. AWA-to-AIA communication is thus regulated by inhibitory synaptic input from surrounding neurons. This inhibition comes from a small set of glutamatergic sensory neurons that work together to gate AIA responses to AWA activation. Consistently, two of these glutamatergic sensory neurons directly sense and are inhibited by diacetyl. Their responses are less reliable, or even non-existent, at low concentrations of diacetyl. The difference in the reliability of AIA responses to different diacetyl concentrations may be explained by differences in the composition of the upstream sensory responses.

Reliable AIA responses appear to require both activation from AWA through an electrical synapse and the release of inhibition from glutamatergic sensory neurons through chemical synapses. AIA acts as a coincidence detector, and its activity represents a readout of global sensory state, providing insight into how AIA represents "food" signals that are sensed by multiple sensory neurons.

This thesis is dedicated to the friends and family whose warmth and humor make me smile every day.

Acknowledgements

I have a lot of people to thank for making the last few years the intellectual and emotional journey it turned out to be. First and foremost, I would like to thank my mentor, Cori Bargmann. Thank you for the scientific and professional support, and for being kind and warm when I needed it most. Thank you for paying attention to disappointing results as much as to the exciting results. You encouraged me to explore my interests and find what inspires me; I cannot express how much your generosity has meant to me.

I would like to thank the entire Bargmann lab, past and present, for making the lab a place I wanted to come to, day after day, year after year. I have learned something from each of you. Thank you Christine for introducing me to nematodes and the lab; Johannes for creating the setup I used so heavily, and for answering my endless questions, even from Germany. Thank you Donovan and Andrew for sharing a space, but mostly for sharing thoughts, drinks and jokes. You have both been huge parts of my experience in the lab. Thank you Xin for being so warm, open, and fun. You always focus on the bright side and your enthusiasm for scientific discovery is infectious. Thank you Aylesse and Phil for being great coworkers and friends, both inside the lab and out. Phil and Sagi, thanks for the countless thoughtful discussions. Finally, thank you Priscilla and Hernan for making things easy.

Thank you to my thesis committee members, Shai Shaham, Vanessa Ruta, and Marc Tessier-Lavigne. I will always cherish your guidance and insight, and you each

helped me think about my project from a different perspective. Thank you to my external committee member, Andrew Leifer, for feedback and ideas.

The Dean's office has been incredibly supportive throughout my time here at Rockefeller. Thank you for removing some of the stress from the PhD process. You were so helpful when I first got here, and somehow even more helpful now as the end approaches. Thank Andrea Morris for career advice and for making it easy to explore non-academic science paths. Your time and support mean a lot to me.

I would like to thank my entire family for encouraging me to explore nature as a child. Thanks to the parents for heavily pressuring me to take a computer programming class in undergrad – solid parenting move. Also, thanks for encouraging me to apply to US programs. It is difficult to imagine how different my PhD would have been if it weren't for that push.

Thank you to my non-lab friends, both in Canada and here in NYC. Thank you to Emma, Peter, Daniel, Gregory, Andrea, and Kathleen for over a decade of openness, support, acceptance, and love. Thank you to Melissa, Dylan, Joan, Iain, Melissa and Avital. You have each been massive parts of my PhD experience. The PhD process can be challenging, but it is way more fun when you are surrounded by warm, loving friends. A big thanks to Lori and the CSA team.

Finally, I would like to thank my partner, Phil. Thank you for the love, support, and confidence boosts. Thanks for being my practice audience, for listening and caring, and for knowing when we need to escape the city. I can't wait for whatever adventure comes after this!

Table of Contents

List of Figures

List of Abbreviations

GPCR	G-protein coupled receptor
fps	frames per second
dia	Diacetyl
Chr	Chrimson
s	second
ns	not significant
WT	wildtype
TeTx	Tetanus Toxin light chain A
5-HT	serotonin
Glut.	glutamate
ACh	acetylcholine
D/V/A/P	dorsal/ventral/anterior/posterior
IAA	Isoamyl alcohol
C. elegans	*Caenorhabditis elegans*
E. coli	*Escherichia coli*
PDMS	polydimethylsiloxane
NaCl	sodium chloride
TRP	Transient Receptor Potential
EPSC	excitatory post-synaptic current

CHAPTER 1: INTRODUCTION

Chemosensation

Sensory systems

Philosophers and scientists have long been fascinated by how humans sense our environments. The Ancient Greek philosopher Democritus suggested that all of our sensation stems from touch, perhaps sensing atoms physically interacting. Aristotle argued that we have five senses: vision (sight), audition (hearing), olfaction (smell), somatosensation (touch), and gustation (taste), an idea solidified over the following centuries in European thought. Early Buddhists described six Ayatana organ-object sense pairs: visible objects/eye; sound/ear; odor/nose; touch/body; taste/tongue; and mental objects/mind. Recent thinking in sensory biology will add thermoception, nociception, equilibrioception, and others to the multiple sensory modalities we use to receive information from our external environments.

Beyond the senses listed above, animals have evolved additional specialized senses suited for their sensory environments and needs. For example, fish have evolved the "lateral line" system of hair cells to sense movement and pressure changes in their surrounding waters. Pit vipers have a pit organ expressing TRPA1 channels to detect infrared radiation emitted by warm-blooded prey as they hunt in the dark (Gracheva et al., 2010).

Animals need to sense external environments in order to find food, seek shelter, find mates, and avoid predators. Many of these actions require the use of multiple sensory organs, as objects and contexts can be represented by multiple sensory cues.

1

For example, birds may use visual and auditory cues to select a mate or locate their prey. Information from these different sensory modalities are integrated throughout the nervous system (see Stein et al, 2009 for many references outlining the benefits of multisensory integration).

Mammals have olfactory subsystems with different roles

Chemosensation is ubiquitous among living organisms. Chemosensation incorporates olfaction, gustation, and the chemosensory irritant system. As with other sensory systems, animals have evolved chemosensory strategies to deal with their particular needs. For example, vultures living in open areas use their vision to find carcasses to eat. Vultures living in canopied environments, however, rely on olfaction and their ability to smell mercaptans released by carcasses (Houston, 1986). I am particularly interested in how animals process chemosensory information, and that will be the focus of this thesis.

In mammals, olfactory receptors account for 1-3% of all active genes (Buck, 2001), pointing to their relative importance. Throughout the evolution of vertebrate olfaction, various classes of olfactory receptors evolved to sample particular areas of chemical space (Bear et al., 2016; see Figure 1-1). Along with the increase in receptor classes came an increase in anatomical structures. Non-human mammals possess a main olfactory system and an anatomically distinct accessory olfactory system, and each anatomical structure houses multiple types of neurons.
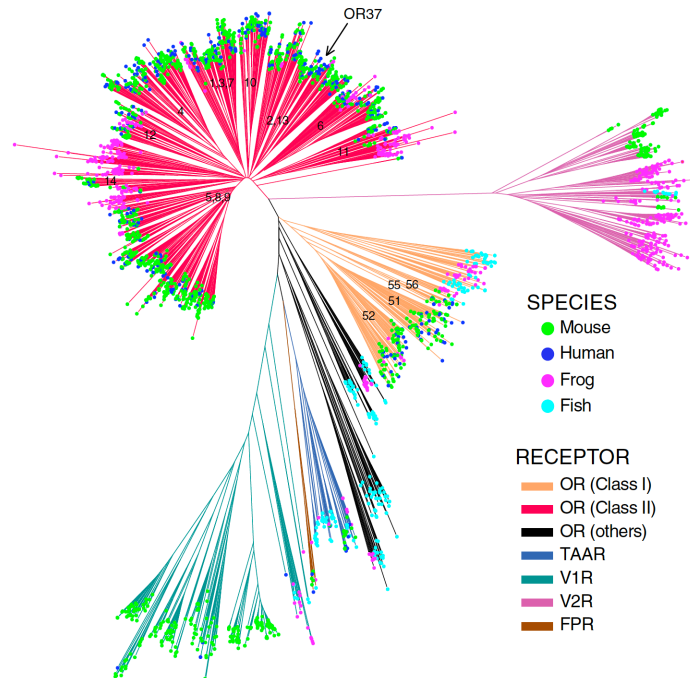
Figure 1-1. **Phylogenetic relationships of vertebrate olfactory receptors**.
Phylogenetic tree consisting of a representative sample of ~2700 functional olfactory
receptors from *Danio rerio* (zebrafish), *Xenopus laevis* (frog), *Mus musculus* (mouse),
and *Homo sapiens* (human) genomes, from Bear et al. (2016). The non-GPCR
receptors in the necklace subsystem are not shown. Line color indicates receptor
class, and dot color indicates species. ORs and TAARs are in the main olfactory
system; V1Rs, V2Rs, and FPRs are in the accessory olfactory system. OR: canonical
olfactory receptor; TAAR: trace amine-associated receptor; V1R: Vomeronasal type
1 Receptor; V2R: Vomeronasal type 2 Receptor; FPR: formyl peptide receptor.

The main olfactory system of mammals consists of three types of neurons:

(1) Canonical olfactory receptor neurons, which each express a single GPCR olfactory

   receptor gene per neuron. Canonical olfactory receptor neurons can detect

   compounds spanning much of chemical space (Bear et al., 2016).

(2) The trace amine-associated receptor (TAAR)-expressing neurons, which each

   express a single TAAR but no canonical olfactory receptors. TAARs are also

GPCRs, distinct from canonical olfactory receptors, and some TAARs are specialized for detecting odors and pheromones that elicit hard-wired behavioral responses (Munger et al., 2009).

(3) The guanylyl cyclase D-expressing neurons in the olfactory subsystem known as the necklace subsystem. Each of these neurons expresses several different olfactory receptors that, unlike other mammalian olfactory receptors, span the membrane only four times and are not GPCRs. These neurons may be specialized for detecting aversive food odors and pheromones (Greer et al., 2016).

The accessory olfactory system also consists of at least three neuron types, housed separately from the main olfactory system. In rodents, the accessory olfactory system is housed in the vomeronasal organ. The accessory olfactory system consists of Vomeronasal type 1 Receptors, specialized to detect volatile pheromones (Del Punta et al., 2002); Vomeronasal type 2 Receptors, specialized to detect water-soluble peptides and proteins (Silva and Antunes, 2017); and formyl peptide receptors, potentially specialized to detect pathogens (Bufe et al., 2012; Riviere et al., 2009; Liberles et al., 2009).

Each of the olfactory neuron subsystems listed above specializes in detecting certain types of odors and pheromones with some ethological relevance to the animal, but there is also overlap between the compounds each subsystem can detect. Some of the olfactory subsystems may have evolved to add to the animal's olfactory repertoire, while other subsystems may have evolved to specify hard-wired behavioral responses to cues of particular importance to the animal.

Humans have ~700 olfactory receptor genes or pseudogenes, but only ~350 of them express active olfactory receptors (Malnic et al., 2004). Humans and other primates lack the accessory olfactory system and the necklace olfactory subsystem that detect various pheromones, among other compounds. Olfaction is nonetheless important for humans; we still sniff our milk to check if it is rancid and have a 75 billion USD global fragrance and deodorant market (Statista). Moreover, human olfaction is tied to emotion and psychological state (Kadohisa, 2013). Unlike other sensory systems, olfactory information bypasses the thalamus and is sent directly from the olfactory bulb to higher cortical areas and to the limbic system (Hoover, 2010).

Odor representation

Olfaction presents a difficult encoding problem. An olfactory system is tasked with sensing many compounds in the environment, but these compounds differ from each other along several dimensions (e.g. chain length, chirality, polarity, aromaticity). To deal with this challenge, olfactory systems have evolved to include an abundance of olfactory receptors that bind odorants with different affinities. The receptors allow the animal to sense many compounds, but then comes the next challenge: how does it make sense of these compounds?

There are two main theories for how the nervous system encodes sensory information: "labeled lines" and "combinatorial coding". Both strategies can be found in sensory systems outside of olfaction. The initial studies in the mammalian olfaction system pointed to a combinatorial coding strategy (Malnic et al., 1999). Since then, however, groups have found evidence for labeled line strategies first in *C. elegans* and

then in insects and mammals. Olfactory systems can employ both highly tuned olfactory receptors for important decisions with no room for error, and broadly tuned olfactory receptors for the ability to sense large swaths of olfactory space. Additionally, odorants can evoke different temporal response patterns in olfactory neurons (e.g. Grillet et al., 2016).

Combinatorial coding

The number of odors an animal can perceive generally outnumbers the number of odorant receptors. Depending on whom you ask, humans can perceive between 10,000 and 1 trillion odors; either way, it is more than the ~350 olfactory receptors we express (Bushdid et al., 2014; Meister, 1015; Gerkin and Castro, 2015). We can discriminate so many odors because each olfactory receptor can recognize multiple odorants at different affinities. Each odorant, in turn, can be recognized by many different olfactory receptors (Dalton and Lomvardas, 2015). Humans have millions of olfactory receptor neurons in humans, each typically expressing a single olfactory receptor (Buck and Axel, 1991). The canonical olfactory receptor neurons that express the same olfactory receptor converge on a few glomeruli in the main olfactory bulb. Each glomerulus contains olfactory receptor neurons that express several different olfactory receptors (Dalton and Lomvardas, 2015). A given pattern of glomeruli activity is thought to encode a particular odorant or small group of similar odorants. This combinatorial coding mechanism takes a limited number of olfactory receptor neurons and uses them to encode a large number of odorants.

Insect olfaction evolved separately from vertebrate olfaction, so it is remarkable that, to a large extent, insect olfaction is organized similarly to mammalian olfaction (Andersson et al., 2015). Like mammals, insect olfactory systems have glomerular architecture and can sense more odorants than the number of olfactory receptors. Si et al. (2019) recently recorded all 21 olfactory receptor neurons in *Drosophila* larvae in response to 34 stimuli at concentrations spanning at least 5 orders of magnitude. They found that each olfactory receptor neuron shared the same activation function for each odorant it responded to, but sensitivity differed between neurons and odors. This implies that each olfactory receptor neuron in *Drosophila* larvae response is tuned fairly broadly.

There is a bias in the chemical stimuli that activate olfactory receptor neurons. For example, a mixture of aldehydes stimulated 59% of a group of 217 mouse olfactory receptor neurons, while a mixture of amines stimulated just 15% (Nara et al., 2011).

Combinatorial Coding + Labeled Lines

The combinatorial coding model relies on olfactory receptors being broadly tuned. They must respond to multiple odorants, or else the code is still limited by the number of receptor genes. These broadly tuned receptors are present in insects, and insects likely employ a combinatorial coding strategy as well. However, there have been several recent examples of finely tuned receptors in insects (Dweck et al., 2013; Grabe et al., 2016).

For example, Dweck et al. (2013) found that *Drosophila* preferentially lay eggs in citrus fruit, that that this behavior is entirely controlled by a single odorant receptor.

Neurons expressing this single odorant receptor sense limonene, and activation of these neurons causes flies to lay their eggs. This seems to confer an evolutionary advantage since wasps that eat the fly larvae are repelled by another turpene detected by the same odorant receptor. This odorant receptor still responds to multiple odorants, but it seems to be solely responsible both for the sensation and for the behavioral response to limonene. ~10% of *Drosophila*'s 60 receptors are thought to be narrowly tuned for specific cues, and the glomeruli they innervate are involved in important functions like mating and avoidance of toxic bacteria and mold (Grabe et al., 2016). Grabe et al. (2016) found that *Drosophila* glomeruli that were innervated by narrowly tuned receptors tended to possess more projection neurons, which may represent functional significance.

One harmonizing explanation for why there may be both combinatorial coding and labeled lines is that the different tuning properties offer different advantages (Haverkamp et al., 2018). For odorants that are highly similar to other odorants but very important for survival, using narrowly tuned receptors would help prevent misinterpretations. Labeled line coding would be reserved for only the most important cues, with the rest of odor space being represented by the remaining broadly tuned receptors, allowing animals to sense many cues that may be related to, say, food.

Olfactory Gestalt

The above studies are all based on single odorants, but many ethologically relevant odor sources release bouquets of volatile odorants. The combined odors may

produce an olfactory gestalt particular to the bouquet. The task of distinguishing the combinations of odorants is even more complicated.

Weiss et al. (2010) found that mixtures of ~30 intensity-matched odors that span olfactory space were perceived similarly by humans, even though the mixtures had no odorant overlap. They termed this smell gestalt "olfactory white". If the odors spanned smaller regions of olfactory space, or if they had unmatched intensities, people could better distinguish them from olfactory white.

The existence of olfactory white in nature may be quite rare. We already know that certain molecules can contribute large fractions of an odor's headspace, and that they may cluster in olfactory space. For example, phenylethyl alcohol, citronellol and geraniol make up ~85% of the rose headspace, with a few dozen odorants making up the rest (Ayci et al., 2005; Jirovetz et al., 2005). The rose does not smell like olfactory white. Likewise, the *Datura wrightii* flower emits 60-80 volatile odors, only nine of which elicit neuronal responses in the *Manduca sexta* moth (Riffell et al., 2009). Moreover, the moth requires the odorant mixture to navigate to the flower, and the mixture produces the same behavioral response at concentrations spanning at least three orders of magnitude. The authors concluded that the moth likely experiences the flower bouquet as a singular percept, or olfactory gestalt.

Chemosensation in *Caenorhabditis elegans*

Up to this point, I have introduced vertebrate and invertebrate olfactory systems. There remains one important model organism with an actively studied olfactory system: *Caenorhabditis elegans*. *C. elegans* is a nematode roundworm that can be found

feeding off the bacteria of rotting fruit (Felix and Braendle, 2010). *C. elegans* can use both volatile and water-soluble cues to find their food at close range, but they rely on volatile odorants emitted by bacteria to find food sources at far range (Grewal and Wright, 1992). *C. elegans* has developed a robust olfactory system to sense those volatile odorants.

C. elegans has a compact nervous system, with only 302 neurons. Researchers knew from an early stage that twelve pairs of sensory neurons (24 total) extended to the animal's nose (Ward et al., 1975). Eleven of these twelve pairs of neurons can sense distinct and partially overlapping chemicals in the environment and represent the animal's primary chemosensory tool kit. We also know how all of these neurons anatomically connect, with a complete electron micrograph wiring diagram of chemical synapses and gap junctions (White et al., 1986). This wiring diagram shows that many of the 12 chemosensory neuron pairs form gap junctions with their contralateral partners, and subsequent studies have shown that contralateral pairs have symmetric activity with some notable exceptions (Bargmann, 2006; Yu et al., 1997; Wes and Bargmann, 2001). Unless the neurons are known to be asymmetric, I will refer to the two neurons by their shared name.

Chemosensory neurons that sense volatile odorants

The early studies into *C. elegans* olfaction used chemotaxis behavior to quantify the number of animals navigating toward or away from a point source and identify the key neurons that sense chemicals. Animals will chemotax toward attractive cues and away from aversive cues. Using laser ablations to kill individual neurons, AWA and

AWC were found to sense discrete sets of odorants, but with some overlap (Bargmann et al., 1993). Out of the 121 volatile compounds initially tested, *C. elegans* chemotaxed toward 50 of them. AWA and AWC were deemed the chemosensory neurons responsible for sensing attractive volatile odorants (Bargmann et al., 1993). By contrast, AWB was found to sense aversive volatile odorants (Bargmann et al., 1990). Further studies found that other sensory neurons are tuned to detect water-soluble compounds, oxygen, pheromones, and carbon dioxide (Macosko et al., 2009; Bargmann and Horvitz, 1991; Gray et al., 2004; Hallem and Sternberg, 2008). The specialization of *C. elegans* sensory neurons for particular sensory modalities or types of chemical cues is reminiscent of the specialization of subsystems within the mammalian olfactory system

Some neurons are polymodal and can sense several aspects of the environment. For example, the ASH neurons can sense hyperosmolarity, heavy metals, aversive concentrations of odor that are sensed by AWA and AWC at lower, attractive concentrations, and even touch (Hilliard et al., 2005; Yoshida et al., 2012; Taniguchi et al., 2014). Multiple sensory neurons are capable of sensing the same odors, and odor sensation at a given neuron is concentration-dependent, just as in mammals (Bargmann et al., 1993; Chou et al., 2001).

Odor encoding in C. elegans: parallels with mammals

C. elegans have many more olfactory genes than, say, *Drosophila* or mice. The *C. elegans* genome encodes ~1300 genes that are predicted to form active chemoreceptors, about 7% of the *C. elegans* genes (Robertson and Thomas, 2006). They belong to 19 families of receptors within 7 superfamilies, and these superfamilies

share no significant sequence similarity. The 1300 predicted olfactory receptors are expressed by only a few neurons. Humans, by contrast, have 350 olfactory receptors and over 10 million olfactory receptor neurons.

The olfactory receptor gene families in *C. elegans* arose independently of both insect and vertebrate olfactory receptor genes. It is therefore remarkable that *C. elegans* olfaction shares so many similarities with mammalian and insect systems. For example, *C. elegans* uses GPCRs to sense odorants, just as in most mammalian olfactory receptor neurons. The ODR-10 receptor, for example, is selective for diacetyl (Sengupta et al., 1996). More recently, a group has shown that STR-2 is an olfactory receptor for 2-heptanone (Zhang et al., 2016). *C. elegans* odorant receptors are found at the ciliated tips of olfactory neurons, just as in the main olfactory system in mammals (Sengupta et al., 1996; Munger et al., 2009).

Both mammalian and *C. elegans* olfactory systems involve multiple signal transduction pathways downstream of olfactory receptors. In mammals, canonical olfactory neurons use cAMP and phosphodiesterase; the accessory olfactory system uses transient receptor potential (TRP) C channels in conjunction with phospholipase C; and the necklace subsystem olfactory neurons expresses guanylyl cyclase D, although its role in signal transduction is unclear (Munger et al. 2009). In *C. elegans*, AWB and AWC neurons use cGMP signal transduction pathways with either phosphodiesterases or receptor guanylyl cyclases and a cyclic nucleotide-gated channel. While AWA neurons use a TRPV channel, phospholipase C, and polyunsaturated fatty acids (Bargmann, 2006).

Combinatorial coding, labeled lines, and temporal coding in C. elegans

Returning to the combinatorial coding and labeled line models of sensory coding, we can ask whether *C. elegans* evolved to use one or the other or both, as insects do. Early experiments led to the conclusion that *C. elegans* olfactory neurons (AWA, AWB, AWC) followed a labeled line architecture. In these experiments, the AWA receptor for the odorant diacetyl, ODR-10, was exogenously expressed in either AWC or AWB neurons of animals lacking *odr-10* in AWA (and defective in behavioral attraction toward diacetyl). When *odr-10* was expressed in AWC, the attraction to diacetyl was restored (Wes and Bargmann, 2001). When *odr-10* was expressed in AWB, the normally attractive diacetyl became repulsive (Troemel et al., 1997). These experiments suggested that activation of AWC would lead to attraction and activation of AWB would lead to repulsion, consistent with the labeled line model. The behavioral response of attraction versus repulsion is determined according to the identity of the activated neuron.

The AWB neuron shares some similarities with the mammalian necklace olfactory subsystem. The necklace subsystem is embedded within the main olfactory system of mammals, but instead of a one-receptor-per-neuron architecture, each necklace subsystem neuron expresses multiple receptors and can sense many innately relevant odorants (Greer et al., 2016). Both AWB and necklace subsystem olfactory neurons thus express multiple olfactory receptors and seem specialized for detecting aversive stimuli. The analogy is incomplete, in part because necklace subsystem neurons use non-GPCR olfactory receptors – an exception in the mammalian olfactory

system. Nonetheless, the mammalian necklace olfactory subsystem, like AWB, may prioritize detection over identification of a particular aversive stimulus.

AWA and AWC can sense discrete but overlapping sets of odorants. For example, only AWC is required for chemotaxis to benzaldehyde, only AWA is required for chemotaxis to low concentrations of diacetyl, but AWA and AWC are redundant for chemotaxis to trimethylthiazole (Bargmann et al., 1993). Each neuron senses multiple odorants spanning olfactory space. Even the two AWC neurons sense different but overlapping odorants. For example, one AWC neuron senses the odorant butanone, but both sense benzaldehyde and isoamyl alcohol (Wes and Bargmann, 2001). This means that *C. elegans* has the architecture of a basic combinatorial code. Whether it uses a combinatorial code to interpret the environment is unknown.

C. elegans sensory neurons can also use temporal features to encode aspects of a stimulus. For example, it was recently discovered that the AWA sensory neurons fire all-or-none action potentials (Liu, Q et al., 2018). AWA's firing properties, however, are dependent upon certain features of the stimulus; AWA fires action potentials to slow but not fast sinusoidal stimulus oscillations, to stimulus ramps, and to small stimulus up-steps. AWA uses a combination of spike number and delay-to-spike timing to encode these stimuli. Consistent with these functional data, at a behavioral level, AWA seems specialized for climbing odor gradients (Larsch et al., 2015).

Chemical and electrical synapses in C. elegans

The electron micrograph wiring diagram of *C. elegans* also provides information about how the neurons are connected. It includes ~7000 chemical synapses and ~900

gap junctions that form putative electrical synapses (White et al., 1986). Chemical and electrical synapses both exist in the vertebrate nervous system as well. While much of the chemical synaptic machinery is conserved between vertebrates and invertebrates, the electrical synaptic machinery is not.

Electrical synapses form when two neurons connect at a functional gap junction. A gap junction consists of two hemichannels, one from each connecting neuron. Each hemichannel is made of multiple connexin subunits in vertebrates, or innexin subunits in invertebrates. Connexins and innexins share no sequence homology, yet they are structurally and functionally very similar (Phelan, 2005). This shared function points to electrical synapses as important features in neuronal communication.

Vertebrate hemichannels have 6-fold symmetry. Invertebrate hemichannels have also been suggested to have 6-fold symmetry (Peracchia, 1973 and others), but a recent 3-D reconstruction of docked *C. elegans* hemichannels showed 8-fold symmetry (Oshima et al., 2016). The 8-fold symmetrical channels appear to have larger pores than vertebrate channels.

Many electrical synapses are symmetrical and bidirectional, but they can also be asymmetrical and allow current or small molecules to flow from one neuron to the other but not vice versa (Marder, 1998). In *C. elegans*, as well as in *Drosophila* and vertebrates, electrical synapse asymmetry is defined by the molecular composition of the gap junction. If a gap junction is heterotypic, with different subunits in the two connecting neurons, the electrical synapse will likely be asymmetric (Liu, P et al., 2013; Miller et al., 2017; Phelan et al., 2008). In *C. elegans*, there are 25 innexin genes, and neurons can express many different innexins and likely form heteromeric hemichannels

within one cell, as well as heterotypic channels across cells (Bhattacharya et al., 2019; Liu, P et al., 2013).

Gap junctions serve several functions in the *C. elegans* nervous system. Gap junctions connect many contralateral neuron pairs, such as AWA-Left and AWA-Right. However, neuron pairs with known functional asymmetries, such as the AWCs and ASE sensory neuron pairs, do not form pairwise gap junctions (White et al., 1986). Gap junctions also connect groups of neurons that must work together, such as premotor command interneurons and motor neurons responsible for coordinating forward versus backward movement (Kawano et al., 2011). Gap junctions can also link multiple sensors (spokes) to a single integrating interneuron (hub) to balance competing sensory inputs, such as attractive and aversive pheromone cues (Jang et al., 2012). The relative benefits of electrical versus chemical synapses in each of these circumstances is unclear.

Thesis overview

Animals must sense a constantly changing external environmental to guide meaningful behavior. The central question of my thesis is: how does an animal integrate the sensory information from its environment? I am focusing on how several sensory neurons contribute to driving and shaping one interneuron's activity.

In Chapter 2, I show that the AWA sensory neuron and AIA interneuron are both robustly activated by diacetyl, but the reliability of responses in both neurons decreases at low concentrations. At all concentrations, the AIA responses lag ~1 second behind AWA responses. AWA responses are required for reliable AIA responses to diacetyl.

However, strong AWA activation is not sufficient to produce reliable AIA responses on its own. This lack of reliability suggests that diacetyl must do more than just activate AWA to elicit robust downstream responses. The responses to strong and weak stimuli elicit AIA responses with similar on-dynamics and magnitude, highlighting that reliability is the main variable in AIA responses to different stimuli. Finally, I show that the gap junction between AWA and AIA likely forms an active electrical synapse. This electrical synapse is asymmetrical, favoring AWA-to-AIA transmission.

In Chapter 3, I show that the reliability of AIA responses to AWA activation increases dramatically in the absence of global chemical synapses. Chemical synapses are therefore net inhibitory onto AIA. I further show that this inhibition is glutamatergic, specifically coming from a small subset of glutamatergic sensory neurons. These sensory neurons work together to gate AIA responses to AWA activation. I conclude that AIA acts as a coincidence detector, requiring both activation from AWA and disinhibition from glutamatergic sensory neurons in order to respond. Consistent with this conclusion, I present data showing that inhibiting AWC, one of the relevant glutamatergic neurons, is also insufficient to produce reliable AIA responses. I conclude the chapter with some preliminary behavior experiments that attempt to address why an AIA coincidence detection mechanism is behaviorally important for the animal.

In Chapter 4, I present experiments on sensory neuron responses. I show that higher concentrations of odor elicit larger and faster sensory responses from more sensory neurons than lower concentrations. In addition to AWA, at least three sensory neuron pairs respond to higher concentrations of the odor diacetyl; one pair responds to the lower concentration. Not all chemosensory neurons sense the odor, indicating that

there is neuronal specificity in odor sensation. The difference in reliability between AIA responses to the higher and lower odor concentrations and direct AWA optogenetic stimulation likely stems from the difference in sensory neuron recruitment.

In Appendix A, I present data on a different interneuron, AIY. I show that, unlike AIA, AIY responses are graded, rising for the duration of the stimulus pulse regardless of concentration. The reliability of AIY responses does not depend on AWA or on chemical synapses, indicating that AIY does not function as a coincidence detector like AIA does. Rather, AIY might integrate the duration or some other feature of the stimulus.

In Appendix B, I show AWA and AIA responses to another odor, isoamyl alcohol, that is thought to be primarily sensed by AWC. AWA responses to isoamyl alcohol are slower than responses to diacetyl, and AIA responses do not lag behind AWA responses. I further show that several stimuli that target different neurons within the chemosensory system all elicit the same stereotyped AIA responses.

My overall conclusion is that AIA activity acts as a readout for the global sensory state of the animal. My discussion will focus on how coincidence detection may work in AIA, why having one neuron represent global sensory state may be advantageous, and what food odors may represent to *C. elegans*, among other topics.

CHAPTER 2: Strong AWA activation is not sufficient to produce reliable downstream AIA responses

Background

Animals make many complicated choices in their lifetimes. They balance nutritious foods with more convenient foods, mating with resting, exploration with safety. All of these decisions require the animals to constantly sample and integrate their external environments and their internal states. If an animal is effective at navigating its environment to locate a sexual partner but cannot detect hunger, it may fail to seek food and starve. If an animal can detect hunger but cannot navigate its environment to locate a food source, it may also starve. I will focus on what this second animal lacks: the ability to make sense of its external environment.

The motivation for the experiments I present in this chapter is to understand how an animal integrates sensory input. I have been using the *C. elegans* olfactory circuit to study how information is processed across one synaptic layer, from a sensory neuron to a first layer interneuron. Specifically, I am probing communication between the olfactory sensory neuron AWA and the interneuron AIA.

AWA, along with AWC, senses attractive volatile odors (Bargmann et al., 1993). AWA is activated by diacetyl at concentrations spanning several orders of magnitude (Larsch et al., 2015). AWA rapidly desensitizes to a given concentration of diacetyl but continues to respond to further increases in diacetyl. AWA may be specialized for detecting fold-change increases in odorant concentration (Larsch et al., 2015). In a property consistent with this hypothesis, AWA fires action potentials in response to

particular stimulus features, such as stimulus ramps and up-steps that could be associated with fold-change increases in odor (Liu, Q et al., 2018).

According to the *C. elegans* electron micrograph wiring diagram, AWA forms a gap junction with the interneuron AIA (White et al., 1986). This gap junction is predictive of an electrical synapse connecting AWA and AIA. AWA is not predicted to form chemical synapses onto AIA, although AIA may form a chemical synapse onto AWA. Although ~10% of synapses in *C. elegans* are predicted to be electrical, electrical synapses are rare for AWA sensory neurons. Of its 15 synaptic partners, AWA forms gap junctions with only AIA and one other interneuron. AWC, a second neuron that detects odors, has no predicted gap junction partners.

AIA is one of four pairs of highly interconnected first layer olfactory interneurons that all receive massive synaptic input from chemosensory neurons (White et al., 1986). AIA is involved in several important functions that involve sensory signaling; for example, aversive learning (Cho et al., 2016; Chalasani et al., 2010), behavioral responses to changing odor concentrations (Larsch et al., 2015), and the integration involved in deciding whether to cross an aversive barrier to reach an appetitive odor source. AIA is generally thought to serve integrative functions. Optogenetically stimulating AIA weakly increases the fraction of animals moving forward (Wang et al., 2017), and silencing AIA decreases the fraction of animals moving forward (Cho et al., 2016; Wakabayashi et al., 2004; Wang et al., 2017).

AIA has calcium increases suggestive of depolarization in response to the addition of several known attractive stimuli, including isoamyl alcohol (Chalasani et al., 2010), pheromones (Macosko et al., 2009), and the AWA-sensed odorant diacetyl

(Larsch et al., 2013). AWA and AIA both appear to depolarize and promote forward locomotion upon addition of an appetitive stimulus. This sign-preserving property is consistent with a connection via a putative electrical synapse.

I wanted to study the relationship between AWA sensory responses and downstream AIA interneuron responses. Several odorants are sensed by AWA, including diacetyl, pyrazine, and trimethylthiazole (Bargmann et al., 1993). The most thorough analysis of AWA neuronal activity used diacetyl (Larsch et al., 2015). Diacetyl is an odor and fermentation byproduct of lactic acid bacteria. It is used to give popcorn that buttery aroma, and more recently in vape e-liquids (Flanigan et al., 2016). Relevant to *C. elegans*, lactic acid bacteria that produce diacetyl have been isolated in rotting fruits with other *Caenorhabditis* species (Choi et al., 2016). Importantly, we know the main olfactory receptor for diacetyl: ODR-10, expressed in AWA. In the absence of ODR-10 receptors, animals do not navigate toward diacetyl (Sengupta et al., 1996), and AWA is not activated by diacetyl (Larsch et al., 2015).

In this chapter, I will show that AWA and AIA are both activated more reliably and with shorter latencies to increasing concentrations of the odor diacetyl. However, stimulating AWA directly with optogenetic stimuli is not sufficient to reliably evoke AIA responses. The AIA responses that are evoked by AWA optogenetic stimulation or by odor are stereotyped in on-dynamics and magnitude, but they differ dramatically in latency and probability. Although not sufficient to evoke AIA responses, AWA activation is necessary for reliable AIA responses to diacetyl. I will provide evidence that AWA likely communicates with AIA via a functional electrical synapse that is asymmetrical, favoring AWA-to-AIA transmission.

Results

AWA is activated in response to diacetyl odor or optogenetic stimulation

Odorants can activate multiple neurons at high concentrations. Diacetyl consistently activates AWA from nM to mM concentrations (Larsch et al., 2015), but to consistently and *selectively* activate AWA, I used an optogenetic approach. Specifically, I used Chrimson, a red-shifted channelrhodopsin (Klapoetke et al., 2014) to directly stimulate AWA. I then recorded the activity of AWA or AIA with the genetically encoded calcium indicators GCaMP2.2b in AWA and GCaMP5A in AIA. Increases in GCaMP fluorescence correlate with increasing calcium concentration and depolarization. For sensory neurons, I measured GCaMP fluorescence changes in the soma. For interneurons like AIA, I measured fluorescence changes in the neuronal process because calcium fluctuations in AIA are more apparent in the process than in the soma (Chalasani et al., 2007; Larsch et al., 2013).

I used a custom-built microfluidics microscopy setup with a programmable LED designed by Johannes Larsch and Dirk Albrecht that allows simultaneous delivery of chemical stimuli to two groups of ~10 paralyzed animals while recording GCaMP fluorescence (Larsch et al., 2013; Figure 2-1A). Previous experiments by Larsch et al. (2015) involved exposing animals to 50 µM retinal, shining 605 ± 25 red light at various intensities to activate Chrimson, and pulsing blue light (470 nm) on a 10 ms duty cycle with 100 ms exposure time to excite GCaMP at an intensity of 10 mW/cm^2 for AWA recordings and 100 mW/cm^2 for AIA recordings. To minimize the amount of retinal used without compromising its ability to prime Chrimson, I reduced the pre-exposure retinal

concentration to 5 µM. I used a red light intensity 15.4 mW/cm^2, similar to Johannes's higher intensities. Finally, I pulsed the blue light with the 10 ms/100 ms duty cycle at 40 mW/cm^2 for both AWA and AIA neurons to make the stimulation protocols consistent when recording each neuron.

Using this revised protocol, I could reliably activate AWA. 85% of AWA neurons were activated within the first second of light exposure (Figure 2-1B, C). Without pre-exposure to retinal or expression of the Chrimson transgene, AWA did not respond to the same light exposure, indicating that GCaMP activation was the direct result of expressing, priming, and activating the Chrimson channel in AWA.

In order to compare the magnitude and dynamics of AWA responses to optogenetic stimulation versus diacetyl, I exposed animals to increasing concentrations of diacetyl. Consistent with Larsch et al. (2015), the magnitude and dynamics of AWA responses differed at different concentrations (Figure 2-1C). AWA responses to optogenetic stimulation resembled responses to 1.15 µM diacetyl in their rapid initiation and rise time, and resembled responses to 115 nM diacetyl in their magnitude.
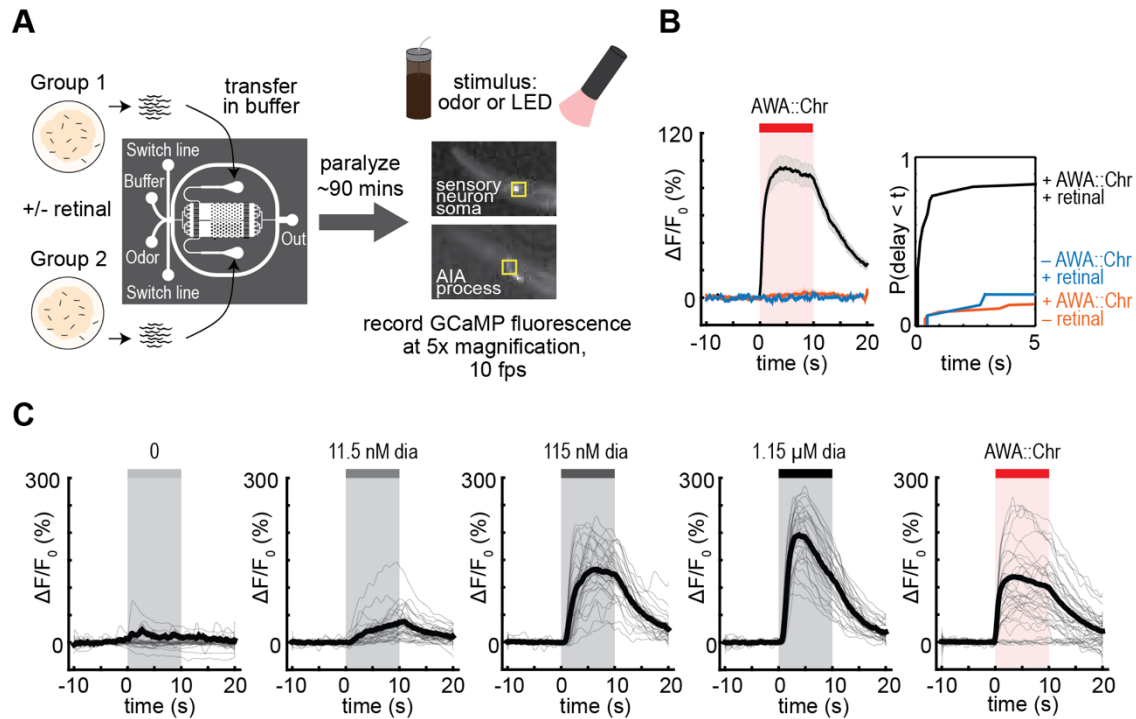
Figure 2-1. **AWA calcium increases in response to diacetyl odor or optogenetic stimulation.**

(A) Schematic of experimental setup. Animals are paralyzed in a microfluidics device and their neural activity is simultaneously recorded while being exposed to odor or light. Two arenas can be recorded simultaneously with up to 10 animals per arena. See Experimental Procedures for details.

(B) AWA requires both retinal pre-treatment and expression of the Chrimson transgene for light activation. Left: Mean AWA calcium responses; shading indicates $\pm$ SEM. Right: Cumulative response time profiles of same data, showing first 5 seconds of light exposure. Transgene but no retinal: n = 48; retinal but no transgene: n = 16; transgene with retinal: n = 74.

(C) Individual AWA calcium responses to pulses of increasing concentrations of diacetyl and to optogenetic stimulation. Bold lines indicate mean. Responses to optogenetic stimulation were down-sampled to 40 traces at random from a complete set of 268 responses.

Strong AWA activation is not sufficient to produce reliable downstream AIA responses

AWA responded to diacetyl at concentrations from 11.5 nM to 1.15 μM. However, AWA responses were more reliable at higher concentrations, with a higher percentage of cells responding, a shorter latency, and an increased response magnitude (Figure 2-2A, B). To ask how the different AWA response properties translated to the downstream AIA interneuron responses, I recorded AWA and AIA simultaneously to pulses of odor. AIA responses also became more reliable and had a higher magnitude at higher odor concentrations (Figure 2-2C-E). At all concentrations, AIA responses were delayed compared to AWA responses, with the AWA-to-AIA lag (Δt_{50}(AIA-AWA)) decreasing to ~1 second as concentration increased (Figure 2-2E, F).

The relationship between AWA and AIA responses to AWA optogenetic stimulation was distinct from the odor response. Whereas AWA responded reliably to optogenetic stimulation, with low and invariable response latency, AIA did not. Only 46% of AWA optogenetic stimulation pulses resulted in AIA activation within 5 seconds, and 56% within 10 seconds (Figure 2-2C, E). Moreover, these responses had highly variable latencies. This was surprising because AWA responses to optogenetic stimulation resembled those to 115 nM – 1.15 μM diacetyl in magnitude and latency (Figure 2-2B, G-I), and these odor stimuli elicited reliable AIA responses. These results reveal a mismatch in the propagation of odor and optogenetic information to the AIA neuron.

Figure 2-2. **Strong AWA activation is not sufficient to produce reliable downstream AIA responses.**

(A and C) AWA GCaMP2.2b (A) or AIA GCaMP5A (C) calcium responses to 10-s pulses of diacetyl or to optogenetic Chrimson stimulation of AWA. AWA and AIA diacetyl responses were recorded concurrently in different animals. Optogenetics experiments were performed separately. AWA calcium traces are the same as in Figure 2-1. Each heat map row represents a calcium trace to a single stimulus pulse; each animal received 2 stimulus pulses. Traces are ordered according to response latency. White line indicates beginning of 10-s stimulus pulse. Resistor symbol in cartoon represents a predicted electrical synapse; thin arrow represents chemical synapse.

(B and D) Mean of the calcium responses shown in (A) and (C), respectively, regardless of response status or latency. Shading indicates $\pm$ SEM.

(E) Cumulative response time profiles of AWA and AIA responses from (A) and (C), reflecting both response latencies and probability. Distributions are truncated to show first 5 s of stimulation. Numbered arrows indicate the delay between the time at which 50% AWA neurons responded versus the time at which 50% of AIA neurons responded (t_{50}).

(F) Difference between AWA$_{t50}$ and AIA$_{t50}$ (Δt_{50}) in response to various stimuli, as shown in (E). The delay decreased as diacetyl concentration increased, but delay was greatest to AWA optogenetic stimulation, despite the short latencies of AWA responses. Bars are mean $\pm$ SEM from bootstrapping (see Experimental Procedures).

(G) Time derivatives of AWA responses to 11.5 nM, 115 nM, and 1.15 μM diacetyl or AWA optogenetic stimulation, aligned to the frame at which activation was initiated. Only pulses that resulted in activation within 5 seconds of stimulus were included.

(H and I) Ten AWA (left) or AIA (right) calcium traces, randomly down-sampled from data in (A) or (C), in response to 1.15 μM diacetyl (G) or optogenetic AWA stimulation (H). AIA responses to AWA optogenetic stimulation are less frequent and have more variable latencies than AIA responses to 1.15 μM diacetyl.

See Appendix D for sample sizes.
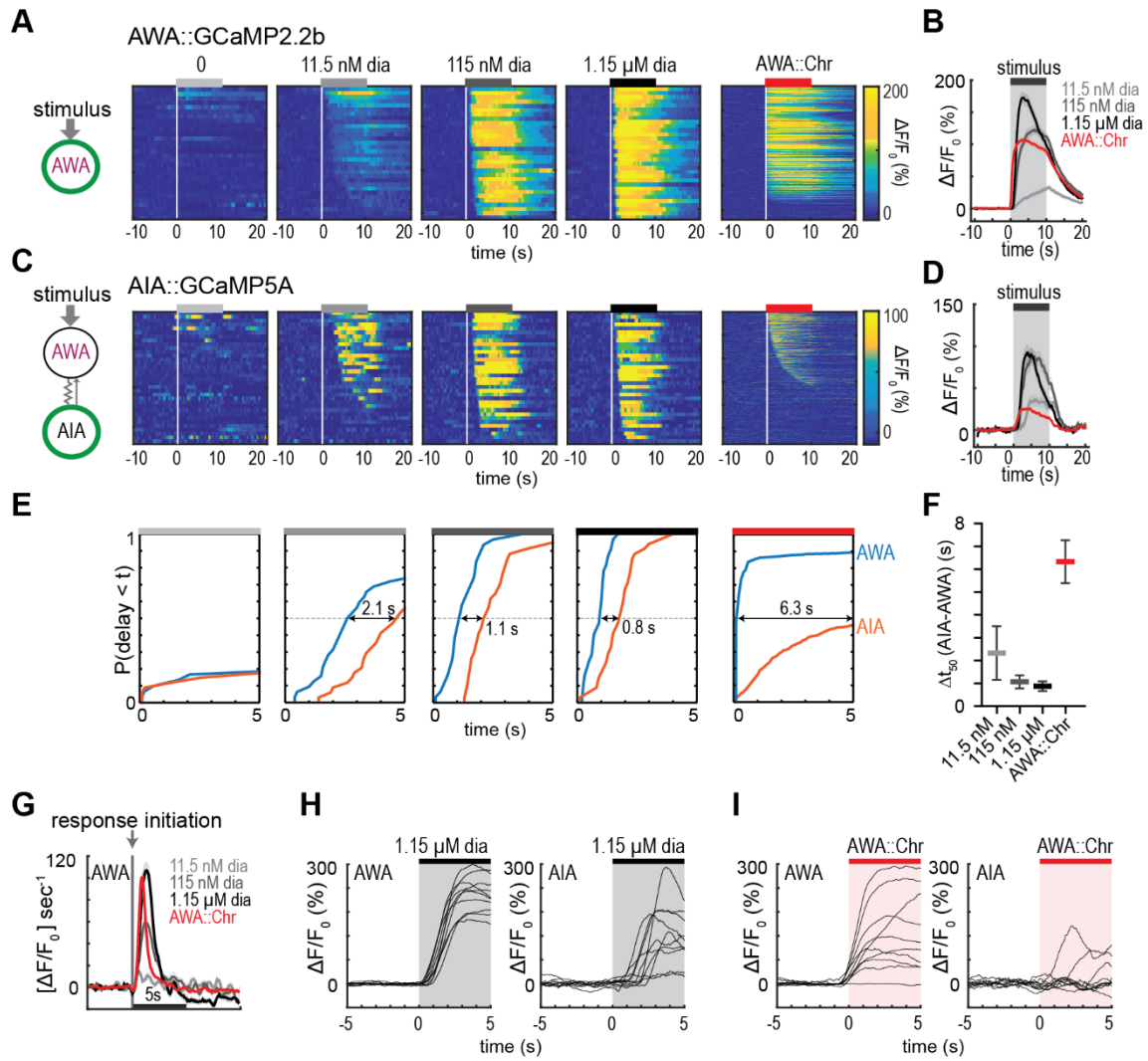
Figure 2-2. **Strong AWA activation is not sufficient to produce reliable downstream AIA responses.**
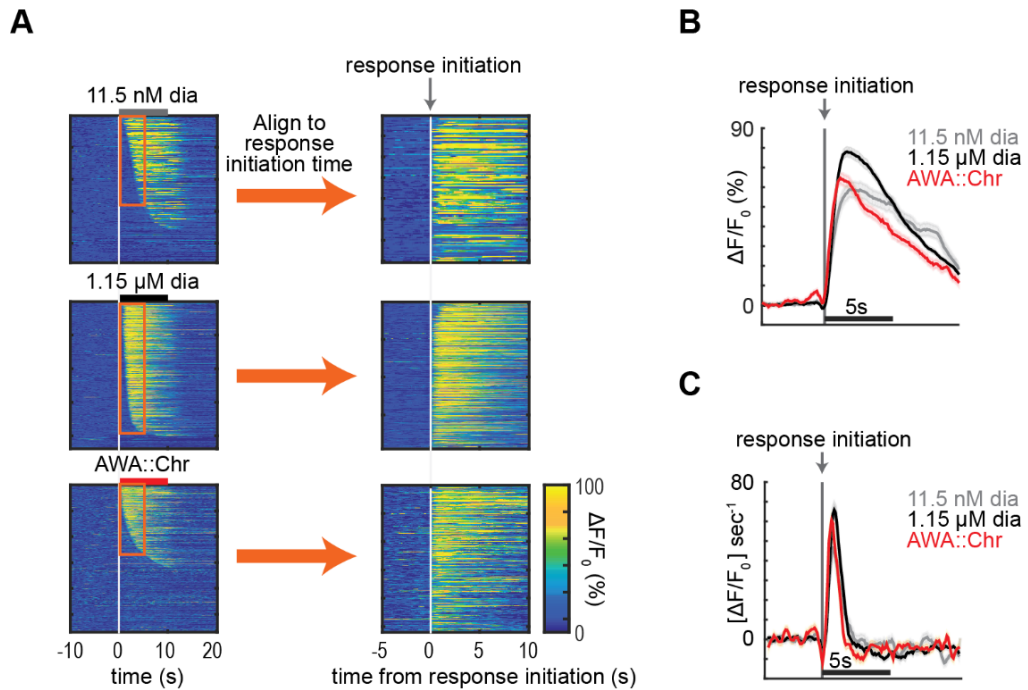
Figure 2-3. **AIA has stereotyped on-dynamics to diacetyl and AWA optogenetic stimulation.**

(A) Heat maps of all AIA responses to 11.5 nM diacetyl, 1.15 μM diacetyl, or AWA optogenetic stimulation, combined over all experiments. Left: responses were aligned to stimulus onset, as in Figure 2-2. Right: Pulses that resulted in activation within 5 seconds of stimulus were aligned to the frame at which response was initiated.

(B) Mean AIA traces shown in (A), aligned to response initiation frame. AIA had similar rise times to all three stimuli. Shading indicates $\pm$ SEM.

(C) Time derivatives of traces shown in (B). Shading indicates $\pm$ SEM.

AIA has stereotyped on-dynamics to diacetyl and AWA optogenetic stimulation

Since AIA responses to AWA optogenetic stimulation were markedly less reliable than AIA responses to odor, I wondered whether these responses differed in other ways. To compare magnitude and on-dynamics, I aligned AIA responses that occurred within the first 5 seconds of stimulus exposure to the time of response initiation (Figure 2-3A). I found that AIA on-dynamics were similar to 11.5 nM diacetyl, 1.15 μM diacetyl, and AWA optogenetic stimulation (Figure 2-3B). The time derivatives of AIA responses to the three stimuli, when aligned to response initiation, were indistinguishable. Thus, the most striking difference in AIA responses to different diacetyl concentrations and to AWA optogenetic stimulation was not in magnitude or in on-dynamics but rather in the probability and latency of a response, that is, in its reliability.
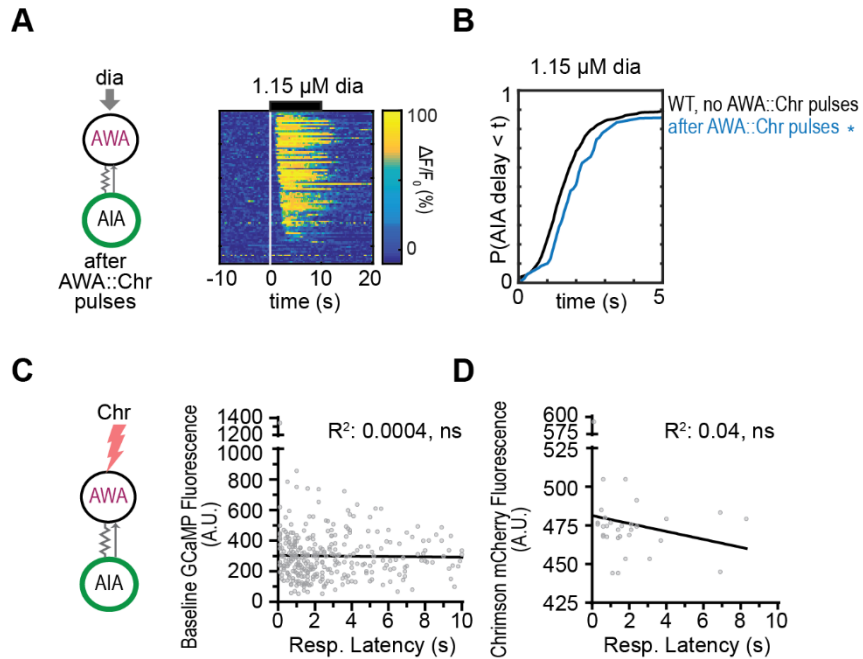
Figure 2-4. **Poor AIA response to AWA optogenetic stimulation is not due to poor Chrimson or GCaMP expression.**

(A and B) AIA neurons that did not respond reliably to AWA optogenetic stimulation do respond reliably to diacetyl.

(**A**) AIA calcium traces in response to 1.15 µM diacetyl recorded immediately after recordings to AWA optogenetic stimulation; one row per trace. Represents a subset of animals used for Figure 2-2C.

(B) Cumulative response time profiles of AIA calcium traces shown in (A), compared to all AIA calcium traces to 1.15 µM diacetyl presented without Chrimson transgene or retinal treatment (same 1.15 µM diacetyl data as in Figure 2-3).

(C) Response latencies of 318 AIA responses to AWA optogenetic stimulation do not correlate with GCaMP fluorescence levels at pre-stimulus baseline.

(D) Response latencies of 31 responses to AWA optogenetic stimulation do not correlate with Chrimson transgene expression levels.

For (B), ns refers to a lack of significance of Kolmogorov-Smirnov test over full 10-s stimulus pulse. See Appendix C for sample sizes and test details. For (C) and (D), ns indicates that the slope of linear regression is not significantly different from 0.

Poor AIA response to AWA optogenetic stimulation is not due to poor Chrimson or

GCaMP expression

Since AIA responses to AWA optogenetic stimulation could have been impacted by retinal pre-exposure or expression of the Chrimson transgene, I wanted to make sure that the AIA neurons that responded poorly to AWA optogenetic stimulation were able to respond normally to diacetyl. Indeed, AIA in animals that had just been exposed to the AWA optogenetic stimulation protocol responded superficially normally to 1.15 µM diacetyl pulses (Figure 2-4A, B). AIA's variable responses to AWA optogenetic stimulation are thus specific to the stimulus and not to the experimental conditions (i.e., presence of retinal, presence of AWA::Chrimson transgene, differing blue light intensities). Moreover, AIA response latency to AWA optogenetic stimulation did not depend on GCaMP fluorescence levels (Figure 2-4C) or AWA::Chrimson transgene expression levels as indicated by bicistronic expression of sl2::mCherry (Figure 2-4D).

AIA response probability and latency to two consecutive pulses of AWA optogenetic

stimulation are independent

In the experimental protocol used for these studies, each animal was exposed to two pulses of a given stimulus, separated by 50 seconds. To control for adaptation or inactivation of neurons by the stimulus, I analyzed responses to the first and second stimulus pulses separately. While the first pulse of AWA optogenetic stimulation did produce slightly more AIA responses than the second pulse, the AIA responses to each pulse had variable response latencies that followed a similar distribution (Figure 2-5A). These two stimulus pulses also produced a similar proportion of AIA responses (62% and 50% over the full 10 seconds), and failures were equally distributed between the first and second pulses (Figure 2-5B). For the animals that responded to both pulses of AWA optogenetic stimulation (35%), there was no correlation between the response latencies to the two pulses (Figure 2-5C).

I performed the same analyses to AIA responses to 11.5 nM and 1.15 µM diacetyl. AIA responses to the first and second pulses of 11.5 nM diacetyl occurred with similar latencies and probabilities (Figure 2-2D-F). AIA responses to the first and second pulses of 1.15 µM diacetyl were superficially similar. However, there was a higher response probability to the first pulse (96% versus 90% over the full 10 seconds) (Figure 2-5G, H) and a small but significant correlation between the AIA response latency to the first and second pulses (Figure 2-5I).

These results indicate that AIA responses to the first and second stimulus pulses were similar for all three stimuli. Therefore, the two stimuli were pooled for subsequent analyses.

Figure 2-5. **AIA response probability and latency to two consecutive pulses of AWA optogenetic stimulation are independent.**

(A, D, and G) Cumulative response time profiles of AIA responses to the first versus second pulse of AWA optogenetic stimulation (A), 11.5 nM diacetyl (D), or 1.15 μM diacetyl (G). Note that all other figures and analyses pool responses from both pulses.

(B, E, and H) Proportion of animals with AIA neurons that respond to only the first pulse, second pulse, both pulses, or neither of two 10-s pulses of AWA optogenetic stimulation (B), 11.5 nM diacetyl (E), or 1.15 μM diacetyl (H). Note that a similar proportion of animals responded to the first pulse only as to the second pulse only in response to both AWA optogenetic stimulation and 11.5 nM diacetyl.

(C, F, and I) Correlations between AIA response latencies to first versus second pulses of AWA optogenetic stimulation (C), 11.5 nM diacetyl (F), or 1.15 μM diacetyl (I). (C) n = 98, no correlation; (F) n = 72, no correlation; (I) n = 187, moderate correlation.

For (A), (D), and (G), asterisks refer to Kolmogorov-Smirnov test significance versus first pulse over full 10-s stimulus pulse. ns: not significant; **: $p < 0.01$; ***: $p < 0.001$. See Appendix C for sample sizes and test details.

For (C), (F), and (I), asterisks refer to significance of linear regression slope differing from 0. ns: not significant; ***: $p < 0.001$.
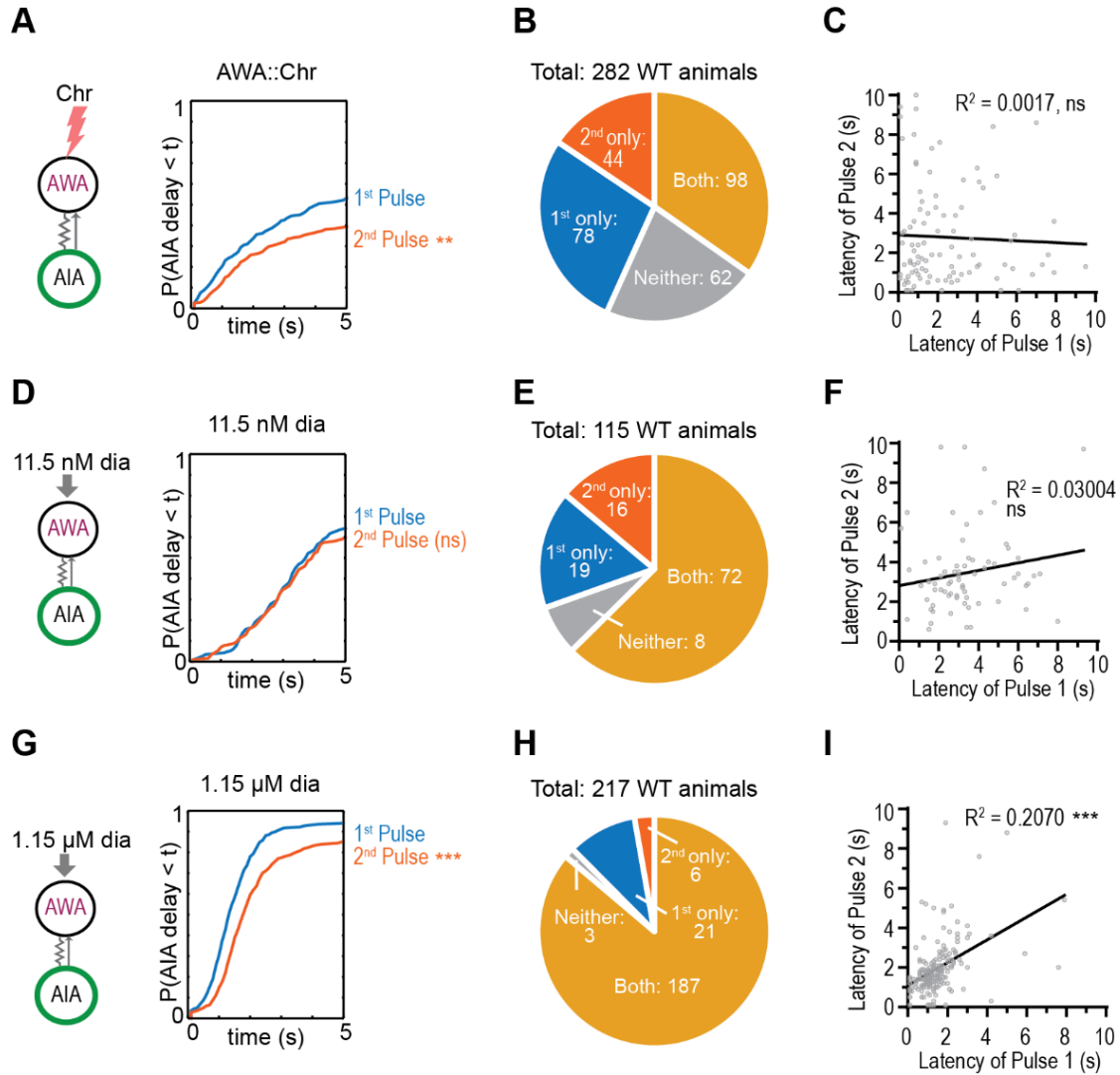
Figure 2-5. AIA response probability and latency to two consecutive pulses of AWA optogenetic stimulation are independent.
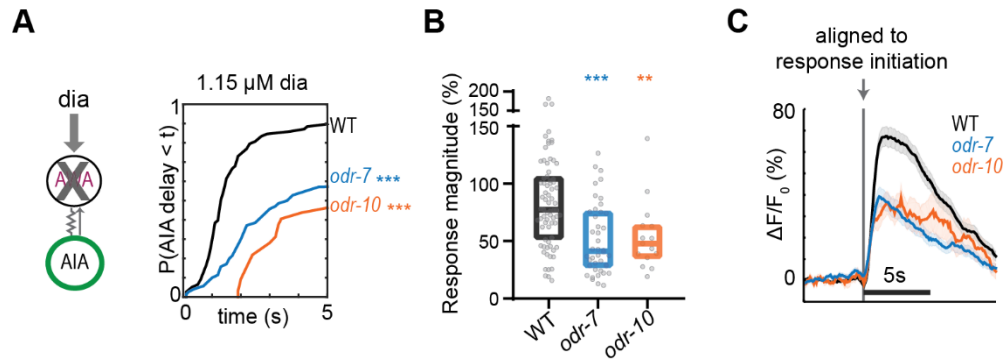
Figure 2-6. **AIA responses to diacetyl rely on AWA.**

(A) Cumulative response time profiles of AIA responses to 1.15 μM diacetyl in WT versus *odr-7(ky4)* (AWA cell fate mutant) and *odr-10(ky32)* (AWA diacetyl receptor mutant) animals.

(B) Magnitudes of AIA responses represented in (A), omitting traces that did not produce a detectable response. Boxes show median and interquartile range.

(C) Means of AIA traces represented in (A), aligned to response initiation frame, including only responses that initiated within 5 seconds of diacetyl exposure. AIA had similar rise times in the three genotypes until it reached 30-40% $\Delta F/F_0$. Shading indicates $\pm$ SEM.

For (A), asterisks refer to Kolmogorov-Smirnov test significance over full 10-s stimulus pulse. ***: p<0.001. See Appendix C for sample sizes and test details.

For (B), asterisks indicate statistical significance of one-way ANOVA with Dunnett's multiple comparisons test. **: p<0.01; ***: p<0.001. See Appendix D for sample sizes and test details.

AIA responses to diacetyl rely on AWA

AWA cell fate mutants (*odr-7*) and animals lacking the AWA diacetyl receptor (*odr-10*) have weaker AIA diacetyl responses (Larsch et al., 2015). Using the analytical framework described above, I repeated these results and found that AIA responses in AWA mutants not only have decreased magnitudes (Figure 2-6B, C), but are also less reliable (Figure 2-6A), consistent with AIA requiring AWA for its diacetyl response. I aligned the AIA responses that initiated within the first 5 seconds of diacetyl exposure to the frame at which the response was initiated rather than to the stimulus onset. The on-dynamics were similar in the AWA mutants and wildtype AIA neurons, but AIA in the mutants had a peak magnitude roughly half than of wildtype. These findings are consistent with AIA requiring AWA for its diacetyl response, as expected, both for reliability and for response magnitude. I conclude that AWA activation is necessary to produce reliable AIA responses to diacetyl, but not sufficient to produce reliable AIA responses on its own.

Transmission of AWA signals to AIA requires gap junction proteins

The *C. elegans* wiring diagram predicts a gap junction between AWA and AIA, but it does not predict the existence of chemical synapses from AWA to AIA. To test these predictions functionally, I measured AIA responses to pulses of 1.15 μM diacetyl in animals expressing tetanus toxin light chain A in AWA (TeTx). TeTx cleaves the synaptic vesicle protein synaptobrevin, and shall therefore eliminate synaptic vesicle release from AWA. AIA responses to diacetyl in *AWA::TeTx* animals resembled wildtype responses, both in their reliability (Figure 2-7A) and in their magnitude (Figure 2-7B). Similarly, AIA responses to AWA optogenetic stimulation in *AWA::TeTx* animals resembled the wildtype (Figure 2-7C). These results support the conclusion that AWA does not require chemical synapses to communicate with AIA.

Gap junctions are formed when a hemichannel from cell A connects with a hemichannel from cell B. These hemichannels are made of subunits called innexins, and 25 distinct genes encode innexins in *C. elegans*. Unfortunately, there is currently no tool to block all innexins in a given cell. I consulted an RNA sequencing data set of larval L2 stage animals that found expression of *unc-9*, *unc-7*, and *inx-4* innexins in AWA (Cao et al., 2017). *unc-9, unc-7*, and *inx-4* were found in AWA in a separate study on innexin expression in adult animals along with an additional innexin, *inx-7* (Bhattacharya et al., 2019). *unc-9* and *unc-7* are the most widely expressed neuronal innexins. I used the double mutant (*unc-7 unc-9*) and triple mutant (*unc-7 unc-9; inx-4*) to investigate whether AWA indeed uses electrical synapses to communicate with AIA. Both the double and triple innexin mutants had less reliable AIA responses to AWA optogenetic stimulation than wildtype animals (Figure 2-7D). The double mutant also

had less reliable AIA responses to both 1.15 µM and 11.5 nM diacetyl pulses than wildtype (Figure 2-7E, F).

The AIA responses to diacetyl pulses in innexin mutants had decreased magnitudes (Figure 2-7H, I). Curiously, this was not the case for AWA optogenetic stimulation (Figure 2-7G), with AIA responses in the triple mutant increasing somewhat. These innexins are broadly expressed, so several other neurons could contribute to this magnitude increase in the triple mutant. Ideally, I could use a genetically-encoded tool to inactivate all innexin subunits in a single cell only after neuronal development, but such a tool does not exist. That said, the AIA responses to 1.15 µM diacetyl in the *unc-7 unc-9* double mutant resembled those in the *odr-7* AWA cell fate mutant from Figure 2-6, both in shifted latency distribution and in decreased magnitude. Taken together, my results are consistent with AWA signaling to AIA via a functional electrical synapse and not a chemical synapse. Moreover, the gap junction likely consists of *unc-7* and/or *unc-9* innexin subunits and potentially others.

Figure 2-7. Transmission of AWA signals to AIA requires gap junction proteins.

(A) Cumulative response time profiles of AIA responses to 1.15 µM diacetyl in WT versus animals expressing a transgene encoding Tetanus Toxin light chain A, which prevents synaptic release, in AWA.

(B) Magnitudes of AIA responses shown in (A), omitting traces that did not produce a detectable response. Boxes show median and interquartile range.

(C) Cumulative response time profiles of AIA responses to AWA optogenetic stimulation in WT versus animals expressing Tetanus Toxin.

(D, E, and F) Cumulative response time profiles of AIA responses to AWA optogenetic stimulation (D), 1.15 µM diacetyl (E), or 11.5 nM diacetyl (F) in WT versus *unc-7(e5) unc-9(fc16)* and *unc-7(e5) unc-9(fc16); inx-4(ok2373)* (double or triple innexin mutant, respectively) animals.

(G, H, and I) Magnitudes of AIA responses shown in (D), (E), and (F), respectively, omitting traces that did not produce a detectable response. Boxes show median and interquartile range.

For (A), (C), (D-F), asterisks refer to Kolmogorov-Smirnov test significance versus WT over full 10-s stimulus pulse. ns: not significant; *: $p<0.05$; **: $p<0.01$; ***: $p<0.001$. See Appendix C for sample sizes and test details.

For (B) and (G-I), asterisks indicate statistical significance of one-way ANOVA with Dunnett's multiple comparisons test. ns: not significant; *: $p<0.05$; ***: $p<0.001$. See Appendix D for sample sizes and test details.
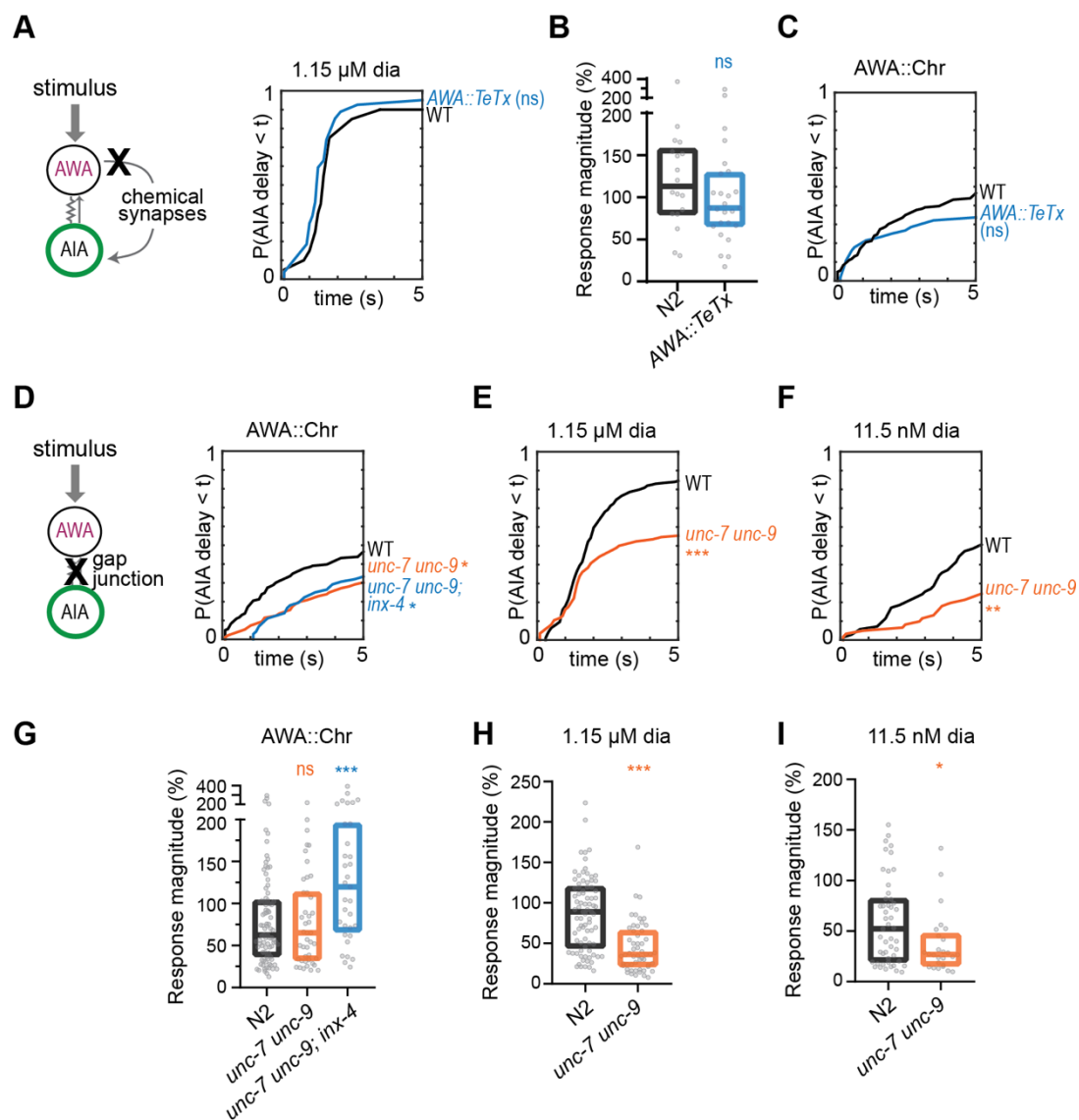
Figure 2-7. Transmission of AWA signals to AIA requires gap junction proteins.

The AWA-AIA electrical synapse is asymmetric

Information flow through electrical synapses can be symmetrical or asymmetrical. If an electrical synapse is symmetrical, current flow from Cell A to Cell B when Cell A is activated would be the same as current flow from Cell B to Cell A when Cell B is activated; the flow would be bidirectional. If the electrical synapse is asymmetrical, current or small molecules would flow more in one direction than the other. To test whether the AWA-AIA electrical synapse is symmetrical or asymmetrical, I expressed the Chrimson transgene in AIA so I could optogenetically stimulate AIA and record the resultant GCaMP fluctuations in AIA and AWA. AIA was rapidly activated by optogenetic stimulation (Figure 2-8A-D). However, AWA responses were variable and infrequent; only 34% of AIA optogenetic stimuli resulted in an AWA response.

Not every AIA neuron undergoing the AIA optogenetic stimulation protocol was activated. Likewise, not every AWA neuron undergoing the AWA optogenetic stimulation protocol was activated. To incorporate the variability, I normalized the post-synaptic response to the response probability in the pre-synaptic neuron that was being directly stimulated (Figure 2-8I, J). The post-synaptic/pre-synaptic response ratio was higher in the AWA-to-AIA direction than in the AIA-to-AWA direction. Thus, the AWA-AIA electrical synapse appears to be asymmetrical.

To characterize the molecular basis of the small AWA responses to AIA optogenetic stimulation, I examined the *unc-7 unc-9* double innexin mutants. These mutants were indistinguishable from wildtype by all criteria (Figure 2-8A-D). Therefore, electrical synapses are less important for AIA to AWA information flow than for AWA to AIA information flow.

41

To test whether AIA requires chemical synapses to activate AWA, I measured AWA responses to AIA optogenetic stimulation in *unc-18* mutants, which are highly defective in pan-neuronal synaptic vesicle release (McEwen and Kaplan, 2008; Weimer et al., 2003; Ventimiglia and Bargmann, 2017). Surprisingly, the AWA responses to AIA stimulation had decreased latency, suggesting that chemical synapses normally inhibit AIA-to-AWA communication (Figure 2-8G, H). Together, these results suggest that electrical and chemical synapses may redundantly carry information from AIA to AWA, since reductions of either process spare the retrograde AIA-to-AWA signal.

Figure 2-8. The AWA-AIA electrical synapse is asymmetrical.

(A) AIA responses to 10-s pulses of AIA optogenetic stimulation in WT and *unc-7(e5) unc-9(fc16)* double innexin mutant animals; one row per calcium trace.

(B) Cumulative response time profiles of calcium traces shown in (A).

(C) AWA responses to 10-s pulses of AIA optogenetic stimulation in WT and *unc-7(e5) unc-9(fc16)* animals; one row per calcium trace.

(D) Cumulative response time profiles of calcium traces shown in (C).

(E) AIA responses to 30-s pulses of optogenetic stimulation in WT and *unc-18(e234)* synaptic transmission mutant animals; one row per calcium trace.

(F) Cumulative response time profiles of calcium traces shown in (E).

(G) AWA responses to 30-s pulses of optogenetic stimulation in WT and *unc-18(e234)* animals; one row per calcium trace.

(H) Cumulative response time profiles of calcium traces shown in (G).

(I) Probability that either AWA or AIA has responded at the end of 10 seconds of AWA or AIA optogenetic stimulation.

(J) Ratios of post-synaptic versus pre-synaptic response probabilities to AWA or AIA optogenetic stimulation, where pre-synaptic refers to neuron being optogenetically stimulated. This ratio is lower in the AIA-to-AWA direction.

Asterisks refer to Kolmogorov-Smirnov test significance versus WT over full 10-s stimulus pulse. ns: not significant; **: $p < 0.01$. See Appendix C for sample sizes and test details.

Figure 2-8. The AWA-AIA electrical synapse is asymmetrical.

44
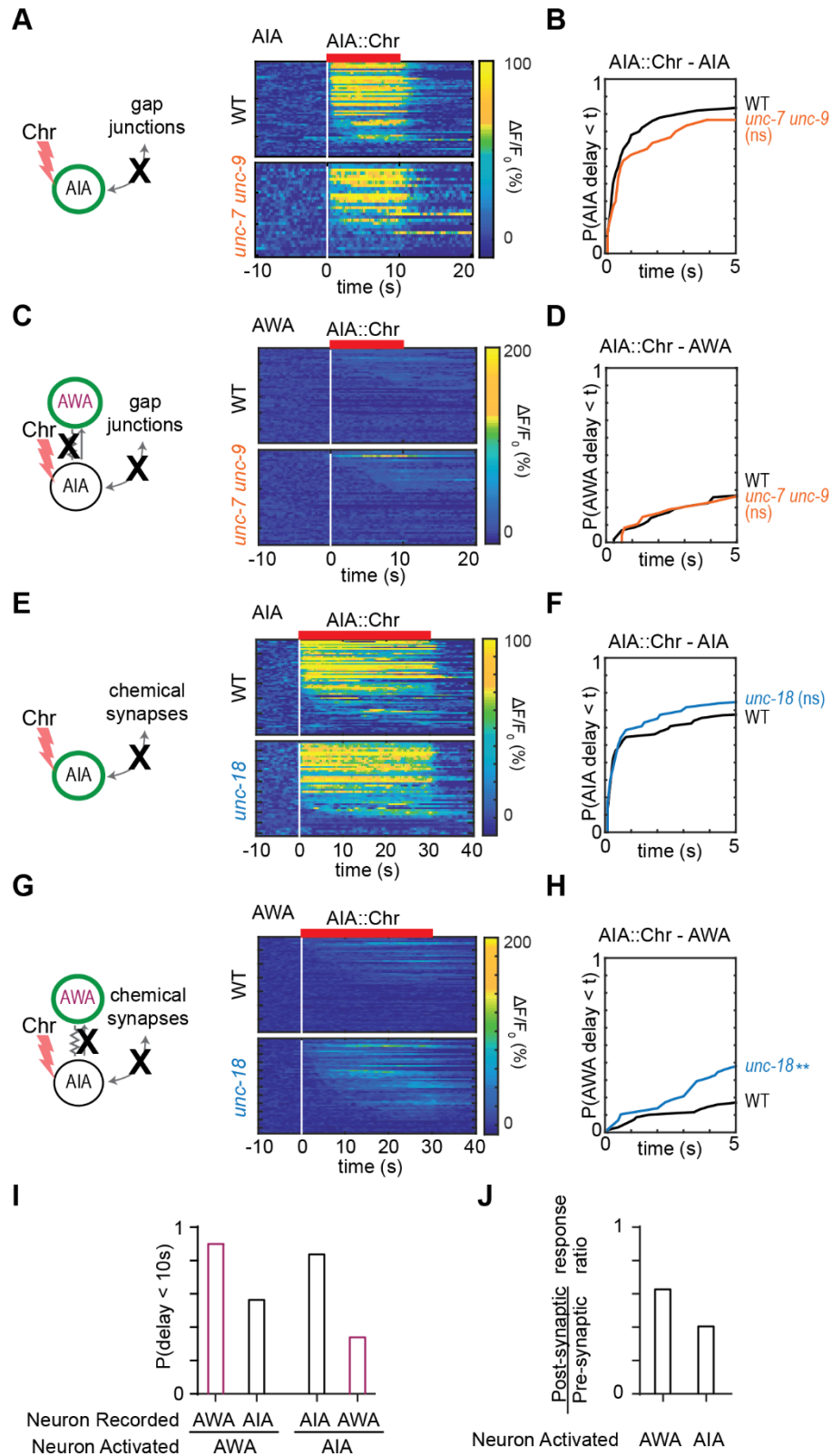
Discussion

AWA to AIA signal transmission is unreliable

I showed in this chapter that strongly stimulating AWA with optogenetics was not sufficient to produce reliable AIA interneuron responses, despite the two neurons sharing a functional electrical synapse. However, when an AIA response *was* triggered, it had stereotyped on-dynamics and magnitude, regardless of the stimulus (see Appendix B for examples of more stimuli). The main difference between stimuli was *if* and *when* the stimulus produced the stereotyped AIA response.

Larsch et al. (2015) previously observed that AIA responses to pulses of diacetyl were stereotyped at concentrations at or above 115 nM diacetyl. However, they stated that AIA responses to the lower concentration of 11.5 nM were "graded and sustained" across the diacetyl stimulation. In my experiments with 11.5 nM diacetyl and optogenetic stimuli, looking at the averaged responses aligned to the stimulus onset appeared to show a graded response without desensitization, but aligning the responses to the onset of AIA activation revealed the same stereotyped AIA dynamics as seen with strong stimuli. Together, these results suggest an all-or-none AIA response to AWA input.

Choosing an optogenetic stimulation protocol

I chose to activate the AWA and AIA neurons with 10 seconds of constant illumination to match the dynamics of previous odor pulses. AWA responses to optogenetic stimulation of AWA resembled AWA responses to 115 nM diacetyl in both

magnitude and dynamics, suggesting that the stimulation fell in a physiological range. AIA responses to AWA optogenetic stimulation were similar using red light at intensities ranging from 6.5 to 15.4 mW/cm^2, the range used here. Because I did not see reliable downstream AIA responses to AWA optogenetic stimulation, I performed pilot experiments with different light stimulus patterns. AWA is tuned to encode certain stimulus features, such as step-like diacetyl increases (Larsch et al., 2015; Liu, Q et al., 2018). I tried to mimic these small odor steps by delivering small increases in light intensity rather than a single, sustained increase. I found that AWA did not desensitize to optogenetic stimulation (Larsch et al., 2015; Figure 2-1), although it does desensitize to odor, so the protocol was not suitable to mimic physiological odor steps.

As a further exploration, I used a flickering optogenetic stimulus protocols (10 ms on, 10 ms off; 100 ms on, 100 ms off) (Tumkaya et al., 2019). The resultant AWA and AIA responses looked similar to constant illumination (data not shown). It would be interesting to try sine wave stimuli changes to mimic the animal's undulatory head motion.

Asymmetry at the electrical synapse

The electron micrograph wiring diagram shows ~900 gap junctions in the *C. elegans* nervous system (White et al., 1986). Majewska and Yuste (2001) determined that these gap junction connect 92% of *C. elegans* neurons. The existence of functional asymmetry, or rectification, provides a mechanism for increasing the sophistication of the network. Asymmetry at the electrical synapse exists in both vertebrates and invertebrates and can be created through the formation of heterotypic gap junctions

(Phelan et al., 2008; Miller et al., 2017; Liu, P et al., 2013). My results suggest that the electrical synapse connecting AWA with AIA allows preferential information transfer from AWA to AIA versus AIA to AWA (Figure 2-8). For communication between a sensory and an interneuron, it may be advantageous for information to flow in one direction and not the other. Asymmetry at an electrical synapse would provide this functional polarity without sacrificing fast transmission speed. At the same time, I speculate that some electrical synapses may be symmetrical, such as those connecting left-right neuron pairs (e.g., the AIA neuron pair consists of one AIA neuron on the left and one on the right side of the animal).

Optogenetically stimulating AIA produced very slow recruitment of AWA (Figure 2-8). This slow recruitment increased somewhat in *unc-18* chemical synapse mutants. The electron micrograph wiring diagram shows a chemical synapse from AIA to AWA (White et al., 1986). AIA is cholinergic (Altun-Gultekin et al., 2001), so I would predict that if AIA inhibits AWA with a chemical synapse, AWA would express either an acetylcholine-gated chloride channel or a G-protein coupled acetylcholine receptor. Based on an RNA sequencing data set, AWA is predicted to express both receptor types: *acc-3*, encoding an acetylcholine-gated chloride channel, and both *gar-1* and *gar-3,* encoding G-protein coupled acetylcholine receptors (Cao et al., 2017).

CHAPTER 3: Glutamate from sensory neurons gates AWA-to-AIA communication and guides behavior

Background

In Chapter 2, I showed that AWA stimulation is not sufficient to produce reliable downstream AIA responses, instead leading to activation with a low probability and high, variable latency. Since I observed robust AIA responses to higher concentrations of diacetyl, which are known to be detected by multiple sensory neurons (Hale et al., 2016), I hypothesized that a non-AWA neuron contributes to the AIA responses to diacetyl.

In Larsch et al. (2015), the authors recorded AIA responses to 1.15 µM diacetyl not only in *odr-7* AWA cell fate mutants (as I did in Chapter 2), but also in *ceh-36* AWC+ASE cell fate mutants and in *odr-7 ceh-36* double mutants. They observed an intermediate AIA response in *odr-7* mutants, intact AIA responses in *ceh-36* mutants, and severely defective AIA responses in the double mutant. I replicated these findings in the double mutants (not shown). Based on these results, I hypothesized that AWA and AWC both contribute to AIA's diacetyl response. This hypothesis is consistent with behavior analysis after laser ablation (Chou et al., 2001).

Unlike AWA, AWC and other sensory neurons form chemical synapses onto AIA. In this chapter, I present evidence that AWA-to-AIA transmission is reliable in the absence of global chemical synapses. More specifically, inhibitory glutamate release from a small group of sensory neurons onto AIA blocks reliable AWA-to-AIA transmission. I conclude that AIA integrates global sensory state, generating a stereotyped response when multiple sensory neurons send coincident and coherent

signals. I present preliminary behavioral experiments to study how coincidence detection in AIA affects behavior.

Results

Chemical synapses are net inhibitory onto AIA

In the previous chapter, I showed that AWA activation is required for reliable AIA responses to diacetyl, but not sufficient to induce reliable AIA responses on its own. To ask how other neurons in the circuit may impact communication from AWA to AIA, I inactivated chemical synapses with the *unc-18(e234)* mutation, which affects a chaperone protein required for synaptic vesicle docking. Synaptic vesicle release is greatly reduced in these mutants, but gap junctions should not be affected (McEwen and Kaplan, 2008; Weimer et al., 2003; Ventimiglia and Bargmann, 2017). I hypothesized that the remaining AIA responses to diacetyl in animals lacking AWA function (Figure 2-6) stemmed from a sensory neuron that formed chemical synapses with AIA, and expected AIA responses to be weaker in the *unc-18* mutant. To my surprise, AIA responses to AWA optogenetic stimulation were more reliable in *unc-18(e234)* mutants than in wildtype (Figure 3-1A). This improved reliability held for each experimental replicate (Figure 3-1B). I tested two additional mutants with defective chemical synapses, *unc-18(e81)* and *unc-13(e51)*, and found that they also had more reliable transmission of optogenetic stimulation from AWA to AIA (Figure 3-1C).

The increased reliability in AIA response could result from a stronger AWA response to the same stimulus, but AWA responses to AWA optogenetic stimulation did

not improve in *unc-13(e51)* versus wildtype animals (Figure 3-1D, E). If anything, AWA

responses to AWA optogenetic stimulation in *unc-13* mutants were lower in magnitude

(Figure 3-1F). To quantify the decreased latency of the AIA response, I calculated the

point at which 50% of AWA versus AIA neurons had responded. The delay between the

two points decreased from 6.3 seconds in wildtype to 1 second in *unc-13* mutants

(Figure 3-1G). The short delay in *unc-13* mutants was comparable to the 0.8 or 1.1

second delay for wildtype responses to 1.15 μM or 115 nM diacetyl, respectively (Figure

3-1H).

A similar increase in reliability in AIA neurons was observed in response to 1.15

μM diacetyl (Figure 3-1I), and this effect was even more pronounced with 11.5 nM

diacetyl (Figure 3-1J). These results indicate that chemical synapses inhibit AIA and

dampen its response to AWA stimulation, whether optogenetic or by odor.

Figure 3-1. Chemical synapses are net inhibitory onto AIA.

(A) WT and *unc-18(e234)* (synaptic transmission mutant) AIA responses to 10-s pulses of AWA optogenetic stimulation, combined over all experiments. WT data are the same as in Figure 2-2.

(B) Cumulative response time profiles of AIA responses shown in (A). Thick lines represent distribution of global data set, faint lines represent distributions from individual experiment blocks.

(C) Cumulative response profiles of AIA responses to AWA optogenetic stimulation in WT and three chemical synapse mutant strains with defective chemical synaptic transmission: *unc-13(e51)*, *unc-18(e234)*, and *unc-18(e81)*.

(D-F) Removing chemical synapses does not improve AWA responses to AWA optogenetic stimulation.

(D) WT and *unc-13(e51)* AWA responses to 10-s pulses of AWA optogenetic stimulation.

(E) Cumulative response time profiles of AWA responses shown in (D).

(F) Magnitudes of AWA responses shown in (D), omitting traces that did not produce a detectable response. Boxes show median and interquartile range.

(G) Cumulative response time profiles of AWA and AIA responses to 10-s pulses of AWA optogenetic stimulation in *unc-13(e51)* animals. Numbered arrow indicates the delay between the time at which 50% of AWA versus AIA neurons have responded (Δt_{50}). AWA and AIA were not recorded simultaneously.

(H) t_{50} of AWA versus t_{50} of AIA (Δt_{50}) in WT and *unc-13(e51)* animals in response to AWA optogenetic stimulation. WT responses to other stimuli (same as in Figure 2-2) are shown for comparison. Bars are mean $\pm$ SEM from bootstrapping (see Experimental Procedures).

(I and J) Cumulative response time profiles of AIA to 10-s pulses of 1.15 µM (I) or 11.5 nM (J) diacetyl in WT and chemical synapse mutants.

For (C), (E), (I) and (J), asterisks refer to Kolmogorov-Smirnov test significance versus WT over full 10-s stimulus pulse. ns: not significant; *: $p<0.05$; **: $p<0.01$; ***: $p<0.001$. See Appendix C for sample sizes and test details.
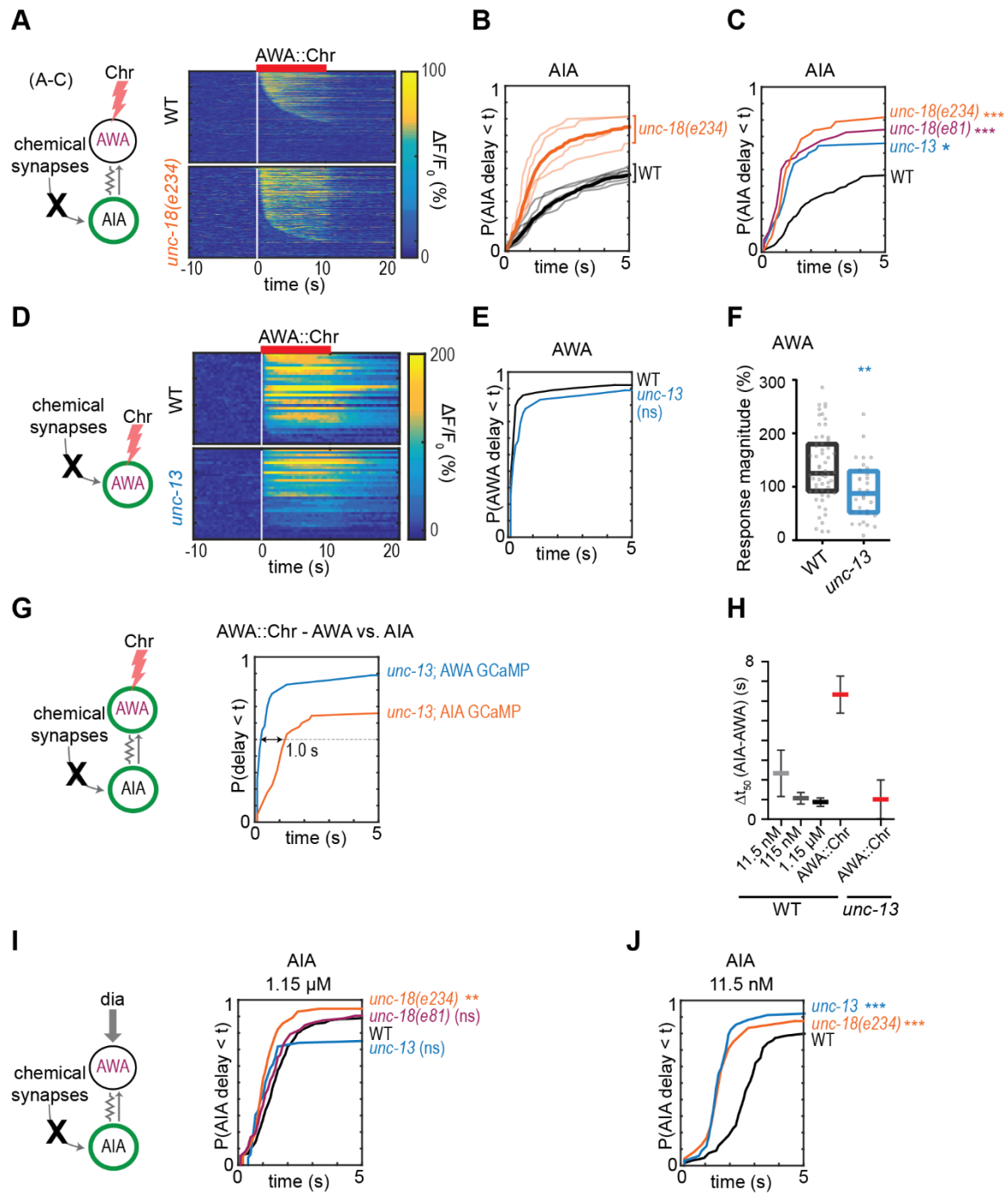
Figure 3-1. Chemical synapses are net inhibitory onto AIA.

Chemical synapses reduce reliability but not magnitude or rise dynamics of AIA responses to AWA stimuli

To further compare the AIA responses in wildtype and synaptic transmission mutants, I subjected traces to quantitative analysis. AIA responses were comparable in magnitude across wildtype, *unc-13*, and *unc-18* animals regardless of whether AWA was stimulated using optogenetics, 1.15 µM diacetyl or 11.5 nM diacetyl (Figure 3-2A-C). I next examined AIA responses to AWA optogenetic stimulation in wildtype and *unc-18(e234)* animals by selecting the AIA responses that initiated within the first 5 seconds of stimulus exposure and aligning them to the initiation of the AIA response (Figure 3-2D, E). Again, the mean AIA response magnitude as well as the calcium rise time to peak were the same in wildtype and *unc-18(e234)* animals. The mean time derivatives for wildtype and *unc-18(e234)* animals, when aligned to response initiation, also overlapped for the rise and peak portion of the response (Figure 3-2F). Thus, chemical synapses alter AIA responses to AWA optogenetic stimulation primarily by altering response latency and probability, not by affecting response magnitude or rise dynamics.

Figure 3-2. Chemical synapses reduce reliability but not magnitude or rise dynamics of AIA responses to AWA stimuli.

(A-C) Magnitudes of AIA responses to 10-s pulses of AWA optogenetic stimulation (A), 1.15 µM diacetyl (B), or 11.5 nM diacetyl (C), in WT versus *unc-13(e51), unc-18(e234),* and *unc-18(e81)* synaptic transmission mutant animals. Data are the same as in Figure 3-1, omitting traces that did not produce a detectable response. Boxes show median and interquartile range.

(D) Heat maps of AIA responses to AWA optogenetic stimulation in WT versus *unc-18(e234)* animals. Left: responses are aligned to stimulus onset, as in Figure 3-1A. Right: pulses that resulted in activation within 5 seconds of stimulus were aligned to the frame at which activation was initiated.

(E) Overlaid means of aligned AIA responses from (D). Note that averages are only comparable for the 5 seconds post-initiation. Rise dynamics and magnitudes are similar in both genotypes. Shading indicates ± SEM.

(F) Time derivatives of responses shown in (D). Left: aligned to stimulus onset. Right: aligned to response initiation frame.

For (A-C), ns refers to a lack of statistical significance of an ordinary one-way ANOVA with Dunnett's multiple comparisons versus WT. See Appendix D for sample sizes and test details.
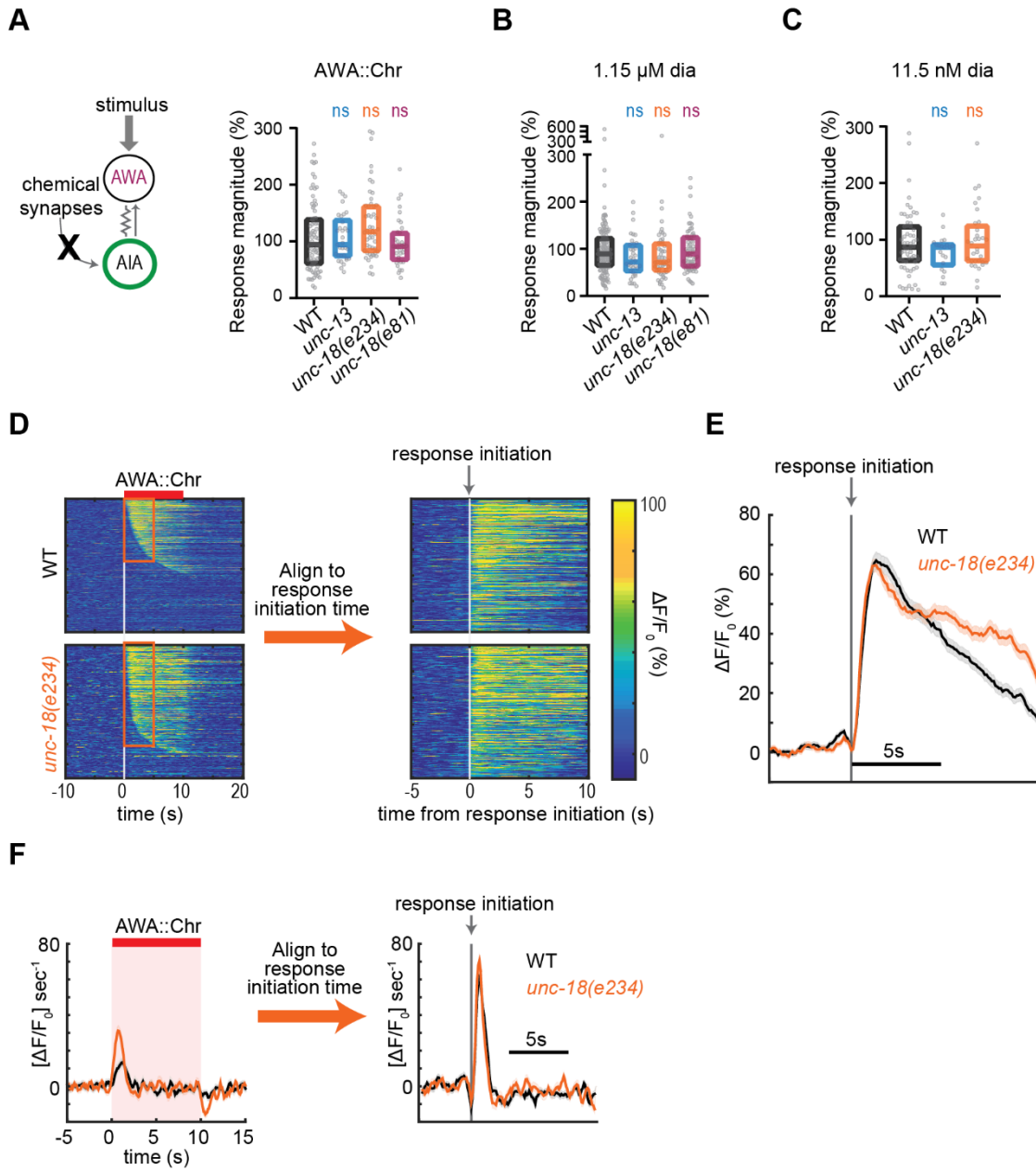
Figure 3-2. Chemical synapses reduce reliability but not magnitude or rise dynamics of AIA responses to AWA stimuli.

Chemical synapses inhibit AIA response decay

unc-18(e234) mutants appeared to have a slower decay in AIA responses to AWA optogenetic stimulation than wildtype (Figure 3-2E). To quantify this effect, I examined the decay of AIA responses that initiated within the first 2 seconds of stimulus exposure, leaving at least 8 seconds after response initiation for comparison. To compare decay rates, I first transformed mean GCaMP fluorescence changes into an approximate calcium concentration by correcting for the nonlinearity of GCaMP, and then log-transformed the calcium responses and fit a line to the 6-second decay portion of the response (2 to 8 seconds after response initiation) (Figure 3-3B). Indeed, the decay half-time was longer in *unc-18(e234)* than in wildtype animals (Figure 3-3C), indicating that chemical synapses shape AIA response decay.

AIA has been shown to use peptides to communicate with sensory neurons (Cho et al., 2016; Chalasani et al., 2010; Tomioka et al., 2006). I therefore looked at the decay of AIA responses to AWA optogenetic stimulation in *unc-31* mutants, which are defective in dense core vesicle exocytosis and peptidergic transmission (Speese et al., 2007). The AIA decay rate was dramatically reduced in these mutants (Figure 3-D, E), suggesting that AIA decay dynamics are regulated by neuropeptides.

To ask if the chemical synapses responsible for AIA response decay were from AIA itself (auto-inhibitory) or another neuron, I optogenetically stimulated AIA for 30 seconds to better measure decay and recorded AIA responses in wildtype and *unc-18* mutants (Figure 3-3F). Again, *unc-18* mutants had slower AIA decay than wildtype animals (Figure 3-3G, H), an effect that was consistent across different intensities of optogenetic stimulation (Figure 3-3I-K).

56

Figure 3-3. **Chemical synapses inhibit AIA response decay.**

(A and D) Mean AIA responses to 10-s pulses of AWA optogenetic stimulation in WT and *unc-18* mutants (A) or *unc-31* dense core vesicle exocytosis mutants (D). Data shown in (A) is further subsampled from data shown in Figure 3-2D, including only responses that initiated within 2 s of stimulus. Responses were aligned to activation initiation frame. Shading indicates $\pm$ SEM.

(B and E) Log transform of calcium decay. $\Delta F/F_0$ traces from (A) and (D), respectively, were transformed into $\Delta Ca^{2+}/Ca^{2+}$ traces, log transformed, and linearly fit for 2-8 seconds post-initiation.

(C, H and K) Linear fits from (B), (G) and (J), respectively, were extrapolated to calculate the number of seconds for AIA calcium levels to decrease to 50% of the peak in WT and *unc-18* animals to find the half-time of aligned AIA responses to AWA optogenetic stimulation.

(F and I) Mean AIA responses to 30-s pulses of AIA optogenetic stimulation using 15.4 mW/cm^2 (F) or 6.5 mW/cm^2 (I) red light in WT and *unc-18* animals. Shading indicates $\pm$ SEM. WT: n = 41; *unc-18*: n = 40.

(G and J) Log fit of calcium decay. $\Delta F/F_0$ traces from (F) and (I), respectively, were transformed into approximated $\Delta Ca^{2+}/Ca^{2+}$ traces, log transformed, and the decay was linearly fit for 3-30 seconds post-stimulus onset.
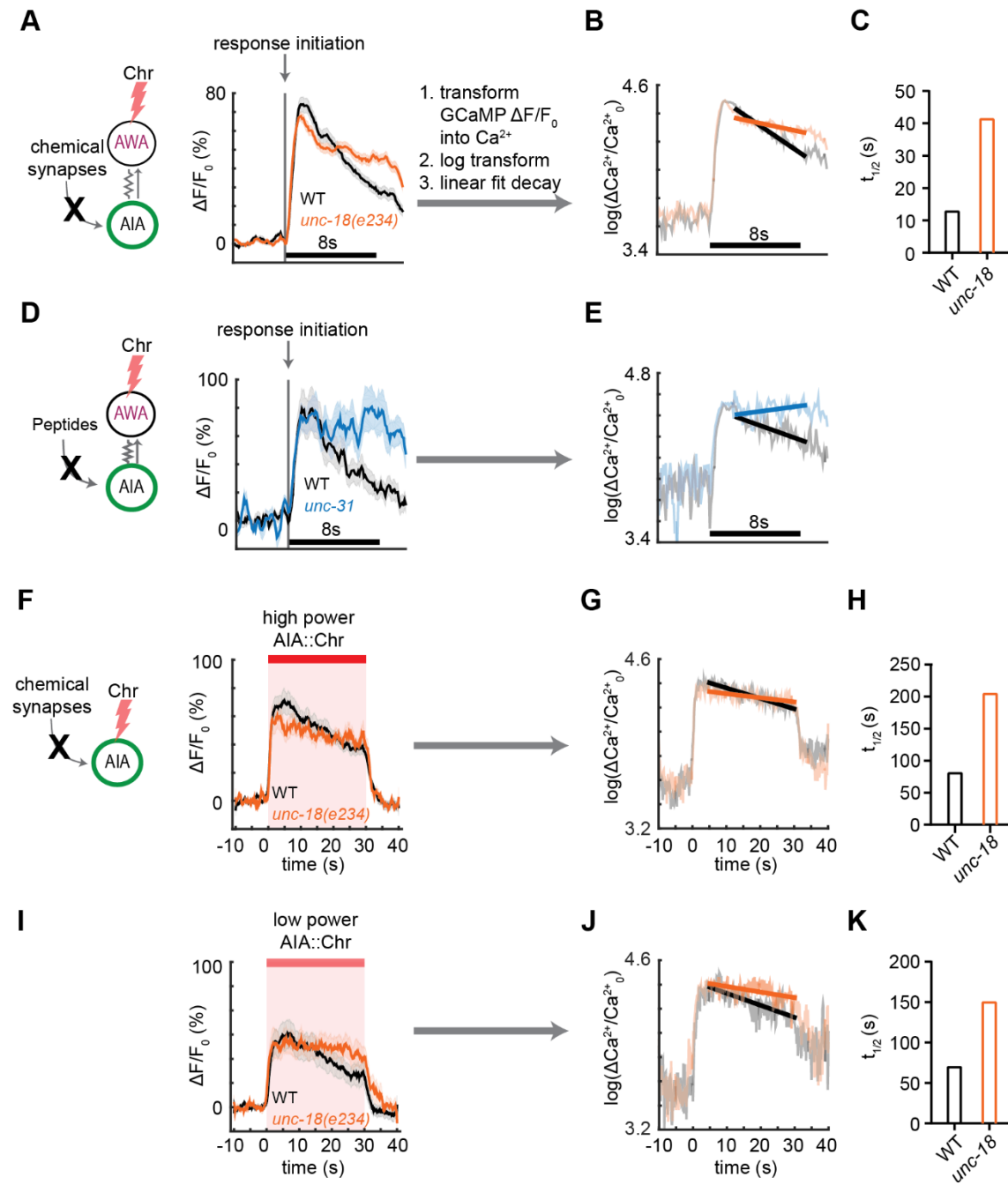
Figure 3-3. **Chemical synapses inhibit AIA response decay.**

Preliminary experiments point to a role for glutamate in AIA inhibition

Having determined that chemical synapses are net inhibitory to AIA (Figure 3-1), and having ruled out AWA as the source of those chemical synapses (Figure 2-7), I examined other neurons in the circuit. The electron micrograph wiring diagram shows many neurons forming chemical synapses onto AIA (Figure 3-4). A majority of these neurons use glutamate as their neurotransmitter, although some use acetylcholine, serotonin, neuropeptides, or unknown signaling molecules.

eat-4 mutants lack the major vesicular glutamate transporter required for glutamatergic signaling in *C. elegans*. AIA responses to AWA optogenetic stimulation or diacetyl odors were slightly accelerated compared to the wildtype, although not as much as in *unc-13* and *unc-18* synaptic transmission mutants (Figure 3-5A-C). By contrast, I observed no acceleration in *unc-31* mutants (defective peptidergic transmission; Figure 3-5D), *unc-25* mutants (defective GABA synthesis; Figure 3-5E), or *cha-1* mutants (defective acetylcholine synthesis; Figure 3-5F). These exploratory experiments pointed to a role of glutamate in AIA inhibition. Rather than pursuing the *unc-13* and *unc-18* synaptic transmission mutants that affect global synapses, I used a more focused approach to examine glutamatergic sensory neurons.

Figure 3-4. Many neurons using various neurotransmitters form synapses onto AIA.

(A) Cartoon representation of most head neurons, showing on the left side. Shaded neurons are either presynaptic chemical synaptic partners or putative electrical synaptic partners with AIA; shading color represents the neuron's neurotransmitter.

(B) List of neurons that form synapses onto AIA and the neurotransmitters and peptides they release. Note the abundance of glutamatergic sensory neurons. Peptide information is based on sources aggregated at *www.wormatlas.org*.

Figure 3-5. Preliminary experiments point to a role for glutamate in AIA inhibition.

(A-C) Cumulative response time profiles of AIA responses to 10-s pulses of AWA optogenetic stimulation (D), 1.15 μM diacetyl (E), or 11.5 nM diacetyl (F) in WT and *eat-4(ky5)* (vesicular glutamate transporter mutant) animals.

(D-F) Cumulative response time profiles of AIA responses to 10-s pulses of AWA optogenetic stimulation in WT versus *unc-31(e928)* (dense core vesicle exocytosis mutant; D), *unc-25(n2324)* (GABA synthesis mutant; B), or *cha-1(p1152)* (acetylcholine synthesis mutant; C) animals.

Asterisks refer to Kolmogorov-Smirnov test significance versus WT over full 10-s stimulus pulse. ns: not significant; *: p<0.05; **: p<0.01. See Appendix C for sample sizes and test details.

Glutamatergic sensory neurons cooperate to inhibit AIA

At least nine interconnected pairs of glutamatergic neurons form chemical synapses onto AIA, six of which are sensory neurons (Serrano-Saiz et al., 2013; White et al., 1986). To narrow in on which neuron or neurons modulate AWA communication with AIA, I selectively blocked glutamate release from four sensory neuron pairs: ASK, AWC, ASE and ASG (Figure 3-6A). This was achieved by expressing flippase under the *tax-4* promoter in animals with an edited endogenous *eat-4* locus; the *eat-4* locus is excised in neurons expressing flippase but functional in the absence of flippase (Figure 3-6B). In animals lacking glutamate release from these four neuron pairs, AWA optogenetic stimulation evoked reliable and short-latency AIA responses similar to those in *unc-18(e234)* synaptic transmission mutants (Figure 3-6C). This effect was not observed with either the modified *eat-4* locus or the flippase expression alone (Figure 3-6D). No single sensory neuron pair accounted for the full effect of preventing glutamate release from ASK, AWC, ASE and ASG (Figure 3-6E-J). Preventing glutamate release from ASK only significantly increased AIA response reliability to AWA optogenetic stimulation (Figure 3-6E), and the combination of AWC and ASE had a small but nonsignificant effect (Figure 3-6H, I). I conclude that ASK and at least one of AWC, ASE and ASG sensory neurons release glutamate to inhibit AIA activation.

Figure 3-6. Glutamatergic sensory neurons cooperate to inhibit AIA.

(A) Simplified diagram of connections between AWA, AIA, and four glutamatergic sensory neurons.

(B) Schematic of cell-selective glutamate knockout genetic strategy. The *eat-4* locus is excised only in the presence of flippase.

(C-J) Cumulative response time profiles of AIA responses to 10-s pulses of AWA optogenetic stimulation in various animals lacking either glutamate release or cellular function of specific sensory neurons. For (E-H), dotted black and blue lines are control and *eat-4-FRT; tax-4p::nFlippase*, respectively, from (C).

(C) Control (*eat-4-FRT* genetic background with no flippase expression), *unc-18(e234)*, and *eat-4-FRT; tax-4p::nFlippase* (glutamate knockout in ASK, ASE, AWC, and ASG) animals.

(D) Control, N2 (used as WT genetic background in all other figures), and N2; *tax-4p::nFlippase* (flippase expression in ASK, ASE, AWC and ASG in animals lacking *eat*-4 excision sites) animals. Control animals are the same as in (C).

(E) *eat-4-FRT; sra-9p::nFlippase* (glutamate knockout in ASK) animals.

(F) *eat-4-FRT; odr-1p::nFlippase* (glutamate knockout in AWC) animals.

(G) *eat-4-FRT; gcy-15p::nFlippase* (glutamate knockout in ASG) animals.

(H) *eat-4-FRT; ceh-36p::nFlippase* (glutamate knockout in AWC and ASE) animals.

(I) WT and *ceh-36(ky640)* (AWC and ASE cell fate mutant) animals.

(J) WT and *che-1(674)* (ASE cell fate mutant) animals.

Asterisks refer to Kolmogorov-Smirnov significance versus *eat-4-FRT* controls (C-H) or WT (I-J) over full 10-s stimulus pulse. ns: not significant; **: $p<0.01$, ***: $p<0.001$. See Appendix C for sample sizes and test details.
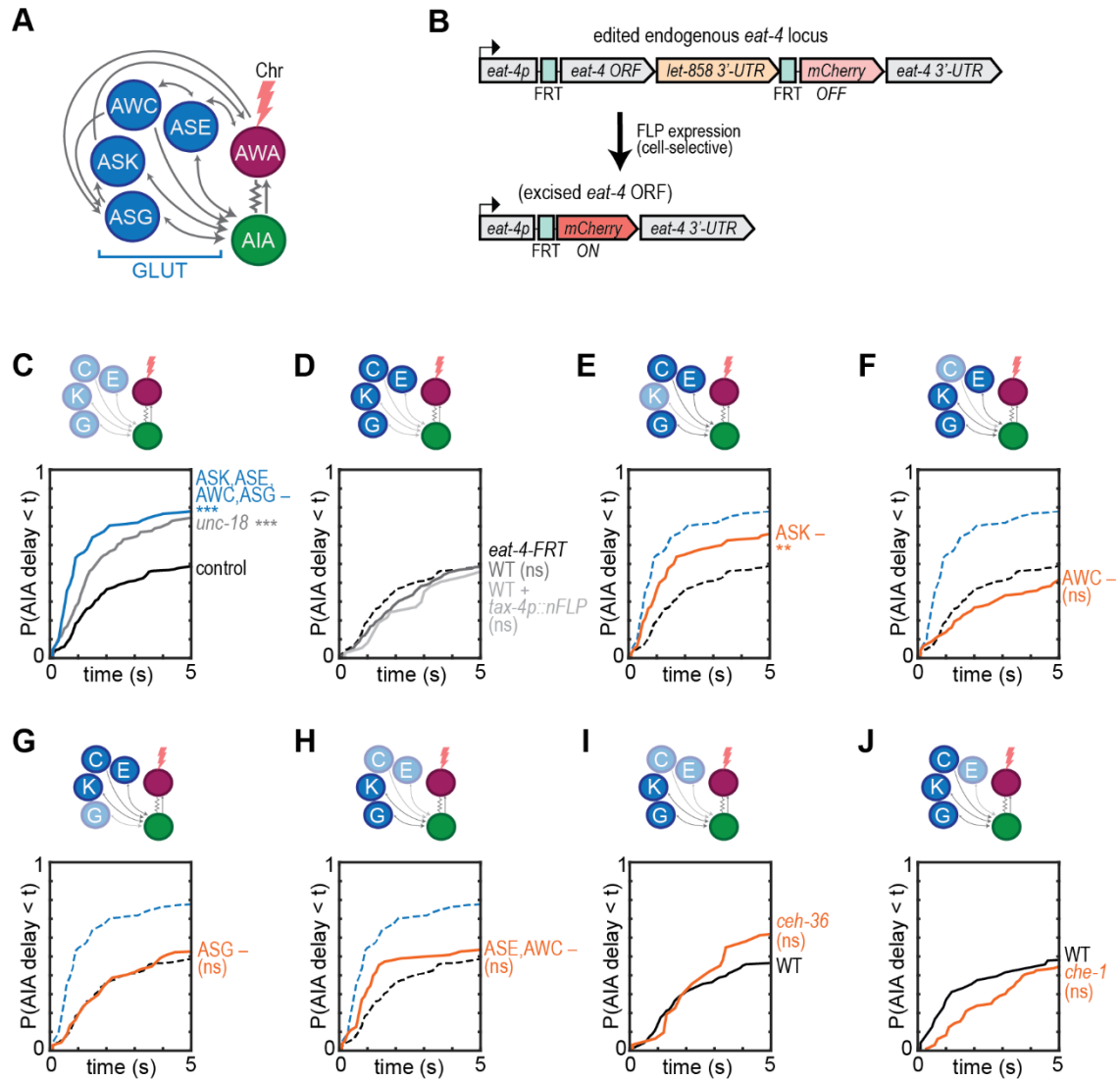
Figure 3-6. Glutamatergic sensory neurons cooperate to inhibit AIA.

Synaptic vesicle release from AWC and ASE is sufficient to prevent AIA activation upon AWA stimulation

To confirm that these sensory neurons tonically inhibit AIA, I selectively expressed wildtype *unc-18* genomic DNA in AWC and ASE in *unc-18(e234)* synaptic mutants, resulting in animals lacking synaptic vesicle release from all neurons except AWC and ASE. In two independent rescue lines, AIA responses were restored to variable, wildtype-like responses (Figure 3-7). This effect was not observed in control *unc-18(e234)* animals expressing a transgene that encoded the *unc-18(e234)* mutation. This result indicates that glutamate release from AWC and ASE is sufficient to inhibit AIA activation by AWA. Together with results from Figure 3-6, I conclude that a small set of glutamatergic sensory neurons tonically inhibits AIA.
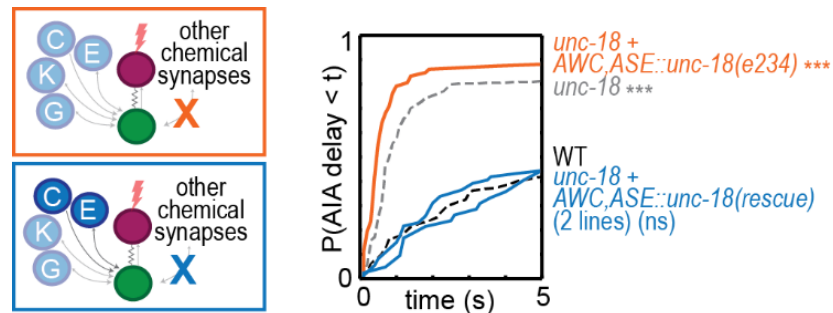
Figure 3-7. **Synaptic vesicle release from AWC and ASE is sufficient to prevent AIA activation upon AWA stimulation.**

Cumulative response time profiles of AIA responses to 10-s pulses of AWA optogenetic stimulation in WT, *unc-18(e234)*, *unc-18(e234)* animals expressing *ceh-36p::unc-18(e234)* genomic DNA (sham rescue), and two lines of *unc-18(e234)* animals expressing *ceh-36p::unc-18(WT)* genomic DNA as an AWC+ASE-specific chemical synaptic rescue. Asterisks refer to Kolmogorov-Smirnov test significance versus WT over full 10-s stimulus pulse. ns: not significant; ***: p<0.001. See Appendix C for sample sizes and test details.

AWC inhibition with a low concentration of butanone is not sufficient to reliably activate

AIA

My results so far suggest that AIA integrates input from multiple sensory neurons, and that stimulation of AWA is not sufficient to activate AIA. I next asked whether disinhibition of glutamatergic input was sufficient to activate AIA. A single AWC neuron, AWC^{ON}, senses and is inhibited by the volatile odor butanone (Wes and Bargmann, 2001). A low concentration of butanone (11.2 nM) consistently inhibits AWC (Cho et al., 2016; their data are replotted in Figure 3-8A), but does not activate or inhibit other sensory neurons (my unpublished data). Delivering pulses of 11.2 nM butanone to AIA did not produce reliable AIA responses, with only ~1/3 of animals responding within 5 seconds of butanone exposure (Figure 3-8B). Thus, a reduction of AWC^{ON} activity, and an associated reduction of glutamate release from AWC^{ON} (Ventimiglia et al., 2017), is not sufficient to activate AIA.
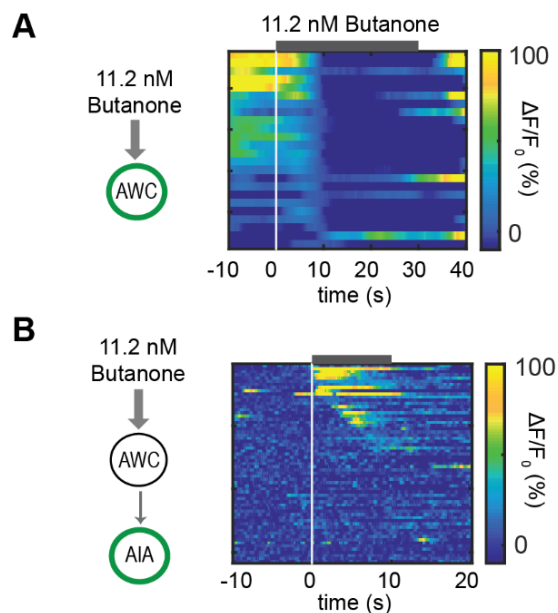
Figure 3-8. AWC inhibition with a low concentration of butanone is not sufficient to reliably activate AIA.

(A) Heat map of WT AWC responses to 30-s pulses of 11.2 nM butanone, n = 25, one row per animal. Re-plotted from Cho et al. (2016); data were produced by Christine Cho.

(B) Heat map of WT AIA responses to 10-s pulses of 11.2 nM butanone, n = 63, one row per animal.

Optogenetically stimulating AWA robustly induces forward movement

During natural behavior, AIA activity suppresses spontaneous reversals and promotes forward navigation toward an attractive stimulus source (Wakabayashi et al., 2004; Larsch et al., 2015). As a quantitative assay for the function of AWA, sensory glutamate, and AIA, I recorded the behavior of animals moving on an agar plate without food (15-20 animals per plate) while I delivered light pulses to optogenetically stimulate AWA (Figure 3-9A). These recordings were done off of food, during the "local search" phase of animal behavior that spans the first 20 minutes after food removal (Lopez-Cruz et al., 2019; Hills et al., 2004; Wakabayashi et al., 2004). During this interval, animals perform many spontaneous reversals, providing a behavior context in which it is possible to measure suppression of reversals and increases in forward locomotion.

Activating the Chrimson transgene in AWA with retinal and light produced a robust enhancement of forward locomotion. 89% of animals were moving forward after ten seconds of stimulation, compared to 70% at baseline. I observed a rebound effect in which animals reduced their forward locomotion below baseline levels for ~10 seconds after the light stimulation ended. These results are consistent with Larsch et al. (2015).

I next examined the sensory glutamate knockout animals. As expected, they did not respond to light stimulation (Figure 3-9C). When the *AWA::Chrimson* transgene was stimulated in the sensory glutamate knockout background, I observed a slightly enhanced effect compared to *AWA::Chrimson* alone (Figure 3-9D-G). In addition, the sensory glutamate knockout animals had an enhanced rebound with less forward locomotion after the end of the light stimulus than the *AWA::Chrimson* strain in the wildtype background.

67

Figure 3-9. **Optogenetically stimulating AWA robustly induces forward movement.**

(A) Experimental setup for optogenetic behavior experiments. Animals are transferred off food to the assay plate and recorded behaving in response to pulses of light. See Experimental Procedures for details.

(B - c) Fraction of animals moving forward during a 20-s light pulse, showing 50 s before and after pulse, with or without retinal pre-treatment.

(B) *eat-4-FRT* background (no flippase), expressing *AWA::Chrimson*.

(C) *eat-4-FRT; tax-4p::nFlippase* (glutamate knockout in ASK, AWC, ASE and ASG).

(D) *eat-4-FRT; tax-4p::nFlippase*, expressing *AWA::Chrimson*.

(E) With-retinal plots from (B), (C) and (D), overlaid for comparison.

(F) Baseline and peak fractions of animals moving forward from (B), (C) and (D).

(G) Difference between baseline and peak fractions of animals moving forward, normalized to baseline, from (B), (C) and (D). Boxes show median and interquartile range.

(H) Baseline and rebound fractions of animals moving forward from (B), (C) and (D).

For (F) and (H), asterisks represent results of paired t-tests between mean baseline and peak (F) or rebound (H) fractions for a given condition, or an unpaired t-test comparing the rebound (H) fraction of *AWA::Chrimson* with or without sensory glutamate knockout, both with-retinal. ns: not significant; *: $p < 0.05$; ***: $p < 0.001$.

For (G), asterisks represent results of unpaired t-tests between with-retinal and without-retinal for a given condition, or an unpaired t-test comparing *AWA::Chrimson* with or without sensory glutamate knockout, both with-retinal. ns: not significant; ***: $p < 0.001$.
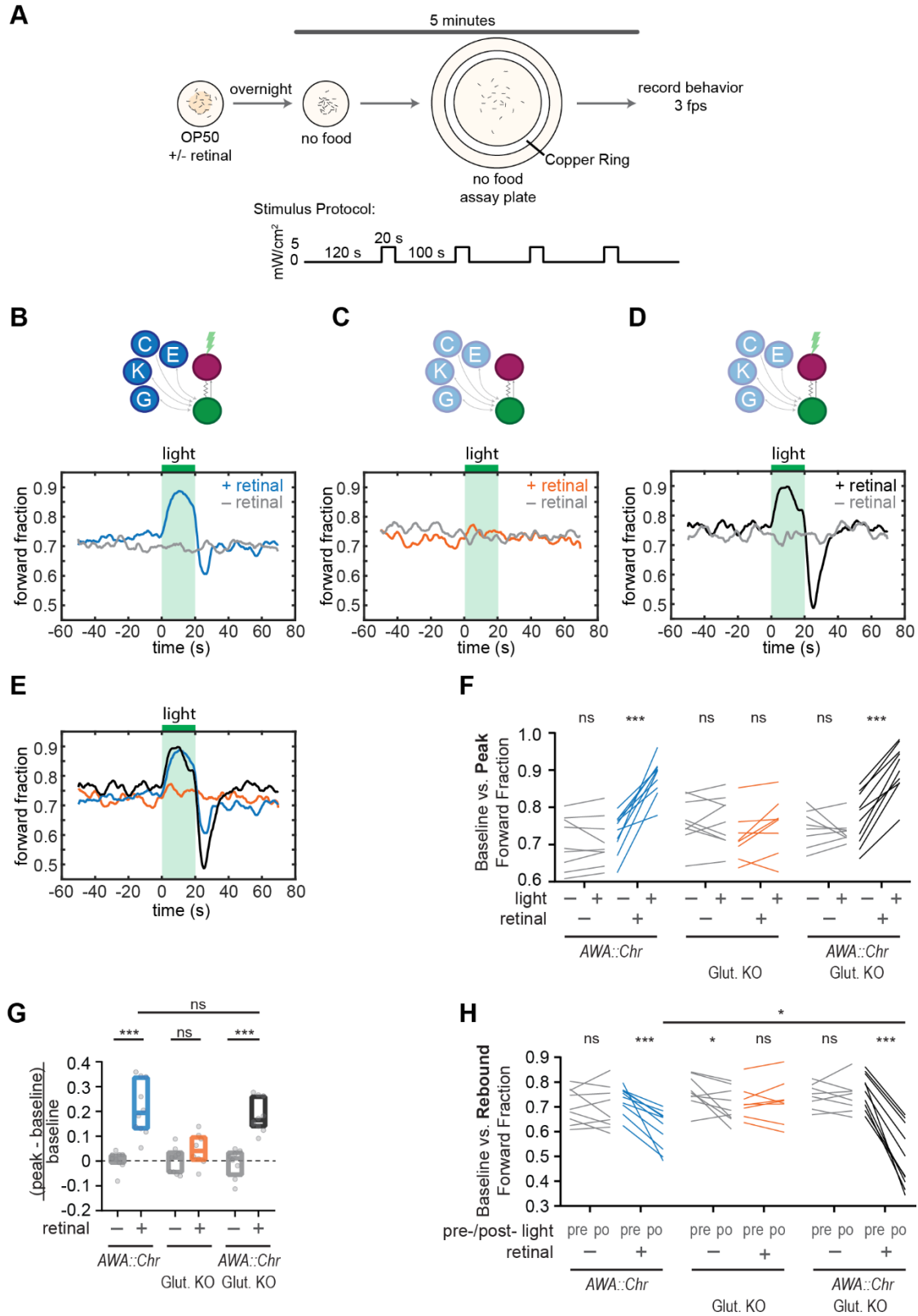
Figure 3-9. Optogenetically stimulating AWA robustly induces forward movement.

Optogenetically inhibiting ASK, AWC and ASE enhances forward locomotion induced by AWA optogenetic stimulation

To confirm and extend these results, I modified the optogenetic protocol:

1. I reduced the light intensity and stimulation pulse duration in an attempt to avoid a ceiling effect (Figure 3-10A).

2. Instead of using sensory glutamate knockout animals, I expressed the *Gt*ACR2 light-activated chloride channel in ASK, AWC and ASE, allowing me to inhibit the neurons upon light exposure. These animals should have normal neuronal function until that point, unlike the sensory glutamate knockout animals that lack glutamate knockout throughout the animals' lifetimes. *Gt*ACR2 effects are also not confined to glutamate.

Optogenetic stimulation of AWA at a low light intensity for 10 seconds resulted in a robust increase in forward movement in a retinal-dependent manner (Figure 3-10B, F). Next, I asked whether inhibiting ASK, AWC and ASE could promote forward locomotion by delivering light pulses to animals expressing *Gt*ACR2 in ASK, AWC and ASE. Indeed, acute inhibition of these sensory neurons resulted in an increase in forward locomotion in a retinal-dependent fashion, although not to the extent that AWA stimulation did (Figure 3-10C, E, F). Finally, simultaneously stimulating AWA and inhibiting ASK, AWC and ASE resulted in a combined effect that was greater than either single stimulation procedure alone, though not significantly so (Figure 3-10G). These results indicate that behavior, like AIA activation, is regulated by the coincident activation and inactivation of appropriate sensory neurons. Interestingly, this experiment did not induce a rebound suppression of forward movement in any genotype, likely because I used lower light intensities for shorter durations.

Figure 3-10. **Optogenetically inhibiting ASK, AWC and ASE enhances forward locomotion induced by AWA optogenetic stimulation.**

(A) Light stimulation protocol for experiment. Note that light pulses are shorter and lower intensity than Figure 3-9.

(B - D) Fraction of animals moving forward during a 10-s pulse of light, showing 50 s before and 60 s after pulse. All animals are WT background.

(B) Animals expressing *AWA::Chrimson*, with or without retinal pre-treatment.

(C) Animals expressing *ASK+AWC+ASE::GtACR2*, with or without retinal pre-treatment.

(D) Animals expressing both *AWA::Chrimson* and *ASK+AWC+ASE::GtACR2*, overlaid with *AWA::Chrimson*-only or *ASK+AWC+ASE::GtACR2*-only with-retinal traces from (B) and (C).

(E) Baseline and peak fractions of animals moving forward from (B-D).

(F and G) Difference between baseline and peak fractions of animals moving forward, normalized to baseline, from (B-D). Data for *AWA::Chrimson* and *ASK+AWC+ASK::GtACR2* in (G) are the same as the corresponding with-retinal data in (F). Boxes show median and interquartile range.

For (E), asterisks represent results of paired t-tests between mean baseline and peak fractions for a given condition. ns: not significant; *: $p<0.05$; ***$p<0.001$.

For (F), asterisks represent results of unpaired t-tests between with-retinal and without-retinal for a given condition. ns: not significant; **: $p<0.01$.

For (G), asterisks represent results of an ordinary one-way ANOVA with a Dunnett's multiple comparisons test, comparing *AWA::Chrimson* with *ASK+AWC+ASE::GtACR2* to either condition alone, all with retinal. ns: not significant; ***: $p<0.001$.
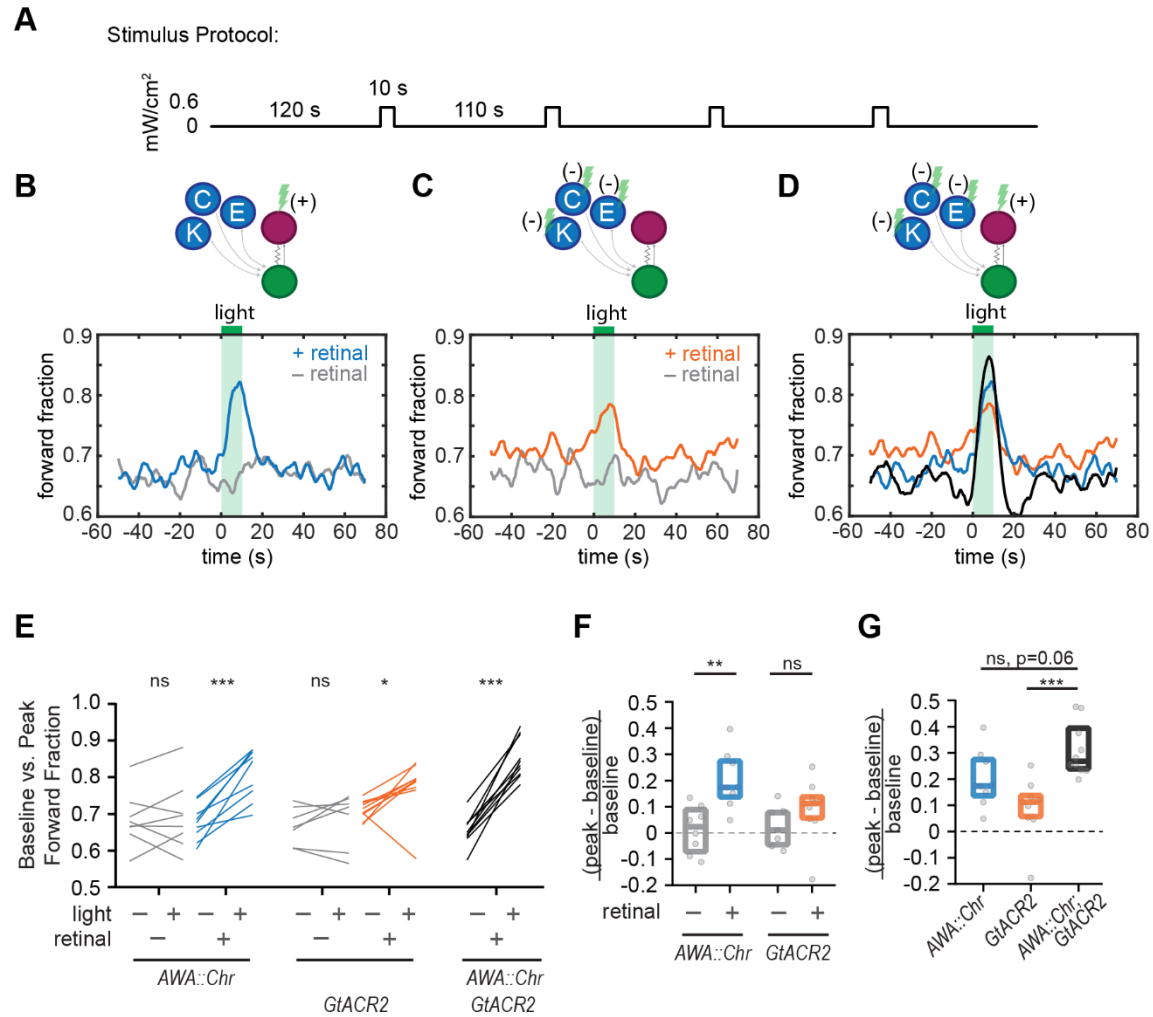
Figure 3-10. **Optogenetically inhibiting ASK, AWC and ASE enhances forward locomotion induced by AWA optogenetic stimulation.**

Preliminary results on AIA's role in induced forward locomotion

As part of the same experiment shown in Figure 3-10, I explored AIA's contribution to forward movement. Since my calcium imaging data point to AIA as a site of sensory integration, I predict that additive or synergistic effects of simultaneously activating AWA and inhibiting ASK, AWC and ASE could be mediated by AIA.

To assess the role of AIA in these optogenetically induced behaviors, I expressed Tetanus toxin light chain A (TeTx, cell-selectively prevents synaptic vesicle release) in AIA in the three strains used above (*AWA::Chrimson*-only, *ASK+AWC+ASE::GtACR2*-only, and the combination). In all three lines, expressing TeTx in AIA shifted the baseline so that more animals were moving forward, regardless of stimulus (Figure 3-11A-C, F). This baseline shift was unexpected based on prior work. In addition, all optogenetically-induced behaviors were reduced in magnitude (Figure 3-10A-F). While this result is promising, more experiments are needed to understand the baseline shift and interpret these changes.
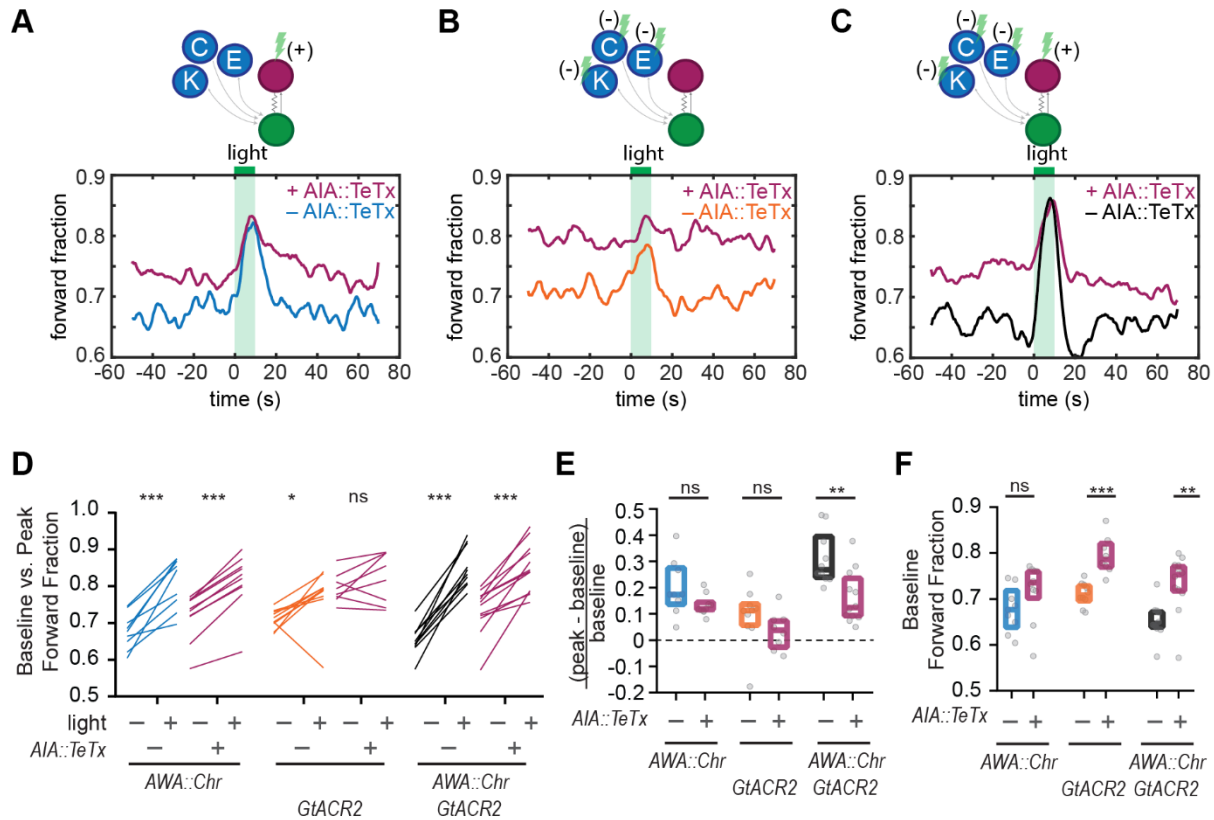
Figure 3-11. Preliminary results on AIA's role in induced forward locomotion.

(A - C) Fraction of animals moving forward during a 10-s pulse of light. Data from animals without *AIA::TeTx* are the same as Figure 3-10.

(A) Animals expressing *AWA::Chrimson*, with or without *AIA::TeTx*.

(B) Animals expressing *ASK+AWC+ASE::GtACR2*, with or without *AIA::TeTx*.

**(C)** Animals expressing both *AWA::Chrimson* and *ASK+AWC+ASE::GtACR2*, with or without *AIA::TeTx*.

(D) Baseline and peak fractions of animals moving forward from (A-C).

(E) Difference between baseline and peak fractions of animals moving forward, normalized to baseline, from (A-C). Boxes show median and interquartile range.

(F) Baseline fraction of animals moving forward from (A-C). Boxes show median and interquartile range.

For (D), asterisks represent results of paired t-tests between mean baseline and peak fractions for a given condition. ns: not significant; *: $p<0.05$; ***: $p<0.001$.

For (E) and (F), asterisks represent results of unpaired t-tests comparing with and without *AIA::TeTx*. ns: not significant; **: $p<0.01$; ***: $p<0.001$.

Discussion

AIA acts as a coincidence detector

In this chapter, I showed that a small set of glutamatergic sensory neurons (ASK, AWC, ASE and ASG) is responsible for inhibiting AIA and preventing reliable AWA-to-AIA communication. This finding suggests that AIA acts as a coincidence detector, responding only when AWA is activated and the glutamatergic sensory neurons relax their inhibition.

Blocking glutamate release from any individual sensory neuron was not sufficient to permit reliable AWA-to-AIA communication, and failed to account for the full effect of blocking glutamate release from four neurons together. This result indicates that several of these neurons must relax their inhibition together to permit reliable AWA-to-AIA communication. Several combinations of neurons appear to have this ability. Rescuing the *unc-18* synaptic transmission mutant in AWC and ASE prevented reliable AWA-to-AIA communication, but preventing AWC and ASE glutamate release using the cell-selective *eat-4* knockout did not enable reliable AWA-to-AIA communication. Preventing ASK glutamate release with the cell-selective *eat-4* knockout, however, did have a significant effect.

When I aligned AIA calcium responses to the initiation of the response itself rather than to the stimulus, wildtype animals and all tested mutants had remarkably stereotyped on-dynamics despite their different response frequencies and latencies. This feature is consistent with AIA acting as a coincidence detector with a characteristic firing property.

The role of AIA in behavior

Using optogenetic methods, I found that inhibiting ASK, AWC and ASE promoted forward locomotion and enhanced AWA stimulation-induced forward locomotion. The next step of this analysis is to assess the role of AIA.

I began this experiment by testing *AIA::TeTx* animals, but determined that the transgene had a shift in baseline behavior opposite to that expected for AIA. One possible explanation for this effect is expression of the transgene in cell types other than AIA. Tetanus toxin is highly potent even at low levels of expression. The promoter used to generate these animals is also expressed in the NSM neurons and may be expressed in other neurons at a low level. Further experiments varying the silencing method or promoter may move this work forward.

In the future, it will be interesting to track chemotaxis to diacetyl in animals lacking the function of different sensory neurons and AIA:

- wildtype +/- *AIA::TeTx* (or another AIA silencing tool)

- *odr-10* (lacking AWA diacetyl receptors) +/- *AIA::TeTx*;

- *tax-4* (lacking sensory transduction in several neurons including AWC, ASE, ASG, ASK, but excluding AWA) +/- *AIA::TeTx*.

As a preliminary hypothesis, I would expect to see a difference in the number of reorientations animals make as a function of distance to the odor source based on AIA activity. I expect that *odr-10* animals would have trouble finding the odor source, as is already known (Sengupta et al., 1996). I would expect that *tax-4* animals would find the odor source within 60 minutes, as previously shown (Coburn and Bargmann, 1996).

However, it is possible that *tax-4* mutants would have an altered reorientation profile that may resemble the wildtype animals expressing *AIA::TeTx*.

Glutamatergic inhibition of AIA

Previous studies have shown that glutamatergic synapses inhibit AIA. Shinkai et al. (2011) demonstrated that animals use the GLC-3 glutamate-gated chloride channel in AIA to integrate information about the conflicting cues of diacetyl (attractive) and copper acetate (aversive). Copper acetate is sensed by ASH (Hilliard et al., 2005), a glutamatergic sensory neuron, so ASH likely inhibits AIA via the GLC-3 channel. Similarly, Chalasani et al. (2010) showed that increases in AIA calcium in response to the attractive odor isoamyl alcohol are reduced in *glc-3* mutants. Isoamyl alcohol inhibits the AWC sensory neurons, and may therefore activate AIA by relieving the glutamate-dependent inhibition from AWC. Other glutamate-gated chloride channels may also be involved, as an RNA sequencing data set predicts that two glutamate-gated chloride channel subunits, encoded by *glc-4* and *avr-15*, are also expressed in AIA (Cao et al., 2017).

The same RNA sequencing data set predicts that AIA expresses the excitatory glutamate-gated cation channels *glr-2* and *glr-4* (Cao et al., 2017), and *glr-2* has been previously identified in AIA using reporter genes (Brockie et al., 2001). AIA expression of GLR-2 has been implicated in ASH-to-AIA communicating as part of arousing animals from state of quiescence (Choi et al., 2015). Thus, glutamate might either excite (via GLR-2) or inhibit (via GLC-3, GLC-4, and AVR-15) AIA depending on context or

signal strength. Direct electrophysiological measurements indicate that glutamate strongly inhibits AIA (Lopez-Cruz et al., 2019).

The delay between AWA and AIA activation to diacetyl odor is ~1 second, which is long enough for inhibition through metabotropic glutamate receptors. AIA expresses the metabotropic glutamate receptor, *mgl-1* (Greer et al., 2008). Chemosensory neurons, including the ones identified in this chapter, inhibit AIA synaptic output via the AIA MGL-1 glutamate receptors in response to food removal (Lopez-Cruz et al., 2019). The role of MGL-1 in off-food foraging behavior is likely on the timescale of minutes, but MGL-1 may also inhibit AIA on the timescale of seconds, such as to attractive odors.

Spontaneous transients versus evoked responses

In this work, I found that ASK is one source of inhibitory glutamate release onto AIA. Similarly, Lopez-Cruz et al. (2019) found that ASK glutamate release leads to AIA activation, showing that spontaneous ASK inhibition transients correlated with AIA activation transients, and that the correlation decreased in *eat-4* glutamate mutants. Lopez-Cruz et al. (2019) also found that the magnitude of AIA calcium transients decreased in *eat-4* mutants. By contrast, I did not observe a decrease in AIA response magnitude in *eat-4* mutants to any of the stimuli tested (AWA optogenetic stimulation, 11.5 nM or 1.15 μM diacetyl). Spontaneous AIA transients may have different properties than evoked responses. A qualitative comparison of spontaneous AIA transients shown in Lopez-Cruz et al. (2019), the evoked responses shown in Larsch et al. (2015), and my own experiments suggest that spontaneous AIA transients lack the stereotyped magnitude of evoked responses. This could be interesting to study in future.

Spontaneous AIA transients were frequent in Lopez-Cruz et al. (2019) but rare in Larsch et al. (2015) and my own experiments. I suspect that the difference in AIA spontaneous activity is due to experiment details, as Larsch et al. (2015) and I used similar experimental conditions (see Experimental Procedures). My focus has been on stimulus-evoked AIA activity, so my results do not depend on spontaneous AIA activity.

AIA calcium decay suggests an inhibitory synaptic input after activation

The AIA calcium response is stereotyped in its decay as well as its onset. Decay kinetics are harder to interpret than rise times because of intrinsic properties of the GCaMP indicator, but differences can nonetheless be noted. I found *unc-18* mutants defective in synaptic vesicle release had sustained and extended calcium responses in AIA after optogenetic stimulation of AWA.

unc-31, a mutant defective in dense core vesicle exocytosis, had dramatically slowed AIA response decays after AWA Chrimson stimulation. This might be related to known peptidergic feedback from AIA to upstream sensory neurons. There are at least three examples of AIA releasing insulin-like peptides to alter upstream sensory responses and learning behavior (Cho et al., 2016; Chalasani et al., 2010; Tomioka et al., 2006). In all cases, the assays involve pre-exposing animals to either odor or salt before testing them for chemotaxis to the same stimulus. Animals that were pre-exposed to the stimulus find the stimulus either aversive or less attractive than animals that were not pre-exposed. The first example is aversive olfactory learning to the normally attractive odor butanone. Cho et al. (2016) found that AIA uses insulin signaling to regulate AWC sensitivity to odor and the localization of EGL-4. EGL-4 is a

protein kinase that must move from the cytoplasm to the nucleus for effective aversive olfactory learning. The second example is olfactory learning to isoamyl alcohol. Chalasani et al. (2010) found that AIA releases the insulin-like peptide INS-1 that diminishes AWC sensory responses to isoamyl alcohol and reduces chemotaxis behavior toward isoamyl alcohol. The third example is in salt learning behavior. Tomioka et al. (2006) found that AIA expresses INS-1 and that both AIA and INS-1 regulate the animal's attraction to salt, likely acting through one of the ASE sensory neurons that senses salt.

The above experiments all involve AIA releasing insulin to regulate sensory responses and behaviors that take several minutes to change. In the case of salt preference (Tomioka et al., 2016), the effect was seen after 20 minutes of pre-exposure, much longer than the few seconds required for AIA responses to begin decaying in my experiments. None of these studies examined AIA decay dynamics.

Although *unc-31* affected the decay of the AIA response, the reliability, on-dynamics, and magnitude of AIA responses were similar in *unc-31* mutants and wildtype animals. This separation suggests that AIA response on-dynamics are independently regulated from the decay dynamics, or perhaps neurons that regulate the timing of AWA-to-AIA transmission also release neuropeptides, but on a slower timescale than they relax inhibition.

Finally, it is worth noting that the decay of AIA responses to *E. coli* OP50-conditioned medium is slower than to other tested stimuli (Figure Appendix B-3). OP50-conditioned medium stimulates many sensory neurons (Zaslaver et al., 2015), and may provide a glimpse at other sensory inputs onto AIA and their regulation.

CHAPTER 4: MULTIPLE SENSORY NEURONS DETECT A SINGLE ODORANT

Background

In the previous chapter, I showed that ASK, AWC and ASE modulate AIA responses to AWA activation. Here, I examine the role of other sensory neurons in diacetyl sensation.

In previous studies, Larsch et al. (2015) showed (and I have replicated) that although AIA responds to 1.15 μM diacetyl in *odr-7* AWA cell fate mutants, it does not respond in *odr-7 ceh-36* double mutants, which lack AWA, AWC and ASE. This result points to AWC and/or ASE as detectors of 1.15 μM diacetyl. Another study measured the calcium responses of several sensory neurons to 1.15 μM diacetyl pulses, and found that ASK, AWB and AWC neurons are activated upon removal of 1.15 μM diacetyl (Hale et al., 2016).

Most studies looking at neuronal responses to diacetyl use higher concentrations than I use in this thesis. At 1.15 mM, Zaslaver et al. (2015) detected only AWA activation and AWC inhibition to diacetyl addition, and Hale et al. (2016) detected only AWA activation to diacetyl addition. For the lower concentrations of diacetyl (11.5 nM), only AWA and AIA responses have been examined (Larsch et al., 2015).

Based on the work presented in Chapters 2 and 3, in combination with the literature, I hypothesized that:

1. At least one of the AWC, ASE, and ASK glutamatergic sensory neurons would respond to addition of 1.15 μM diacetyl.

2. The glutamatergic neuron should be inhibited by 1.15 µM diacetyl, and therefore its inhibition can disinhibit AIA.

3. Fewer non-AWA sensory neurons will respond to 11.5 nM than to 1.15 µM diacetyl.

In this chapter, I show that multiple sensory neurons respond to 1.15 µM diacetyl, fewer respond to 11.5 nM diacetyl, and none other than AWA respond to AWA optogenetic stimulation. The sensory neuron responses to diacetyl are direct for two neurons and indirect for a third.

Results

ASK, AWC and ASE respond to 1.15 µM diacetyl, and ASK responds to 11.5 nM diacetyl

Based on the results in Chapter 3, ASK, AWC and ASE were the primary candidates for non-AWA sensory neurons that respond to diacetyl. Therefore, I measured their calcium responses to 1.15 µM and 11.5 nM diacetyl. All three neurons responded to the higher concentration of diacetyl (Figure 4-1A, D, G), with ASK responses being the largest and most reliable. ASK and AWC were inhibited by odor addition, which is consistent with the hypothesis that they reduce their release of inhibitory glutamate to disinhibit AIA. By contrast, ASE was activated by 1.15 µM diacetyl.
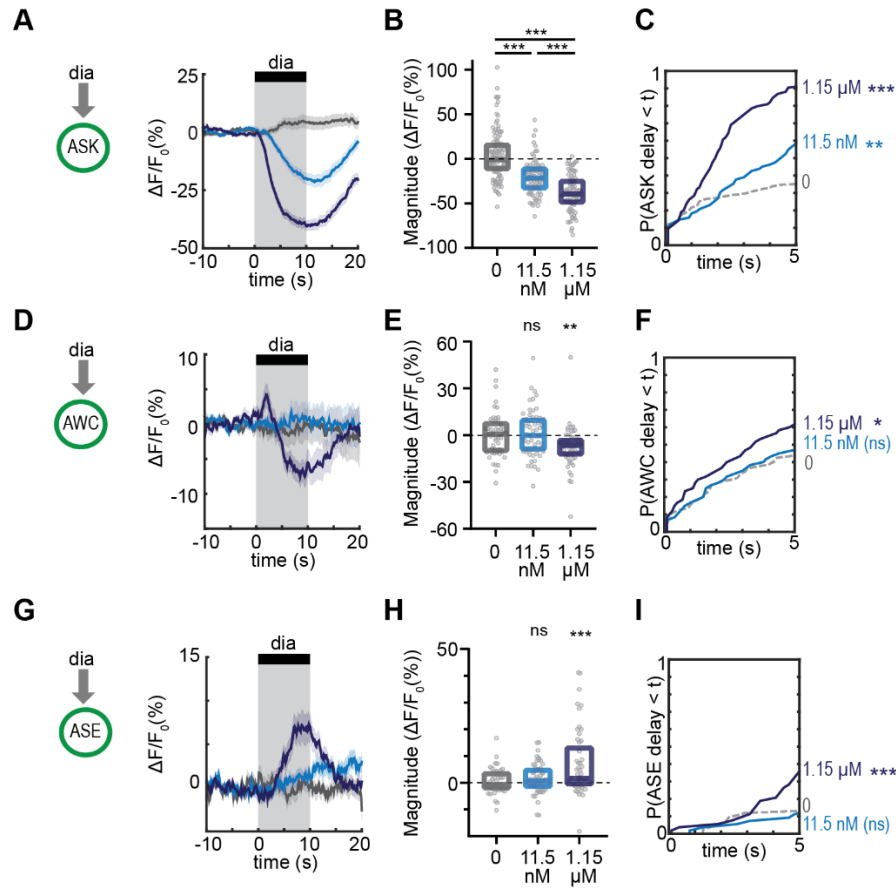
Figure 4-1. ASK, AWC and ASE respond to 1.15 μM diacetyl, and ASK responds to 11.5 nM diacetyl.

(A, D, and G) Mean ASK (A), AWC (D), and ASE (G) responses to 10-s pulses of 0, 11.5 nM, and 1.15 μM diacetyl. Shading indicates ± SEM.

(B, E, and H) Magnitudes of responses shown in (A), (D), and (G), regardless of whether stimulus pulse produced a detectable response. Boxes show median and interquartile range.

(C, F, and I) Cumulative response probability profiles of responses shown in (A), (D) and (G). Only the first 5 s are shown.

For (B), (E), and (H), asterisks indicate statistical significance of one-way ANOVA with Dunnett's multiple comparisons test. ns: not significant; **: $p < 0.01$; ***: $p < 0.001$. See Appendix D for sample sizes and test details.

For (C), (F), and (I), asterisks refer to Kolmogorov-Smirnov test significance over full 10-s stimulus pulse. ns: not significant; *: $p < 0.05$; **: $p < 0.01$; ***: $p < 0.001$. See Appendix C for sample sizes and test details.

At the lower concentration of 11.5 nM diacetyl, ASK was still inhibited, but to a lower extent than observed with 1.15 µM diacetyl (Figure 4-1A-C). ASK responses to 11.5 nM diacetyl were smaller in magnitude and less reliable than to 1.15 µM diacetyl. Neither AWC nor ASE detectably responded to 11.5 nM diacetyl (Figure 4-1D-I), consistent with a previous study showing that AWC supports chemotaxis to high but not low levels of diacetyl (Chou et al., 2001).

ASK and AWC sense diacetyl directly, whereas ASE responds indirectly

ASE calcium responses to diacetyl were delayed relative to other sensory neurons, a feature that often represents indirect signaling via synaptic connections (Thiele et al., 2009). Indeed, I found that ASE failed to respond to 1.15 µM diacetyl in *unc-18* synaptic transmission mutants (Figure 4-2A-B). Responses to NaCl, which ASE senses directly (Suzuki et al., 2008), were normal in these mutants (Figure 4-2C). To test whether AWA was responsible for ASE activation, I recorded ASE responses in *odr-10* AWA diacetyl receptor mutants; ASE responses to diacetyl were unchanged (Figure 4-2A-B). I conclude that ASE does not directly sense 1.15 µM diacetyl, but rather receives chemical signals from a non-AWA sensory neuron that does.

ASK and AWC both responded normally to 1.15 µM diacetyl in both *unc-18* and *odr-10* mutants (Figure 4-2D-G). These results are consistent with direct diacetyl detection by ASK and AWC at this concentration.

Figure 4-2. ASK and AWC sense diacetyl directly, whereas ASE responds indirectly.

(A, D, and F) Mean ASE (A), ASK (D), and AWC (F) responses to 10-s pulses of 1.15 µM diacetyl in WT versus *unc-18(e234)* synaptic transmission versus *odr-10(ky32)* AWA diacetyl receptor mutants. Note that ASE responses in *unc-18* are greatly diminished. Shading indicates ± SEM.

(B, E, G) Magnitudes of responses shown in (A), (D), and (F), regardless of whether stimulus pulses resulted in detectable activation or inhibition. Boxes show median and interquartile range.

(C) Magnitudes of ASE responses to the removal of 100 mM NaCl after 10-s exposure in WT versus *unc-18* versus *odr-10* animals. Boxes show median and interquartile range.

Asterisks either indicate statistical significance of an unpaired t-test comparing 1.15 µM to buffer responses, or a one-way ANOVA with Dunnett's multiple comparisons test versus WT. ns: not significant; **: $p<0.01$; ***: $p<0.001$. See Appendix D for sample sizes and test details.
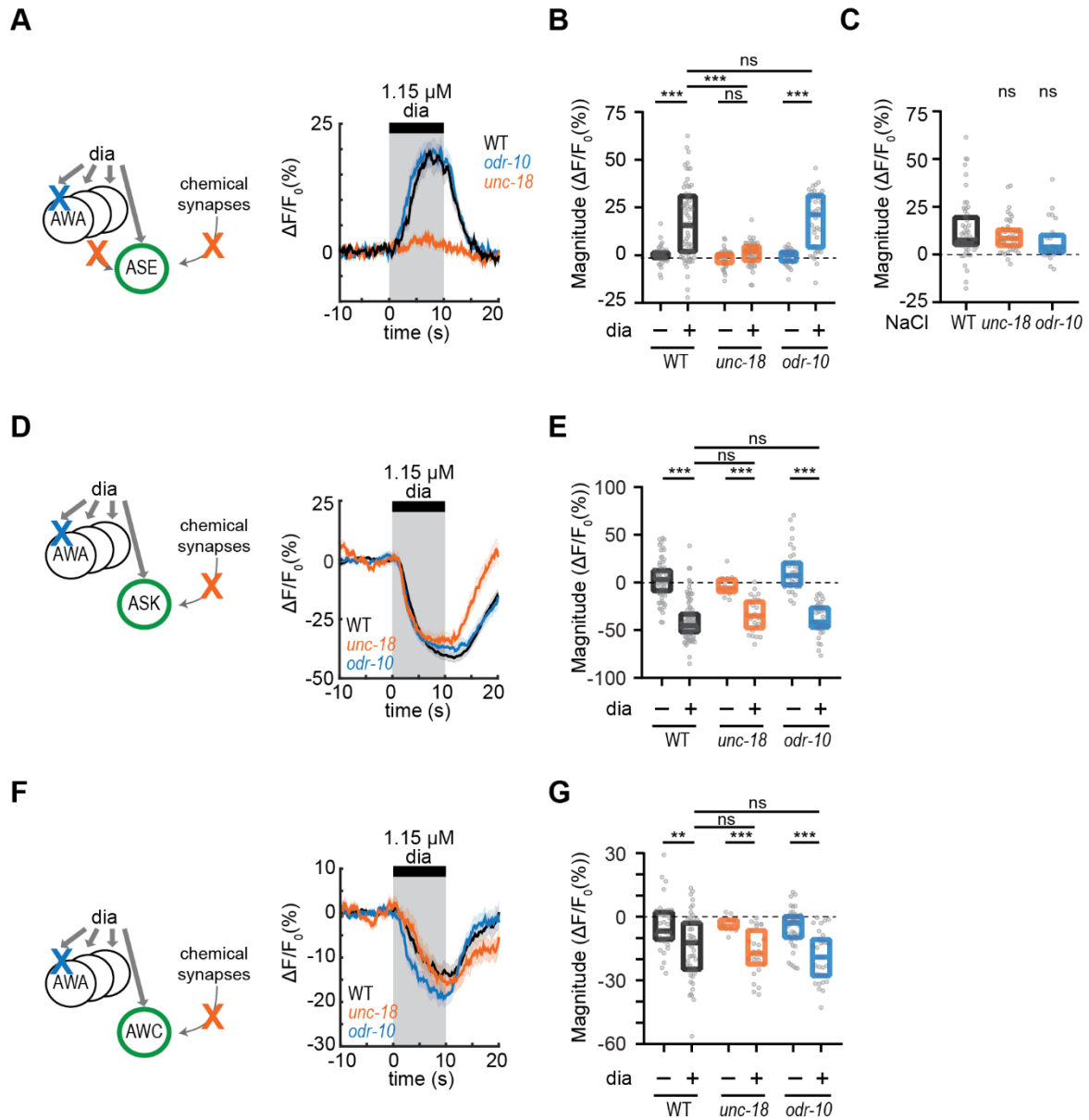
Figure 4-2. ASK and AWC sense diacetyl directly, whereas ASE responds indirectly.

Sensory responses to diacetyl show neuronal specificity

Finally, I examined diacetyl responses in ASH, another glutamatergic sensory neuron pair that forms chemical synapses onto AIA. ASH is a major nociceptive neuron in *C. elegans* and is known to be polymodal. ASH is activated by nose touch, heavy metals, quinine, osmotic shock (Hilliard et al., 2005) and to aversive concentrations of the odorant isoamyl alcohol (Yoshida et al., 2012). Relevant to us, it has been shown to be activated by aversive concentrations of diacetyl (11.5 mM) (Taniguchi et al., 2014), and inhibited upon to the removal of 1.15 µM diacetyl in L3 larvae but not in adults (Hale et al., 2016). ASH did not respond to 1.15 µM diacetyl, but did respond to a NaCl control stimulus (Figure 4-3).
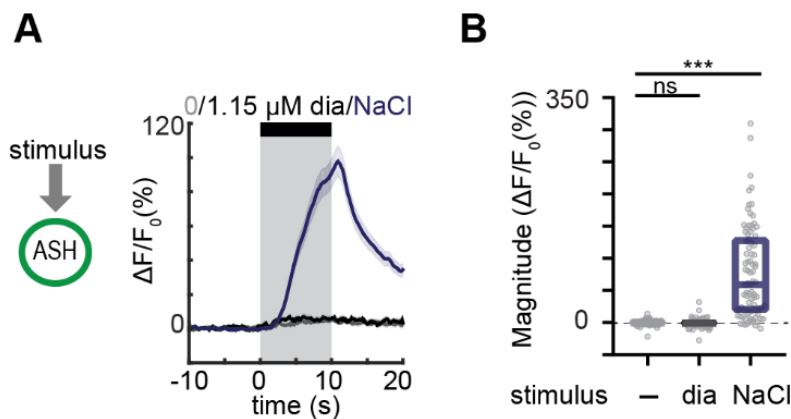
Figure 4-3. ASH does not respond to 1.15 µM diacetyl.

(A) Mean ASH responses to 10-s pulses of 0 or 1.15 µM diacetyl or 100 mM NaCl in WT animals. Shading indicates ± SEM.

(B) Magnitudes of responses shown in (A), regardless of whether stimulus pulses resulted in detectable activation. Boxes show median and interquartile range. Asterisks indicate statistical significance of a one-way ANOVA with Dunnett's multiple comparisons test versus buffer. ns: not significant; ***: $p < 0.001$. See Appendix D for sample sizes and test details.

ASK, AWC and ASE do not respond to AWA optogenetic stimulation

Sensory neurons in *C. elegans* are highly interconnected based on the wiring diagram (White et al., 1986), so it is plausible that AWA could activate other sensory neurons. Despite this interconnectedness, none of the other sensory neurons (ASK, AWC and ASE) responded to AWA optogenetic stimulation (Figure 4-4A-E).
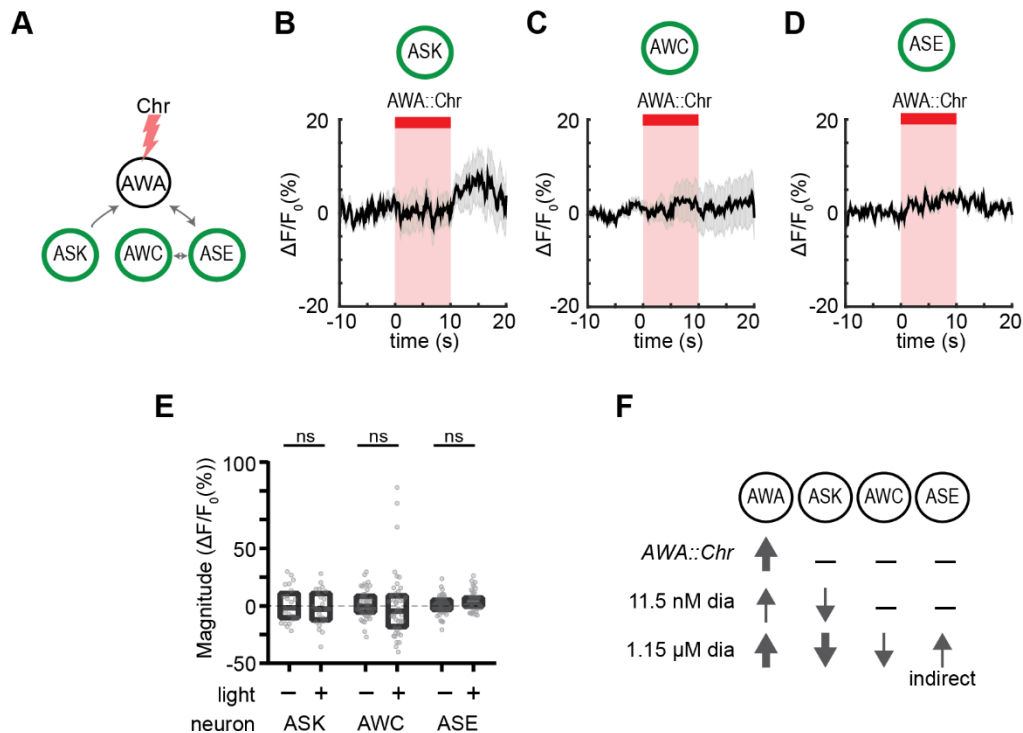
Figure 4-4. ASK, AWC and ASE do not respond to AWA optogenetic stimulation.

(A) Simplified schematic of connections between sensory neurons, defined by the *C. elegans* wiring diagram (White et al., 1986).

(B-D) Mean ASK (B), AWC (C), and ASE (D) responses to 10-s pulses of AWA optogenetic stimulation. Shading indicates ±SEM.

(E) Magnitudes of responses shown in (B-D). Magnitude changes during pre-light period were used as controls. Boxes show median and interquartile range.

(F) Summary of sensory neuron responses to various stimuli. Upward arrows indicate activation; downward arrows indicate inhibition.

ns refers to lack of significance in paired t-tests comparing pre-light and within-light periods in same neurons. See Appendix D for sample sizes and test details.

Discussion

The differences in AWA, ASK, AWC and ASE responses to AWA optogenetic

stimulation, 11.5 nM diacetyl, and 1.15 µM diacetyl can be summarized as follows (see

Figure 4-4F): AWA is activated by all three stimulation protocols, but less reliably to 11.5

nM diacetyl. ASK is inhibited by diacetyl addition at both concentrations, with lower

response magnitude and more variable latencies to 11.5 nM diacetyl. AWC is inhibited

by 1.15 µM but not by 11.5 nM diacetyl. ASE is activated by 1.15 µM diacetyl through

an indirect synaptic connection, and it does not respond to 11.5 nM diacetyl.

Optogenetic stimulation of AWA does not affect AWC, ASK, or ASE.

These results show that multiple sensory neurons respond to 1.15 µM diacetyl

(AWA, ASK, AWC and ASE). ASK and AWC are inhibited by diacetyl; they release

glutamate at rest and diacetyl inhibits this release. Only AWA and ASK respond to the

lower concentration of 11.5 nM diacetyl.

These results are consistent with the results shown in previous chapters as well

as prior studies. Hale et al. (2016) did not detect ASK or AWC inhibition by diacetyl, but

they did detect ASK and AWC activation to diacetyl removal, consistent with my

findings. Their GCaMP lines appear to photobleach during their long recordings (they

delivered 120-second odor pulses), so it is possible that the photobleaching interfered

with their detection of inhibition. Zaslavar et al. (2015) detected only AWA activation and

AWC inhibition by 1.15 mM diacetyl, 1000-fold more than used here. They counted only

ΔF/F values above 20% as responses, so it is possible that they missed small ASE

responses, or that ASE and ASK do not respond to diacetyl at such high concentrations.

For ASK, this may indeed be the case; Hale et al. (2016) observed ASK activation upon

removal of 1.15 µM diacetyl but not 1.15 mM diacetyl. Similarly, AWC is inhibited by 9

µM or 900 µM isoamyl alcohol but not by 90 mM isoamyl alcohol (Yoshida et al., 2012).

The ASE neuron pair consists of an asymmetrical bilateral pair, ASEL and ASER.

The two ASE neurons respond differently to salt increases and decreases (Suzuki et al.,

2008). Based on experiments not shown here, I have consistently observed activation of

both ASE neurons by diacetyl pulses.

ASE responds to 1.15 µM diacetyl but does not sense 1.15 µM diacetyl directly.

There are at least two additional examples of *C. elegans* sensory neurons responding to

a stimulus without directly sensing it (Thiele et al., 2009; Leinwand et al., 2015). The

sensory neuron ADF is activated by increases in salt concentration, but requires

synaptic connections from an unknown neuron for this response (Thiele et al., 2009).

More relevant to my data, ASE neurons are inhibited by the attractive odor

benzaldehyde, and activated upon benzaldehyde removal (Leinwand et al., 2015).

Activation of ASE neurons upon benzaldehyde removal depends on insulin signaling,

but not chemical synapses, from AWC neurons, which sense benzaldehyde directly. It

would be interesting to explore the role of the indirect activation of ASE by diacetyl in

shaping AIA responses.

Additional Notes

In contrast with Hale et al. (2016), who observed activation of yet another sensory

neuron, AWB, upon 1.15 µM diacetyl removal, I observed that AWB was activated by

1.15 µM diacetyl addition rather than removal in the majority of experiments (not

shown). AWB showed day-to-day inconsistencies such that either all animals responded

or none did for the entire day. I never saw activation of AWB upon diacetyl removal, and stopped pursuing AWB for three reasons:

1. My primary interest is AWA-to-AIA signaling. AWB is cholinergic and not glutamatergic, and the acetylcholine biosynthesis mutant *cha-1* did not appear to enhance AIA responses to AWA optogenetic stimulation (Figure 3-5C).

2. When I tested AIA responses to AWA optogenetic stimulation in *odr-1* mutant animals, which have defective AWB and AWC signal processing (L'Etoile and Bargmann, 2000), these mutants had wildtype-like responses (data not shown).

3. When I tested AIA responses to AWA optogenetic stimulation in an *AWB::Caspase* line, which kills AWB, they were unaffected. I confirmed that these animals had defective chemotaxis to 2-nonanone, a known volatile repellant sensed by AWB.

I conclude that AWB does not gate AIA responses to AWA optogenetic stimulation, but cannot rule out a role for AWB in AIA diacetyl responses.

CHAPTER 5: PERSPECTIVES

Summary

In this thesis, I show that activating the sensory neuron AWA is not sufficient to elicit a reliable response in the AIA interneuron, and that these neurons are connected by a functional, asymmetrical electrical synapse. AIA calcium responses to the odor diacetyl became more reliable as concentration increased, with a consistent ~1-second lag compared to AWA responses. AIA responses to AWA optogenetic stimulation, as well as to a low concentration of diacetyl, were more reliable in synaptic transmission mutant animals. This led to the hypothesis that chemical synapses inhibit the transmission of information from AWA to AIA. I showed that indeed glutamate release from a small set of sensory neurons that synapse onto AIA inhibits AIA activation by AWA. Glutamatergic sensory neurons thus gate AWA-AIA communication. Finally, I showed that the same glutamatergic sensory neurons respond, both directly and indirectly, to the addition of diacetyl. Their responses were concentration-dependent, potentially explaining the difference between AIA response reliability to varying concentrations of diacetyl.

These results point to AIA acting as an integrator of sensory information, with AIA activity serving as a coincidence detector and a readout of global sensory state. In this chapter, I will discuss the implications of these findings.

How *C. elegans* encode "food"

Odor quality is represented by combinations of sensory neurons

Many bacteria release bouquets of odorants. Odorants are directly sensed by one or multiple olfactory receptors with different affinities, which are expressed in one or multiple sensory neurons. In *C. elegans*, different sensory neurons respond to odors – even the same odor – with different magnitudes, dynamics, and signs. These response properties are dictated by properties intrinsic to the sensory neuron and olfactory receptors. The sensory neurons signal the presence of odor to AIA, which does not respond reliably to input from a single sensory neuron. With each additional coherent input from a sensory neuron, AIA responses and subsequent behavior become more reliable, potentially with increased computational speed. AIA activation is stereotyped and signals that "yes, this sensory signal is real and attractive" based on the global upstream sensory state. The sensory neurons act through AIA and other interneurons to bias the animal into a forward-moving state. Based on the wiring diagram, various interneurons may integrate partly overlapping elements of the animal's sensory environment and internal state.

Animals use volatile odorants to navigate toward a source of bacteria, but they can use both water-soluble and volatile odorants to inform decisions at a closer range (Grewal and Wright, 1992). I will focus this discussion on how an animal may interpret the volatile cues of a food source.

93

Detection versus identification

C. elegans face the classic evolutionary struggle of breadth versus specificity, or detection versus identification. Mammal and insect nervous systems have thousands of olfactory neurons that each express one olfactory receptor gene (with exceptions), allowing them to use combinatorial coding at a cellular level to distinguish between odors (Malnic et al., 1999; Buck and Axel, 1991). The *C. elegans* nervous system is much more compact, with only 11 chemosensory neuron pairs. The animal's anatomy imposes constraints on the amount and type of information the animal can encode.

Using these few sensory neurons, *C. elegans* are able to sense and respond to an amazing diversity of stimuli. Each chemosensory neuron responds to multiple stimuli and expresses many putative chemoreceptor genes (Troemel et al., 1995; Taniguchi et al., 2014; Vidal et al., 2018; Cao et al., 2017). At a first-order level, olfaction uses a "labeled line" architecture, in which activating a particular sensory neuron results in a characteristic behavioral response. For example, when the AWA receptor for diacetyl is expressed in AWC or AWB instead of in AWA, diacetyl is either attractive (in AWC) or repulsive (in AWB), linking the sensory neurons to particular behavioral responses (Troemel et al., 1997; Wes and Bargmann, 2001). Combining these two principles, behavioral switching from attraction to low odor concentrations to repulsion from extremely high odor concentrations is associated with the expression of different receptors on different neurons. For example, diacetyl is sensed by AWA via the ODR-10 receptor at concentrations spanning many orders of magnitude. However, pure diacetyl is sensed by the SRI-14 receptor in ASH, which mediates aversive responses

(Taniguchi et al., 2014). Similarly, isoamyl alcohol is sensed by AWC and AWA at low concentrations and ASH neurons at high concentrations (Yoshida et al., 2012).

The above findings suggest that *C. elegans* prioritize the ability to detect many odors over the ability to discriminate them at a chemical level. Perhaps the animal just needs to detect a signal that represents "food", and the animal will navigate toward it. However, animals are still able to behaviorally discriminate between attractive odors and make decisions between different signals that represent "food". For example, animals can distinguish between the AWC-sensed odors butanone and benzaldehyde. Butanone is sensed by only one of the AWC neurons, AWC^{ON}, while benzaldehyde is sensed by both AWCs, so there is some degree of combinatorial coding for discrimination within a single asymmetric pair of neurons (Wes and Bargmann, 2001). Another example is 3-methyl-2-butenoate and isoamyl alcohol. Both odorants are sensed by AWC and likely AWA (Hsueh et al., 2017). Both compounds produce the same AWC^{ON} calcium responses, yet animals strongly prefer 3-methyl-2-butenoate to isoamyl alcohol. We do not know the mechanism underlying this preference or how other sensory neurons contribute to the preference.

With its small nervous system, *C. elegans* could have a slightly more elaborate combinatorial code if left-right neural pairs in addition to AWC encoded different odorant identities. However, I have observed symmetrical responses in the two AWA neurons, and they connect to each other via a gap junction, a feature associated with left-right symmetry. Itskovits et al. (2018) observed that activity in the two AWA neurons is not always matched as an animal responds to a diacetyl gradient. Perhaps AWA has left-right asymmetry at a dynamic, rather than a developmental, level.

In summary, *C. elegans* can both sense many food odors and distinguish between some odors, potentially employing a combinatorial strategy, with different combinations of neurons sensing different odors. It seems to combine a labeled line architecture with combinatorial coding.

Diacetyl is an ecologically relevant odor

Throughout this thesis, I have used diacetyl as my main odor stimulus. Diacetyl was one of the original attractive volatile odorants discovered to elicit robust chemotaxis responses in *C. elegans* (Bargmann et al., 1993). Even then, it was known that bacteria could produce diacetyl as a metabolic byproduct, and it was already being used in the food industry. *C. elegans* are found in rotting fruit with bacteria (Felix and Braendle, 2010), so it made sense that diacetyl may be a natural chemoattractant.

In 2015, several *Caenorhabditis* species closely related to *C. elegans* were isolated in Korea from rotting yuzu (citrus) fruit (Choi et al., 2016). These fruits contained the lactic acid bacteria *Lactobacillus* and *Lactococcus*. The wild bacterial isolates produced large quantities of diacetyl, and that diacetyl drives *C. elegans* attraction to the wild bacteria isolate through the ODR-10 diacetyl receptor. The robust attraction of *C. elegans* to lactic acid bacteria isolated and grown on yuzu fruit or in lab media, and its ODR-10 dependence, suggests that diacetyl can be an ecologically relevant odor.

Interestingly, lactic acid bacteria produce ~4x more diacetyl when grown in media containing both glucose and citrate compared to glucose-only, and 15x more than citrate-only (Choi et al., 2016). The diacetyl levels did not correlate with bacterial cell

count, indicating that diacetyl may not only signal the presence of bacteria, but the presence of a rich source of well-resourced bacteria.

The above study suggests that *C. elegans* uses diacetyl as a proxy for well-resourced bacteria. One single odorant drove the entire chemotaxis response to an attractive bacterial source. Moreover, the attraction to the bacterial source disappeared when animals were pre-exposed to diacetyl. We do not know how much diacetyl contributes to the headspace of lactic acid bacteria, but other bacterial species that *C. elegans* deems attractive emit multiple odorants (Worthy et al., 2018a). Assuming that lactic acid bacteria are no different, diacetyl as a single odor dominates the attraction toward lactic acid bacteria.

The above experiments do not answer the question of whether lactic acid bacteria are themselves a particularly nutritious food source, or whether they co-habitate rotting fruit with other nutritious foods sources, or perhaps signal a relative lack of pathogenic bacteria. Diacetyl could be used as a proxy for any of these.

Completely separate from Choi et al. (2016), lactic acid bacteria were isolated with *C. elegans* in apples, orange and cactus fruits from Spain and France (Samuel et al., 2016). *Lactobacilli* were present in all of their samples, particularly in the cactus fruit. Although other bacterial genera were even more predictive, *Lactobacilli* were predictive of whether *C. elegans* were proliferative or non-proliferative in a given apple sample. Interestingly, Samuel et al. (2016) found that *C. elegans* tend to proliferate more in apple samples with lower bacterial diversity, and these samples had highly similar microbial communities. Specific mixtures of bacteria may make a given habitat conducive to proliferation.

It is plausible that an odorant could represent something other than the bacteria that released it. Worthy et al. (2018a) used bacteria naturally isolated with *C. elegans* and tested animal preference to a non-pathogenic natural isolate versus the lab-grown *E. coli* control strain. They were given this choice in two ways, one based on volatile components alone (bacteria on lid of assay plate), the other based on the bacteria themselves (bacteria on assay plate). For most bacterial strains, the results were consistent between the two assays. In two strains, however, animals chose the isolated strain based on volatile cues alone but chose the lab *E. coli* strain if they were allowed to sample the bacteria. This may indicate that the isolated strains release repulsive soluble cues, but it could also mean that the attractive volatile cues are signaling the co-presence of a more nutritious food source – a signal that makes more sense for wild bacterial consortia than for lab monocultures.

Based on the above studies, I am drawn to the (untested) idea that diacetyl as a single odorant may guide animals toward relatively nutritious and non-pathogenic consortia of bacteria, regardless of how nutritious the lactic acid bacteria that releases diacetyl may be. Whether this is true or not, diacetyl appears to be an ecologically relevant odor, and it is the only volatile odor required to drive attraction to lactic acid bacteria (Choi et al., 2016).

Bacteria release odor bouquets; odor responses are non-additive

A single olfactory odorant is sufficient to drive chemotaxis toward its source. This is hardly new information; it has been the premise of chemotaxis experiments for decades. New results demonstrate that this is a property of the odor released by

98

nematode pathogens. For example, one compound released by the nematode-trapping fungus *Arthrobotrys oligospora* is sufficient to lure *C. elegans*, even in the presence of the competing attractant isoamyl alcohol (Hsueh et al., 2017).

Other pathogens release multiple odors to attract *C. elegans*. For example, the pathogenic bacteria *Serratia marcescens* is attractive to *C. elegans*; animals choose to navigate toward *S. marcescens* over lab *E. coli* strains. The *S. marcescens* headspace has five prominent volatile compounds: acetone, butanone (used in this thesis; Figure 3-8), dimethyl disulfide, dimethyl sulfide, and ethyl acetate (Worthy et al., 2018b). At the concentrations found in the headspace, acetone and butanone are attractive, and the others are neutral or mildly repulsive. However, if the odor bouquet lacks acetone but has butanone or vice versa, *C. elegans* will still chemotax to the source, indicating that acetone and butanone are partially redundant in luring *C. elegans* to *S. marcescens*. Both acetone and butanone odors are sensed by the AWC^{ON} neuron, and animals lacking AWC^{ON} but not AWC^{OFF} chose the lab *E. coli* strain over *S. marcescens*. Thus, the relative attractiveness of two bacterial species could be provided by just a couple of odors. We do not know whether acetone is additionally sensed by AWA neurons, but the AWA neurons were not required for the chemotaxis response to *S. marcescens*.

Another pathogenic bacteria, *Bacillus nematocida*, lures *C. elegans* in order to colonize the nematode gut (Niu et al., 2010). Volatile odorants released by *B. nematocida* include two attractive odors: 2-heptanone and benzaldehyde (Niu et al., 2010). However, the luring of *C. elegans* requires only 2-heptanone (Deng et al., 2013). Benzaldehyde is sensed by both AWC neurons (Wes and Bargmann, 2001), but only

AWC^{ON} is required for chemotaxis toward 2-heptanone (Zhang et al., 2016). Taken together, these studies support the idea that there may be multiple attractive odorants in a bacterial bouquet, but one odorant in that bouquet may be most important for *C. elegans* chemotaxis.

Nonpathogenic bacteria also release bouquets of volatile compounds, including multiple odorants that are individually attractive to *C. elegans*. One study examined the headspace of nonpathogenic bacteria that had been isolated together with *C. elegans* from natural environments (Worthy et al., 2018a). Four of the six attractive bacterial strains released isoamyl alcohol, another attractive odorant used in this thesis (Appendix B). One strain released isoamyl alcohol but was not attractive. This strain had only 1 mM isoamyl alcohol in its headspace; the four attractive strains had 6-45 mM isoamyl alcohol in addition to other compounds.

The most attractive of the natural bacterial strains (JUb5) produced 6 mM isoamyl alcohol in addition to acetone, butanone, 2-methyl-1-butanol, and two compounds that are not attractive on their own (Worthy et al., 2018a). JUb5 was the only bacterial strain with isoamyl alcohol + acetone + butanone, along with some others. Another strain had a higher concentration of isoamyl alcohol, 2-methyl-1-butanol, acetone, and some other odors but no butanone; this strain was much less attractive than JUb5.

What does this tell us? First, all of the odors used in this thesis are ethologically relevant. The identification of microbes from the natural habitat of *C. elegans* provide insight into that habitat that were not available when I started my thesis work. Second, bacteria tend to release bouquets of volatile odorants rather than single compounds.

Third, the components of the bouquet need not be additive; one odorant can drive an entire response. Fourth, multiple odorants in a bouquet may be sensed by the same sensory neuron. Finally, the concentration of the volatile odorant matters. Attraction to volatile compounds is concentration-dependent, including these ethologically relevant odorants (Worthy et al., 2018a has dose-response curves for several). With respect to my work, levels of diacetyl released by bacteria depends on the growth conditions (Choi et al., 2016). It would be interesting to see the relationship between nutrient abundance, levels of volatile compounds in bacterial headspace, and animal attraction to the bacteria.

Mapping sensory neurons function in chemotaxis

Chemotaxis to individual volatile odors has been repeatedly shown to depend upon AWA and/or AWC. The level of redundancy of AWA and AWC for chemotaxis behavior varies with odor (Bargmann et al., 1993). For trimethylthiazole, AWA and AWC are fully redundant; for isoamyl alcohol, they are partially redundant (with AWC more important than AWA); and for butanone, only AWC[ON] matters. For diacetyl, AWA is most important for chemotaxis at low concentrations and AWC has a redundant role at higher concentrations (Chou et al., 2001).

The initial chemotaxis assays that identified AWA and AWC as the sensory neurons responsible for detecting volatile attractive odors were end-point assays; animals were scored for accumulation at an odor source after 60 minutes (Bargmann et al., 1993). It is possible that a single neuron is required for the animal to direct its chemotaxis, but other neurons may improve the animal's efficiency at tracking the

source. For example, animals lacking functional ASK, AWC and ASE may still find a diacetyl source within 60 minutes through AWA-driven signaling, but they may have altered behavior or timing in doing so compared to wildtype animals. Our lab is equipped for this analysis. Relevant to this possibility, one group recently published work suggesting that AWC may serve a corrective function as AWA guides chemotaxis toward diacetyl (Itskovits et al., 2018). They propose that animals turn inappropriately away from the gradient, at which point AWC senses a decreased concentration and consequently depolarizes to initiate a corrective turn to align the animal with the gradient. This model relates to AWC's response to odor removal rather than odor addition, and it suggests a role for a non-AWA neuron in diacetyl chemotaxis.

Another potential factor is odor concentration. It is possible that we are performing assays at concentrations that stimulate only a subset of relevant sensory neurons, whether too high or too low. It remains difficult to measure the odor concentrations experienced by animals in the traditional chemotaxis assays. We can, however, simultaneously record calcium activity in a limited number of neurons and record behavior as an animal navigates odor gradients at set odor concentrations within a microfluidic device (Larsch et al., 2013). For example, Larsch et al. (2013) recorded AWC^{ON} calcium activity in animals navigating an isoamyl alcohol gradient that reached a peak concentration of 1 mM isoamyl alcohol. We can begin to match the gradient odor concentrations to the concentrations of odors found in the headspace of attractive bacteria. For example, headspaces of several attractive bacteria contained 6-45 mM isoamyl alcohol, and the headspace of an attractive albeit pathogenic bacteria contained 500 μM butanone (Worthy et al., 2018a; 2018b).

Having multiple neurons sense multiple odorants may help the animal make decisions in complex environments. In standard chemotaxis assays, animals choose between an odor source and a drop of solvent, with nothing else on the plate. In the wild, they would be choosing between bacterial sources in odor-rich environments such as compost. I found only one published non-pathogenic bacterial choice assay with neuronal ablations. The authors showed that *ceh-36* mutants (improper AWC and ASE function) had a partial defect in choosing bacteria that wildtype animals found highly attractive in a preference assay (Abada et al., 2009). Further experiments of this sort could be highly informative.

How we categorize sensory neurons

Based on previous studies, ASK was designated as a gustatory and pheromone-sensing neuron (Macosko et al., 2009; Bargmann and Horvitz, 1991). While ASK is indeed important for sensing water-soluble molecules and pheromones, ASK can also sense volatile odorants (this thesis). An analogy can be made to the mammalian vomeronasal organ, which was initially thought to sense water-soluble pheromones but is now understood to sense multiple other stimuli, including volatile odorants (Zufall and Leinders-Zufall, 2007). Particularly in the compact nervous system of *C. elegans*, we should keep in mind that cells capable of sensing water-soluble compounds may also express the chemoreceptors required to sense volatile compounds.

Coincidence detection as a means for integrating sensory information

AIA as a coincidence detector

AIA responds to the activity of multiple upstream sensory neurons. It becomes active when multiple sensory neurons respond to a stimulus, acting as a coincidence detector. What is the biological role of this property?

A coincidence detection mechanism may help animals filter out noisy background stimuli. Some filtering takes place in the sensory neurons themselves, as exemplified by the 1-second delay between stimulus onset and AWA firing an action potential (Liu, Q et al., 2018). AIA's coincidence detection adds another layer of filtering, as it requires the simultaneous activity or inactivity of a suite of sensory neurons.

AIA activation events to various stimuli are stereotyped in magnitude and on-dynamics (Figure 2-3, Appendix B). These on-dynamics remain stereotyped in several mutants (Figure 2-6, 3-2, Appendix B). The magnitudes and dynamics of upstream sensory neuron responses change with odor concentration, but AIA condenses the rich sensory information into a uniform response. For AIA responses, the concentration of a given odorant may be more important than its identity. Thus AIA responds robustly to 1.15 µM diacetyl, which stimulates AWA, ASK and AWC, but not to 11.5 nM diacetyl, which stimulates the neurons less robustly (AWA, ASK) or not at all (AWC). AIA signals are representative of the presence of sufficient relevant stimuli to warrant a potential response.

Each sensory neuron signals to multiple interneurons, providing the possibility that different interneurons encode different aspects of stimulus information. In addition

to AIA, AWA also connects with AIY, but via a chemical synapse (White et al., 1986). Unlike AIA, AIY responses to diacetyl rise slowly and continuously until the end of the stimulus pulse (Appendix A). AIY responses to 11.5 nM are similar in magnitude to AIY responses to 1.15 μM, so AIY does not encode the magnitude of the AWA responses or the additional contribution of AWC or ASK. In other words, unlike AIA, AIY does not function as a coincidence detector. Because AIY responses increase in magnitude as the stimulus persists, AIY might encode the duration of the stimulus. AIA responses are unsuited to encode stimulus duration, since AIA responses rise sharply to peak and begin decaying within ~2 seconds, regardless of how long the stimulus persists. Unlike AIA, AIY responded reliably to diacetyl pulses (Appendix A). AIA may thus serve a unique role in the *C. elegans* chemotaxis circuitry.

Neural delays are actively encoded by the chemosensory circuit

AWA and AIA are both activated by diacetyl or isoamyl alcohol at concentrations spanning at least 3 orders of magnitude (Figure 2-2, Appendix B). In the case of diacetyl, AIA responses lag behind AWA responses by ~1 second at all concentrations tested (Figure 2-2). In the case of isoamyl alcohol, AWA and AIA respond at essentially the same time (Figure Appendix B-1), suggesting that the timing of AIA responses is determined by the timing of AWA activation. I suspect that this delay in AWA response occurs within AWA itself, whether through slow receptor properties or intrinsic cell properties. I speculate that AWC and perhaps other sensory neurons are inhibited (and thus AIA is disinhibited) before either AWA or AIA are activated. Once AWA is activated, AIA responds with no noticeable lag. In the case of diacetyl, I speculate that the timing

of AIA responses is instead determined by the timing of the glutamatergic sensory neurons. Following this logic, I examined the timing of the ASK and AWC inhibition by diacetyl, expecting that their inhibition would match the timing of AIA activation. Indeed, this is the case (Figure 5-1A).

Time delays are a common feature in neuronal coding schemes, including olfaction (Bathellier et al., 2010). AWA fires action potentials to depolarizing stimuli with a delay of ~1 second (Liu, Q et al., 2018). After the first stimulus, however, AWA fires action potentials without a delay upon further stimulus increases (Figure 5-1B). In my odor experiments, I am delivering pulses rather than steps of increasing concentration, so I am only testing neuronal responses to the initial exposure to odor. It would be interesting to see two things: (1) whether ASK and AWC would be further inhibited by odor up-steps, or whether they act as switches (odor is or is not present), and (2) whether the lag between AWA and AIA responses to subsequent odor up-steps is shorter than the lag upon initial odor exposure.

The second experiment, involving diacetyl upsteps, has already been performed and published in Larsch et al. (2015; see Figure 5-1C). I hope to revisit these data and analyze the AWA-AIA lag times. If the delay disappears after the initial odor increase, the AWA-AIA lag to diacetyl pulses may be at least partially a result of the time filter in AWA. Perhaps both mechanisms play a role; the initial response to diacetyl may depend on both the AWA action potential delay and the delay resulting from slower inhibition of glutamatergic sensory neurons. Subsequent increases in odor may elicit immediate AWA action potentials, potentially overriding the necessity for further ASK or AWC hyperpolarization.
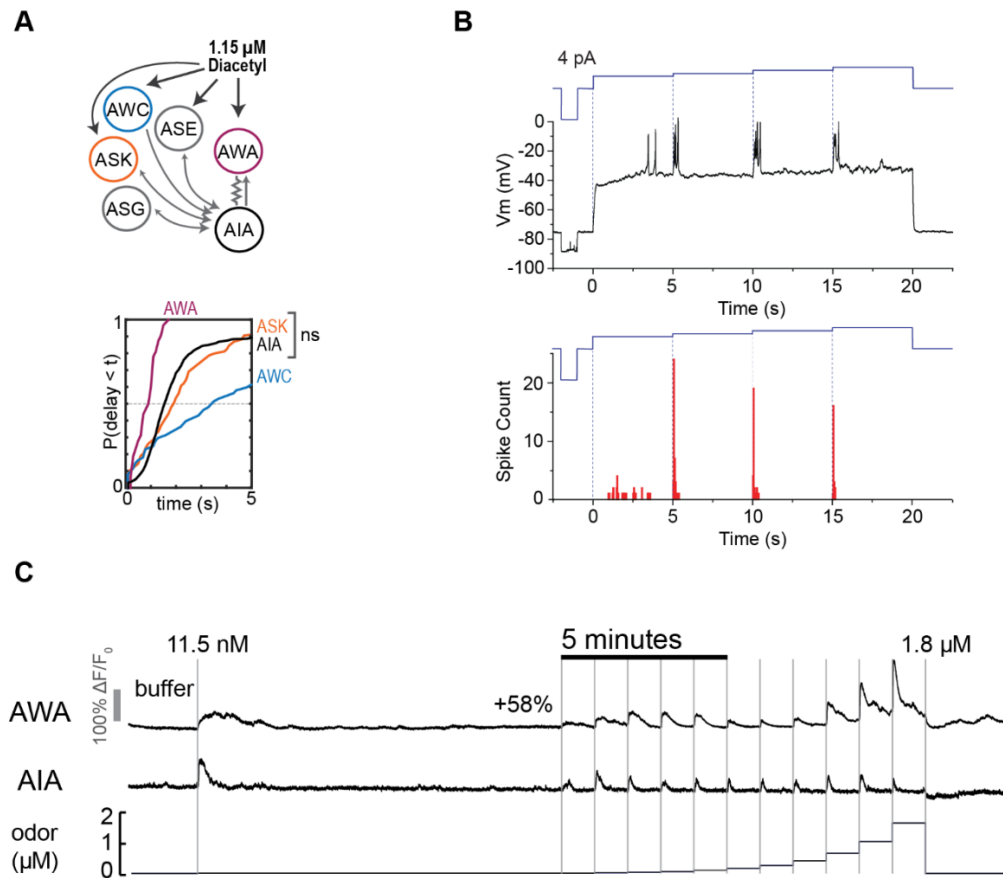
Figure 5-1. Clues about what determines the AWA-AIA time lag.

(A) Cumulative response time profiles of AWA, ASK, AWC and AIA responses to 10-s pulses of 1.15 μM diacetyl. AWA responses as in Figure 2-2; AIA responses as in Figure 2-4; ASK and AWC responses as in Figure 4-1. Only the first 5 s are shown. ns indicates lack of Kolmogorov-Smirnov test significance between ASK and AIA cumulative response time profiles over full pulse. See Appendix C for details.

(B) Top: AWA neuron firing action potentials in response to step-like current injections. The first step was 4 pA; all subsequent steps were 1 pA. Each step lasted 5 seconds. Bottom: Histogram of 37 AWA neurons undergoing current injection protocol shown above. The first spike is always delayed, but subsequent spikes are not. From Liu, Q et al. (2018); data were produced by Qiang Liu.

(C) Mean AWA responses to an initial diacetyl concentration increase from 0 to 11.5 nM, 10 minutes at 11.5 nM, followed by 12 consecutive concentration increases of 58% per step, reaching a final concentration of 1.8 μM diacetyl. Each step lasted 60 seconds. Modified from Larsch et al., 2015; data were produced by Johannes Larsch.

According to Qiang Liu, AIA may also fire action potentials, but without the 1-second delay seen in AWA (unpublished observations). This would help to explain why AIA has a comparatively large and fast response to 11.5 nM diacetyl when the excitatory input from the AWA electrical synapse is small and graded. Philip Kidd and I are working to optimize a protocol for imaging AWA expressing a new voltage sensor in response to odor pulses, and hope to try the voltage sensor in AIA as well to elucidate its action potential firing (Piatkevich et al., 2018).

The RIA interneuron uses neurite compartmentalization

Integration in interneurons can use compartmentalized information as well as temporal information. Another *C. elegans* interneuron, RIA, uses signal compartmentalization to integrate sensory and motor information as an animal steers toward an odor source. RIA differentially localizes sensory and motor signals to separate compartments of its neurite (Hendricks et al., 2012; Ouellette et al., 2018; Liu, H et al., 2018). Briefly, RIA receives input and sends feedback inhibition to two different motor neurons, one responsible for dorsal movement, the other responsible for ventral movement. The two motor neurons each form synapses onto a distinct compartment of the RIA neurite, so activity in the two compartments of the RIA neurite oscillates with head swings. RIA also receives sensory input, and these synapses inhibit or activate the entire neurite. The motor and sensory signal components are additive within a given compartment, so the negative feedback from RIA to the motor neurons is impacted by the sensory information. RIA thus steers the animal in the direction of the attractive odorant because of the signal compartmentalization.

Combining excitatory and inhibitory inputs can occur through compartmentalization

AIA integrates excitation from AWA with disinhibition from several glutamatergic sensory neurons. This balance of excitatory and inhibitory sensory inputs can be found elsewhere in nature; for example, in the cross-inhibition of the retina (Werblin, 2010).

Another highly relevant example of this balance exists within the *C. elegans* chemosensory system for salt responses. The ASE neurons, in addition to responding to diacetyl (Figure 4-1), are considered the main salt sensors. ASE neurons form an asymmetric pair. Unlike most left-right pairs of sensory neurons, ASE-Left (ASEL) and ASE-Right (ASER) do not form gap junctions with each other, and they have asymmetrical activity patterns (Suzuki et al., 2008). ASEL is activated by increases in salt concentration and inhibited by decreases in salt concentration. ASER does the opposite; it is inhibited by increases in salt concentration and activated by decreases.

Both ASEL and ASER form glutamatergic synapses onto the interneuron AIB. AIB responses to salt match the ASER responses, so that salt increases inhibit AIB and salt decreases activate it (Kuramochi and Doi, 2019). Kuramochi and Doi (2019) found that ASEL and ASER work together to tune the downstream AIB response. When salt levels increase, ASEL releases glutamate onto inhibitory glutamate-gated chloride channels concentrated on the distal portion of the AIB neurite (Figure 5-2B). When salt levels decrease, ASER releases glutamate onto both excitatory AMPA-type ionotropic receptors and metabotropic glutamate receptors on the proximal portion of the AIB neurite. The authors did not present an analysis of the timing of AIB responses, and how each input neuron contributes to it, which would be interesting to see.

I was curious whether the excitatory and inhibitory inputs onto the AIA neurite were compartmentalized in a similar manner to AIB. I thus consulted the electron micrograph wiring diagram (White et al., 1986; wormwiring.org). Each AIA neuron has one neurite beginning at the cell body and extending anterior to form a gap junction with its contralateral partner (i.e. AIALeft connects with AIARight). AIA forms synapses all along its neurite, and AIA may be pre- or post-synaptic at these synapses. AIA is post-synaptic to ASK, AWC and ASE, as discussed. The synapses received from ASK, AWC and ASE are all located along the distal portion of the AIA neurite (Figure 5-2A). By contrast, the AWA-AIA electrical synapse is located at the proximal portion, near the cell body. Synaptic connections onto AIA are thus spatially segregated, and just like AIB, the inhibitory connections are distal and the excitatory connections are proximal.

Conceptually, ASEL/ASER/AIB signaling shares features with AWA/AWC/ASK/AIA signaling (Figure 5-2B). In both cases, a sensory neuron (or pair) directly senses and is activated by a stimulus, and at least one other sensory neuron directly senses and is inhibited by the stimulus. Both the activated and inhibited neurons connect to a downstream interneuron. The activated neurons form connections more proximally to the cell body, while the inhibited neurons form connections more distally. Finally, in both cases, multiple sensory neurons have been shown to detect the stimulus, both directly and indirectly (salt: Thiele et al., 2009; Zaslaver et al., 2015).

There are some key distinctions between the two circuits. One difference is in the synaptic mechanisms used. In the case of salt responses, ASEL and ASER both use glutamate and chemical synapses. In the case of odor responses, AWC uses glutamate and chemical synapses, but AWA uses an electrical synapse.
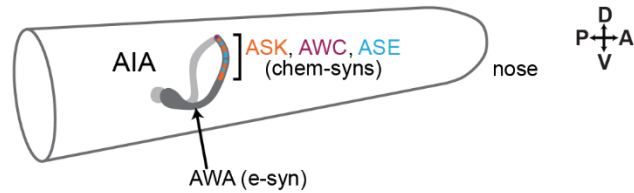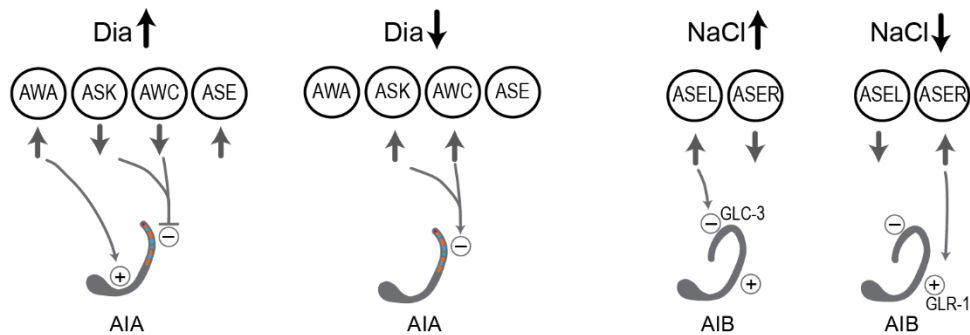
Figure 5-2. AIA receives excitatory and inhibitory input in separate regions of its neurite.

(A) Location of synapses onto AIA neurite. Approximate locations of ASK, AWC and ASE chemical synapses and AWA electrical synapses are shown along the AIA neurite (gray). Only one of the AIA neurons is shown.

(B) The balance of excitation and inhibition on the AIA neurite in response to 1.15 µM diacetyl addition and removal resembles the balance of excitation and inhibition on the AIB neurite in response to salt increases and decreases. In both cases, excitation and inhibition are provided by different neurons with opposite signs.

In AIB, excitatory and inhibitory inputs from ASE neurons are compartmentalized along the neurite. In RIA, signals are also compartmentalized along the neurite. To my knowledge, no one has reported differential calcium responses along the AIA neurite. However, a hint in the direction of AIA compartmentalization comes from the fact that AIA calcium responses are restricted to the neurite and not propagated to the cell body. Localization of voltage-activated calcium channels in the process may be a mechanism to restrict calcium signals locally and temporally. Consistent with AIA acting as a coincidence detector, the inputs may be subthreshold until AIA potentially fires an action potential.

Chemical and electrical synapses in the nervous system

Chemical and electrical synapses working together

The reason I began studying the AWA-AIA connection was because they are connected by a putative electrical synapse and not a chemical synapse in the AWA-to-AIA direction. I found that the electrical synapse was regulated by chemical synapses from other neurons. There are several examples of "mixed synapses", where chemical and electrical synapses exist in close proximity and regulate each other. In the fish Mauthner cell, chemical synapses initiate potentiation in electrical synapses at mixed synapses (Pereda, 2014). In the connection between a *C. elegans* command interneuron and motor neurons, electrical synapses are strongly and unexpectedly rectifying in the direction of the command interneuron (Liu, P et al., 2017). The purpose of these electrical synapses and their rectification is to amplify chemical synapses in the direction of the motor neurons. Similar mechanisms operate at synapses between interneurons and motor neurons in fish (Song et al., 2016).

The mixed synapses in the above have chemical and electrical synapses between the same neurons (e.g. command interneuron and motor neurons in *C. elegans*). The AWA-AIA synapse is different because the AWA-AIA electrical synapse is regulated by chemical synapses from other neurons.

The interactions between the AWA-AIA electrical synapse and the inhibitory glutamatergic synapses may be analogous to the synapses of the inferior olive. In the inferior olive, the principal cells are coupled via electrical synapses, firing synchronously in clusters. These principal cells uncouple when a nearby neuron releases GABA at an

inhibitory chemical synapse, reducing or blocking current flow at the electrical synapse (Pereda et al., 2013). GABA at the inferior olive synapse may play a role like that of inhibitory glutamate on AIA.

Neuromodulators can also impact electrical synaptic activity (Pereda, 2014). These are probably not the dominant factor in AWA-to-AIA transmission since *unc-31* peptide release mutants did not affect information transfer from AWA to AIA (Figure 3-5).

Tools (or lack thereof) to identify and study electrical synapses

A major impediment to studying electrical synapses is the absence of well-established tools for modulating their function. In *C. elegans*, there are 25 innexin genes, some with multiple isoforms, and each neuron expresses multiple innexins (Altun et al., 2009; Bhattacharya et al., 2019; Cao et al., 2017). The diversity of innexins makes it difficult to silence all potential electrical synapses in a given neuron by genetic knockout. Moreover, most individual innexin genes are expressed widely across the nervous system. Innexins are also involved in neuronal development of *C. elegans*, so genetic mutants may have unknown development effects (Starich et al., 2003; Chuang et al., 2007). Better genetic or pharmacological tools for acute disruption of innexins would be a helpful addition to this part of circuit analysis.

Innexin expression

Electron micrographs show the presence of gap junctions connecting *C. elegans* neurons (White et al., 1986), but they do not provide information about which innexins

form the gap junctions. The first attempt to map innexin expression in the whole animal used GFP reporter lines, with an innexin's promoter driving GFP expression (Altun et al., 2009). This initial study was very informative, but like many reporter gene studies, it was incomplete. For example, this study did not identify AWA or AIA. Since then, innexins have been studied with antibodies (Starich et al., 2014), and with fosmid-based reporter constructs and CRISPR/Cas9 genome editing strategies (Bhattacharya et al., 2019). This latest study revealed that all neurons in adults express between one and ten innexin genes, averaging ~six different innexins per neuron (Bhattacharya et al., 2019). The results from the latest study overlap extensively with the innexin profile from an independent single-cell RNA sequencing dataset (Cao et al, 2017).

Among the innexin genes, *unc-7* and *unc-9* are widely expressed in neurons. The other subunits may modify their function and specificity. For example, the particular combinations of innexins at a gap junction can affect its rectification and conductance properties (Liu, P et al., 2013).

Electrical synapse connectivity

Anatomically defined gap junctions are traditionally shown to function as electrical synapses using paired electrophysiological recordings (Bennett et al., 1963). In *C. elegans*, the gold standard of paired recordings between two neurons has only been attained in a single paper demonstrating electrical synapses between a motor neuron and a command interneuron (Liu, P et al., 2017).

Another traditional method of inferring which neurons are electrically coupled is to look at chemical coupling. In dye coupling experiments, a low molecular weight dye

injected into one neuron flows through gap junctions into another. Photoactivatable

caged fluorescent dyes have also been used (Schumacher et al., 2012). Following this

model, genetically encoded fluorescent-tagged peptides can pass through gap junction

to label paired cells (Qiao and Sanes, 2016). Another new genetically encoded tool

based on chemical coupling incorporates sub-cellular spatial resolution. This tool,

named PARIS, involves expressing a light-sensitive hydrogen pump in Cell A and a

fluorescent pH sensor in Cell B (Wu et al., 2019). The hydrogen that is pumped from

Cell A passes through gap junctions and is sensed as a pH change in Cell B, causing

the fluorescent sensors in Cell B to light up. These new techniques will likely be very

useful in confirming the function of predicted electrical synapses in the *C. elegans* and

may be useful for studying asymmetries at the synapses.

Innexin perturbation

Pharmacological agents for inhibiting gap junctions are notoriously nonspecific in

most species. Moreover, since vertebrate connexins and invertebrate innexins are not

similar in sequence, they are not expected to generalize in their pharmacological

properties.

A genetic tool to inhibit UNC-9-containing gap junctions exploits a gain-of-

function allele of *unc-1*, which encodes a stomatin-like membrane protein that co-

localizes with and gates UNC-9 gap junctions in muscle (Chen et al., 2007). The gain-

of-function *unc-1(n494)* allele produces a protein that blocks UNC-9 function, and this

inhibition can be rescued by expressing an UNC-9-GFP fusion protein. This approach

has the benefit of being cell-specific; the *unc-1(n494)* is expressed under a promoter of

116

choice. The *unc-1(n494)* genetic tool has been useful to study certain circuitry (Jang et al., 2017), but it does not have the temporal specificity to rule out developmental effects. More importantly, we only know it to inhibit UNC-9-based gap junctions and are unsure about its effects on other innexins.

To overcome the temporal specificity issue, it may be possible to use genetic approaches like miniSOG protein fusions, which generate toxic superoxides upon illumination, to ablate specific innexins in a cell-selective manner with temporal control. miniSOG fused to VAMP2 and synaptophysin has been used to ablate chemical synapses (Lin et al., 2013). Both AWA and AIA express five unique innexins (Bhattacharya et al., 2019), but it may not be necessary to inactivate all of them individually with miniSOG if they form heteromeric hemichannels.

Another genetic approach that has been used successfully to destroy innexins in *C. elegans* is the auxin-degradation approach (Liu, P et al., 2017). A degron was inserted to the C-terminus of the UNC-7 innexin protein using CRISPR/Cas9, and an extrachromosomal array was used to achieve cell-selective expression of a TIR1 F-box protein. The TIR1 F-box protein activates a ubiquitin ligase that, in the presence of auxin, destroys the degron-tagged protein – in this case, UNC-7. The main issue is, once again, the diversity of innexin genes expressed in AWA and AIA.

Does AIA integrate motor state?

In the past few years, there have been studies showing that ensembles of *C. elegans* neurons are activated at the same time as part of a large-scale motor program (e.g. Nguyen et al., 2016; Kato et al., 2015). To study large numbers of neurons at the

same time, the authors expressed GCaMP only in the cell nuclei so the signals could be resolved and cells could be identified. Because AIA calcium fluctuations are observable in the neurite rather than the cell body (Chalasani et al., 2007; Larsch et al., 2013), we do not know whether AIA is part of such a large-scale motor program. Moreover, we recorded AIA activity in paralyzed animals, so we cannot directly correlate AIA activity with behavior. One study found that AIA transients correlated with behavior, with calcium increases during forward movements and calcium decreases during reversal in *npr-1* (neuropeptide Y receptor) mutants (Laurent et al., 2015). However, this group did not look at wildtype animals or establish causality, and they found this correlation in spontaneous AIA transients rather than in evoked responses.

Optimally, we could image AIA activity in a freely moving animal navigating an odor gradient. This type of experiment has already been done to pulses of diacetyl (Larsch et al., 2013), showing that it is feasible in a microfluidics system. Our lab now has an experimental setup that would allow for AIA calcium imaging in an animal chemotaxing toward odor on a plate rather than in a microfluidic chip. If carefully analyzed, this experiment could help determine the relative importance of motor versus sensory states.

Activity in other interneurons has been linked to behavioral state. For example, Gordus et al. (2015) found that the interneuron AIB integrates sensory input with motor commands such that the ability of AWC to transmit its isoamyl alcohol responses to AIB depends on the downstream motor state. However, my results indicate that the variability in AIA responses stems from sensory activity, with no indication that motor state matters for odor- or optogenetic-evoked AIA responses. AIA and AIB are both first

layer amphid interneuron pairs and receive synaptic input from many of the same sensory neurons. However, AIB activity reflects the downstream motor state of the animal, while AIA activity seems to reflect the upstream sensory state of the animal.

Kaplan et al. (2018) published a review article arguing that we should avoid grouping all interneuron responses together. Rather, they claim that we should analyze interneuron activity by first separating traces into high versus low pre-stimulus activity to distinguish between forward and reversal states in case the interneuron is part of a forward or reverse ensemble, just as Gordus et al. (2015) did when studying AIB activity. However, unlike AIB, AIA does not show largescale background fluctuations, so this analysis would not have been necessary.

Even if AIA integrates only upstream sensory state and it is not part of a motor program, AIA activity could still reflect states of the animal beyond its external environment. Sensory neuronal activity can reflect internal state as seen, for example, with ASK, whose spontaneous activity fluctuates more with time after removal from food (Skora et al., 2018; Lopez-Cruz et al., 2019).

AIA and behavior

AIA integrates upstream sensory information, but what is the purpose of a signal from AIA? The general design motif of having intermediary structures like AIA that integrate sensory information to bias motor output is found throughout the animal kingdom. The current thought in the field is that no single first layer interneuron is absolutely required for chemotaxis behavior. Rather, each interneuron biases

behavioral choices such that AIA and AIY increase the probability of forward states versus reversal/reorientation states, and AIB and AIZ do the opposite.

The four first layer interneurons are not the only interneurons involved in producing meaningful animal behavior. I have also mentioned RIA in this discussion; RIA, along with RIB and RIM, are classified as "second layer" interneurons. All of these interneurons receive input from at least one sensory neuron and from several other interneurons. AIA synapses heavily and directly onto AIB and AIZ but not onto RIA, RIB or RIM. This is unusual for a first layer interneuron; AIB, AIY and AIZ all synapse directly onto all three of RIA, RIB and RIM (White et al., 1986).

Interneurons may be differentially required for different strategies that together enable chemotaxis behavior. Chemotaxis behavior consists of klinotaxis and klinokinesis. Klinotaxis involves the animal using head undulations to sample the environment and steer along the steepest gradient toward an attractive odor source (Iino and Yoshida, 2009). Klinokinesis, on the other hand, involves frequent reorientations to correct the animal's trajectory (Pierce-Shimomura et al., 1999).

The first layer interneurons, including AIA, seem to be more heavily involved in klinokinesis than klinotaxis (Iino and Yoshida, 2009; Luo et al., 2014). On the other hand, RIA seems to be more heavily involved in klinotaxis, as is consistent with its compartmentalized activity based on head undulations (Henricks et al., 2012; Ouellette et al., 2018; Liu, H et al., 2018). There may be additional strategies that remain to be described. AIA is known to affect learning and foraging, as well as spontaneous behavior (Wakabayashi et al., 2004; Lopez-Cruz et al., 2019; Cho et al., 2016). Understanding its integrative role through a combined genetic, behavioral, and

functional approach, as I have used here, provides an opportunity for many future

discoveries.

EXPERIMENTAL PROCEDURES

Nematode Growth

I used standard genetic and molecular biology techniques. *C. elegans* strains were maintained at 22-23ºC on nematode growth medium (NGM; 51.3 mM NaCl, 1.7% agar, 0.25% peptone, 1 mM $CaCl_2$, 12.9 µM cholesterol, 1 mM $MgSO_4$, 25 mM KPO_4, pH 6) plates seeded with LB-grown *Escherichia coli* OP50 bacteria grown in as a food source. Animals had constant access to food for at least 3 generations prior to any experiment. The Bristol N2 strain was used as wildtype. All experiments were performed on young adult hermaphrodites, picked as L4 larvae the evening before an experiment. See Appendix E for a complete list of strains used.

Stimulus Preparation

Odor solutions were freshly prepared each experimental day. I prepared diacetyl solutions by serially diluting from a pure stock of diacetyl (2,3-butanedione; Sigma-Aldrich 11038, CAS 431-03-8; stored at 4ºC) into S Basal buffer (0.1 M NaCl, 5.74 mM K_2HPO_4, 7.35 mM KH_2PO_4, 5 µg/ml cholesterol, pH 6-6.2). I used S Basal + 100 mM NaCl to confirm that ASE neurons of all genotypes had comparable direct responses to salt, and that ASH neurons were capable of responding to osmotic stimuli. Solutions used for calcium imaging of immobilized animals additionally contained 1 mM of (-)-tetramisole hydrochloride (Sigma L9756) to paralyze the body wall muscles. (-)-Tetramisole binds to acetylcholine receptors in the body wall muscles (Lewis et al., 1980). All odor solutions were stored in brown glass vials.

For non-diacetyl odor solutions used in Figure 3-8 (butanone) or Appendix B, I prepared the following solutions fresh on the day of the experiment:

- 11.2 nM butanone (Fluka 04380, CAS 78-93-3), stored at room temperature and serially diluted into S Basal.

- 1 μM ascaroside C3 in S Basal. Ascaroside C3 was synthesized by Rebecca Butcher's lab and stored as 10 mM in ethanol at -20°C.

- 0.9, 9, or 90 μM isoamyl alcohol (EMD AX-1440-6, CAS 123-51-3), stored at 4°C and serially diluted into S Basal.

- OP50 conditioned medium in NGM. NGM buffer without agar or cholesterol (but with peptone) was used as the control buffer. I seeded 30 mL NGM buffer with a colony of OP50 bacteria the night before the experiment, and culture was shaken at 37°C overnight. The morning of the experiment, I measured the optical density as ~2 and filtered the bacteria (0.22 μm Millex GP) to yield the conditioned medium, which contains bacterial metabolites and secretions but not bacterial cells.

Calcium Imaging of Single Neurons in Immobilized Animals

Larvae were selected as L4s the evening before the experiment and picked to new OP50 plates. For optogenetic experiments, I seeded plates of 5x concentrated OP50-seeded LB with or without 5 μM all-trans retinal, serially diluted from a 500 μM stock (stored at -80°C in glycerol). These plates were dried in darkness for 2 hours with plate lids partially off. Animals were transferred without food and housed overnight in complete darkness.

Immediately before the start of an experiment, animals were selected for visible GCaMP fluorescence, gently washed in S Basal buffer, and loaded into custom-

fabricated two-arena polydimethylsiloxane (PDMS; Sigma 761036, made from 9:1 base:

curing agent, Sylgard 184) imaging devices. These devices were de-gassed in a

vacuum dessicator for at least 5 minutes and flooded with buffer before ~10 animals of

two genotypes or conditions were loaded into separate arenas. Animals were paralyzed

in darkness for ~90 minutes in buffer + tetramisole before the start of the experiment.

Experiments were performed on a Zeiss AxioObserver A1 inverted microscope fit

with a 5x/0.25 NA Zeiss Fluar objective. An Andor iXon3 DU-897 EM-CCD camera was

mounted to the microscope using a 0.63x c-mount adapter to increase field of view. 474

nm wavelength light was delivered by a Lumencor SOLA-LE lamp at 165 mW/cm^2 for

odor-only experiments and at 40 mW/cm^2 for experiments involving optogenetics to

avoid blue light activation of the Chrimson channel. Videos were acquired at 10 fps (100

ms exposure time), with light pulsed at a 10 ms duty cycle (sample was illuminated for

10 ms every 100 ms). I used Metamorph 7.7.6 software to control image acquisition and

light pulsing in addition to rapid stimulus switching (National Instruments NI-DAQmx

connected to an Automate Valvebank 8 II actuator that controls a solenoid valve), odor

selection (two Hamilton 8-way distribution valves), and activation of an external red LED

for Chrimson stimulation (Mightex Precision LED Spot Light, 617 nm, Part number PLS-

0617-030-S, attached to Chroma ET605/50x filter to narrow band to 605 ± 25 nm). For

Chrimson experiment in Figure 3-3I-K (low power AIA::Chr), red light intensity was 6.5

mW/cm^2. For all other Chrimson experiments, red light intensity was 15.4 mW/cm^2.

Animals received two pulses of the tested stimulus, with the exception of the

butanone experiments in Figure 3-8, in which animals received only one pulse. In

experiments with multiple odor concentrations, I delivered lower concentrations first. In

optogenetics experiments with diacetyl controls, or diacetyl experiments with NaCl controls, the control was delivered last.

Raw fluorescence values were measured using a custom ImageJ script from Larsch et al. (2013), which measures the average intensity of a 4x4 pixel square and subtracts the local background intensity. For all sensory neurons, the square captured the soma; for AIA, it captured the middle of the neural process. Animals that were moving too much for the tracking script were discarded. For experiments with odor delivery, I delivered a pulse of fluorescein dye at the end of the experiment to ensure proper flow. Experiments with improper flow were discarded. All genotypes and conditions were tested on at least 2 separate days.

Determining Response Latency Times

For neurons activated by odor (AWA, AIA, ASE, ASH), each background-subtracted raw fluorescence trace was first normalized to generate dF/F_0, where F_0 was the median of the 10 seconds (100 frames) before the odor pulse onset. Traces were then smoothed by 5 frames such that each frame t represented the mean of t-2 to t+2. For neurons inhibited by odor (ASK and AWC), each background-subtracted raw fluorescence trace was similarly smoothed, then scaled such that the minimum value was 0 and the maximum value was 1. Note that ASK and AWC traces were only scaled for determining response latency times; magnitudes were calculated differently, and they were plotted unscaled.

An activating neuron's calcium trace was deemed a "response" if a frame t within the stimulus pulse met the following criteria: (1) the mean fluorescence of t:t+12 was

greater than 4 standard deviations above the mean of the 10-s pre-odor fluorescence, and (2) the time derivative of $t:t+1$ is greater than 1 standard deviation of the time derivative of the 10-s pre-odor fluorescence fluctuations. An inhibited neuron's calcium trace was deemed a "response" if a frame t met within the stimulus pulse met the following criteria: (1) the mean fluorescence of $t:t+10$ was below 2 standard deviations below the mean of the 10-s pre-odor fluorescence, and (2) the mean time derivative of $t:t+6$ was either below 2 standard deviations of the time derivative of the 10-s pre-odor fluorescence fluctuations, or below -30%/second.

In both cases, the response latency was the first frame at which the above criteria were met. The above criteria were optimized based on agreement with measurements taken by eye, using 40 wildtype AIA calcium traces to AWA Chrimson stimulation for activation criteria and 30 wildtype AWC calcium traces to 1.15 µM diacetyl for inhibition criteria.

To compare the variability of response latencies, I compared the cumulative distributions of response latencies. I used the Kolmogorov Smirnoff test to compare these distributions since this test would capture both the latencies and probability of response. Although the figures show only 5 s of stimulus, the Kolmogorov Smirnoff test compared distributions of the full 10 s pulse. Details of each test, including the D test statistic, can be found in Appendix C.

Comparing AWA-AIA Lag Times

To calculate the mean lag between AWA and AIA responses to AWA Chrimson stimulation, 11.5 nM, 115 nM, and 1.15 µM diacetyl, I subtracted the frame at which 50% of AWA neurons had responded from the frame at which 50% of AIA neurons had responded to a given stimulus. I performed this calculation 1000 times from randomly bootstrapped sampled populations pulled from the complete data sets presented in the heat maps of Figure 2-2 for wildtype and Figure 3-1 for *unc-13*. The randomly bootstrapped sampled populations had the same *n* as the true population, sampled with replacement. The standard deviation of this calculation was used as the standard error of the bootstrapped mean.

Measuring Magnitudes

Each background-subtracted raw fluorescence trace was first normalized to generate dF/F_0. For all neurons (AWA, AIA, AIY, ASK, AWC, ASE, ASH), F_0 was the median of the 10 seconds (100 frames) before the odor pulse onset. Traces were then smoothed by 5 frames such that each frame *t* represented the mean of *t*-2 to *t*+2.

For ASK, AWC, ASE, and ASH, the response magnitudes to pulses of buffer, diacetyl, NaCl (for ASH), and AWA Chrimson stimulation (for ASK, AWC, and ASE) were calculated by subtracting the mean of the second (10 frames) prior to odor delivery from the mean of the final second (10 frames) within the odor pulse. ASE response magnitudes to NaCl removal were calculated by subtracting the mean of the final second (10 frames) within the NaCl pulse from the mean of the 4th second (10 frames) after NaCl removal. Because AWA and AIA responses often adapt within the 10-s

stimulus pulse, I defined AWA and AIA response magnitudes as the maximum fluorescence level within the 10-s pulse (after the smoothing).

To statistically compare magnitudes between genotypes or conditions, I used either an ordinary one-way ANOVA with Dunnett's multiple comparisons test for experiments with more than two conditions, or an unpaired t-test for experiments with only two conditions. For the majority of AIA magnitude comparisons, I included only calcium traces that represent detectable non-zero responses as described in the Determining Response Latency Times section to eliminate the effect of low response reliability in the magnitude analysis. For sensory neuron magnitudes to various stimuli, I included all calcium traces to determine whether there was an appreciable response to a given stimulus.

For ASK, AWC, ASE and ASH responses to diacetyl or NaCl, response magnitudes to the stimulus was compared to those measured during pulses of buffer using an unpaired t-test. For ASK, AWC and ASE responses to AWA Chrimson stimulation, response magnitudes to the light pulse were compared to the fluorescence differences of a similar window during the 10-s period before the light pulse using a paired t-test. See Appendix D for statistical test details.

Comparing AIA Decay Dynamics

To compare the decay times of AIA responses to sensory stimuli (Figure 3-3A-C, Appendix B3), I first aligned the detectable non-zero responses that initiated within the first 2 seconds (20 frames) of stimulus presentation to allow for comparison of dynamics for 8 seconds after the response initiated. To compare the decay times of AIA

responses to AIA optogenetic stimulation, I filtered for detectable non-zero responses initiated within the first 2 seconds but did not align them since their latencies were consistently short as is. I took the mean of these filtered early responses and transformed them from GCaMP $\Delta F/F$ to an approximated $\Delta Ca^{2+}/Ca^{2+}$ value using the following values for GCaMP5A: Hill coefficient = 2.7, maximum in vitro $\Delta F/F$ = 17.4, and the Ca^{2+} affinity K_d = 307 nM (Akerboom et al., 2012). This transformation was as follows: $\Delta Ca^{2+}/Ca^{2+} = K_d / ((Max\Delta F/F)/(\Delta F/F) - 1)^{1/HillCoefficient}$, and serves as an estimate of calcium concentration changes within the dynamic range of the GCaMP5A calcium indicator. I then took the natural log transformation of the calcium traces and fit a line to the decay portion of the signal.

For the 10-second sensory stimuli pulses, I could only compare the aligned traces for 8 seconds post-initiation. The linear fit was thus from 2 to 8 seconds post-initiation of response. For the 30-second AIA optogenetic stimulation, the linear fit was from 3 to 30 seconds after stimulus presentation. In both cases, the lines were extrapolated to find the half-time in seconds.

Behavior Experiments

L4 stage animals were pre-picked the day before the experiment onto freshly seeded OP50 plates with 5 μM retinal, as described in the Calcium Imaging of Single Neurons in Immobilized Animals section. Animals were housed overnight in complete darkness. No-retinal controls were picked onto freshly seeded OP50 plates prepared in parallel with the retinal plates.

To prepare for the experiment, I transferred 15-20 animals from their retinal plates to an unseeded plate. Once they crawled for several body lengths to clean off excess food, I transferred them to the assay plate. The assay plates were circular NGM plates with a diameter of 150 mm. Just before transferring animals to the assay plate, I placed a filter paper ring with a 100 mm inner diameter and soaked the filter paper with 20 mM $CuCl_2$. The $CuCl_2$ served to restrict animals to the ~80 cm^2 recording area. After 5 minutes had elapsed from the moment the animals were transferred to the unseeded plate, the experiment began.

Lopez-Cruz et al. (2019) had an intermediate step in their protocol, transferring animals from their overnight bacterial lawn to a plate with a uniform, edge-less lawn for 45 minutes to avoid effects of food history. He was carefully studying behavior related to food history, so this was necessary. I decided to instead transfer animals directly from their overnight bacterial lawn to the transfer plate just before the experiment because, anecdotally, this decreased forward movement, placing our baseline further from the ceiling. This strategy seemed to work since our baselines were ~70% instead of ~80%, which I would expect from the exact protocol used by Lopez-Cruz et al. (2019).

Animals were recorded behaving off of food for 10 minutes at 3 frames per second. Using a 15 MP PL-D7715 CMOS camera (Pixelink), controlled by Streampix software (Norpix). To stimulate either Chrimson or GtACR2, I used a custom MATLAB program to control an external LED (Solis High Power LED, 525 nm, ThorLabs), which delivered green light at 5 mW/cm^2 for the experiment shown in Figure 3-9, and 610 µW/cm^2 for the experiment shown in Figures 3-10 and 3-11. Light was pulsed at 10 Hz with a 50% duty cycle. I delivered one 20-s light pulse (for Figure 3-9) or 10-s light pulse

(for Figures 3-10, 3-11) every 2 minutes for a total of 4 pulses. Experiments were conducted on two identical camera-computer-LED setups adjacent to each other, separated by blackout paper to prevent cross-activation. Plates of different conditions were staggered and counterbalanced between the two setups.

To analyze the differences between each condition, I tracked the behavior using a custom MATLAB program, as previously described (Pokala et al., 2014; Lopez-Cruz et al., 2019). The program tracked trajectories of all of the animals recorded, along with the behavior of the animals at each frame. When animals collided, the trajectories would break, resulting in a collection of track fragments without specific animal identifiers. I filtered out short tracks, leaving only track fragments that were uninterrupted for 30 seconds (90 frames), and used these track fragments to calculate the fraction of animals moving forward in each frame, regardless of when the forward movement was initiated. I then aligned the 4 pulses and averaged the fraction reorienting over all experiments (7-12 experiments per condition, performed over 4 days). The curves shown in Figures 2-8, 2-9 and 2-10 are the combined curves over all experiments, smoothed by 10 frames.

To measure the effects of a given manipulation, I used unsmoothed fractions for individual experiment plates, and each experiment included all four stimulus pulses. The "baseline" was the mean forward fraction of the 50-second window preceding the light pulse. The "peak" was the mean of the 2-second window spanning from 8 to 10 seconds into the light pulse. The "rebound" was the mean of the 2-second window spanning from 4 to 6 seconds after the light pulse terminated.

To test whether light exposure produced an increase in forward locomotion, I performed paired t-tests comparing the baseline fraction to the peak fraction for a given experiment plate. To test whether the increase was retinal-dependent, I performed an unpaired t-test comparing the normalized change in forward fraction ((peak-baseline)/baseline) of with-retinal to no-retinal. To test whether ASK+AWC+ASE+ASG glutamate KO enhanced the *AWA::Chrimson*-induced effect, I performed an unpaired t-test between the normalized changes in *AWA::Chrimson* + ASK+AWC+ASE+ASG Glutamate KO and *AWA::Chrimson* alone (for Figure 3-8). To test whether *AWA::Chr* + *ASK+AWC+ASE::GtACR2* produced larger increases in forward locomotion than either *AWA::Chrimson* or *ASK+AWC+ASE+GtACR2* alone (for Figure 3-9), I performed an ordinary one-way ANOVA with two Dunnett's multiple comparisons. To test whether *AIA::TeTx* impacted induction of forward locomotion, I performed unpaired t-tests.

Note on Spontaneous Activity

Spontaneous AIA transients were more frequent in Lopez-Cruz et al. (2019) than in Larsch et al. (2015) or my own experiments. Larsch et al. (2015) and I used similar experimental procedures that were slightly different from those used in Lopez-Cruz et al. (2019). The differences were as follows:

(1) Microfluidic device. Lopez-Cruz et al. (2019) used a "trapped chip" PDMS device that confines a single animal to a small channel with its nose poking out into a steady stream of buffer. Their flow rate was dictated by a vacuum supply. I used a non-restrictive device PDMS device that can hold several animals with their entire

bodies exposed to a steady stream of buffer. My flow rate was dictated by gravity flow.

(2) Paralysis. Lopez-Cruz et al. (2019) did not paralyze their animals. I paralyzed my animals with tetramisole (acetylcholine agonist) for ~90 minutes before beginning an experiment.

(3) Time off food. Lopez-Cruz et al. (2019) performed their experiments beginning 6 minutes after food removal and finished recording 56 minutes after food removal. I performed experiments ~90 minutes after food removal. Lopez-Cruz et al. (2019) found that AIA spontaneous activity increased with time spent off food, so additional time off food likely would not account for reduced spontaneous activity.

(4) Buffer used. Lopez-Cruz et al. (2019) used NGM buffer, whereas I used S Basal buffer for the majority of experiments. I have also used NGM buffer for the OP50-conditioned medium responses shown in Appendix B. During those experiments, I did not see many spontaneous responses, so I do not think this was the root of the discrepancy.

(5) Light pulsing. Lopez-Cruz et al. (2019) used constant blue light to excite GCaMP, whereas I used pulsed blue light (10 ms light per 100 ms).

Three hypotheses to test are whether AIA spontaneous activity: increases when the animal is confined, increases when the animal is exposed to non-pulsed illumination, or decreases upon prolonged exposure to tetramisole. My focus has been on stimulus-evoked AIA activity, so my results do not depend on spontaneous AIA activity. That said, it may be worth establishing the exact nature of the spontaneous AIA activity and whether it correlates with small movements in the trapped chip.

Appendix A: Diacetyl responses in the interneuron AIY are inhibited but not gated by chemical synapses

Background

The majority of this thesis focuses on the interneuron AIA and the upstream sensory neurons that sense diacetyl. In Appendix A, I would like to explore another interneuron pair: AIY. AIY, together with AIA, AIB, and AIZ, are the four "first layer amphid interneuron" pairs, generally thought to play integrative roles. AIY and AIA both inhibit reversals, while AIB and likely AIZ promote reversals (Wakabayashi et al., 2004). These four interneuron pairs interconnect with each other in potentially informative ways (Figure Appendix A-1). For example, AIA forms chemical synapses onto AIB but not vice versa, suggesting that AIA may inhibit turning in part by suppressing AIB activity. AIY and AIZ have opposite roles not only in promoting forward movement, but also in isothermal tracking. Likewise, AIY forms chemical synapses onto AIZ but not vice versa, suggesting that AIY may inhibit turning in part by suppressing AIZ activity. AIY and AIZ can also regulate the interneuron RIA with opposite effects (Mori and Ohshima, 1995).
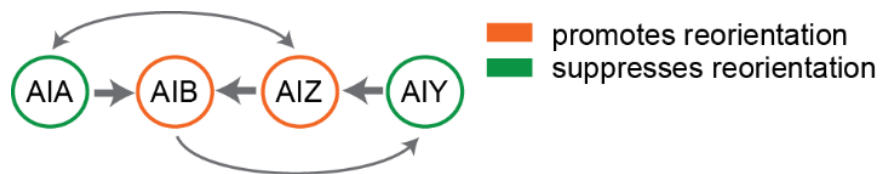
Figure Appendix A-1. First layer amphid interneurons are interconnected. AIA and AIY suppress turning behavior, whereas AIB and AIZ promote turning behavior. AIY and AIZ generally have opposite functions, and AIA is thought to inhibit AIB.

Other than promoting forward locomotion, AIA and AIY share other characteristics. They are both activated by 1 µM diacetyl (Larsch et al., 2013) and

exhibit responses in the neurite process rather than in the cell body (Larsch et al., 2013, Chalasani et al., 2007). Moreover, neither AIA nor AIY alone is required for chemotaxis to salt, but ablating AIA and AIY together decreases the salt chemotaxis index (Iino and Yoshida, 2009), suggesting a degree of functional redundancy. AIY also receives chemical synapses from AWC, ASE and ASG (Figure A-2A), three of the glutamatergic sensory neurons involved in gating AWA-AIA communication. However, AIY receives chemical input from several sensory neurons that AIA does not, suggesting that AIY has distinct integration roles from AIA. For example, AIY is a major synaptic target of the main thermosensory neuron pair, AFD, and AIY has been shown to play a large role in thermotaxis (Tsalik and Hobert, 2003). AIA and AIY also differ in their connections with AWA. The electron micrograph wiring diagram shows AWA connecting to AIY via chemical synapses rather than electrical synapses as it does for AIA (White et al., 1986), leading us to wonder whether a similar coincidence detection mechanism exists in AIY.

In Appendix A, I present preliminary calcium imaging results in the AIY interneurons. I first show that AIY responds to low concentrations of diacetyl (11.5 nM), lower than previously tested. These responses rely on AWA for their magnitude. AIY responds more reliably to diacetyl than AIA in the absence of AWA function. AIY responses to diacetyl have faster on-dynamics in the absence of chemical synapses, but the timing of the response initiation does not change.

Results

Diacetyl responses in the AIY interneuron are smaller but reliable without AWA activity

I measured AIY responses to 1.15 μM diacetyl in both wildtype and *odr-10* AWA diacetyl receptor mutants, as I did for AIA for Figure 2-6. AIY responses were smaller in magnitude in the *odr-10* mutants (Figure Appendix A2B, C). Unlike AIA, however, the reliability of the AIY response did not differ dramatically between wildtype and *odr-10* (Figure Appendix A2D). The response latencies were slightly increased in *odr-10* mutants, but the overall response probability was similar (Figure Appendix A2D, E). Moreover, the *odr-10* mutation did not change the time of the peak response (Figure Appendix A2E, F). I conclude that, unlike AIA, AIY responses to 1.15 μM diacetyl are reliable in the absence of AWA input. However, the AIY response magnitude is greatly reduced in the absence of AWA activity.

As shown in Chapter 4, fewer sensory neurons respond to the lower concentration of 11.5 nM diacetyl than to 1.15 μM diacetyl. Therefore, I compared AIY responses in wildtype and *odr-10* mutants to 11.5 nM diacetyl. Again, AIY response magnitudes were decreased in the *odr-10* mutants (Figure Appendix A2G, H, J). Unlike 1.15 μM diacetyl, AIY responses to 11.5 nM diacetyl were less reliable in *odr-10* mutants (Figure Appendix A2I). When AIY responses did occur, they looked very similar in magnitude to those at higher concentrations of diacetyl (Figure Appendix A-2J).

AIY responses to diacetyl were graded, increasing slowly over the stimulus time. Their magnitude and dynamics did not appear to be concentration-dependent in wildtype or *odr-10* mutants. Taken together, AWA activity is more important for the reliable diacetyl responses in AIA than in AIY. In addition, a fraction of AIY response at all diacetyl concentrations comes from non-AWA sensory neurons.

Figure Appendix A-2. Diacetyl responses in the AIY interneuron are smaller but reliable without AWA activity.

(A) Simplified circuit diagram of synaptic connections onto AIY. Note that AWA forms a chemical but not electrical synapse onto AIY.

(B) Mean AIY responses to 10-s pulses of 1.15 μM diacetyl in WT versus *odr-10(ky32)* (AWA diacetyl receptor mutant) animals. Shading indicates ± SEM.

(C) Magnitudes of AIY responses shown in (B), omitting traces that did not produce a detectable response. Boxes show median and interquartile range.

(D) Cumulative response time profiles for AIY responses shown in (B). Note that profile is shifted in *odr-10* mutants but reaches similar response probability within ~3 seconds.

(E) Start and peak times of AIY activation responses shown in (B), omitting traces that did not produce a detectable response. Boxes show median and interquartile range.

(F) Difference between peak and start times of AIY activation responses calculated in (E). Boxes show median and interquartile range.

(G) Mean AIY responses to 10-s pulses of 11.5 nM diacetyl in WT versus *odr-10* mutant animals. Shading indicates ± SEM.

(H) Magnitudes of AIY responses shown in (G), omitting traces that did not produce a detectable response. Boxes show median and interquartile range.

(I) Cumulative response time profiles for AIY responses shown in (G).

(J) Mean of WT and *odr-10* AIY traces shown in (B) and (G), including only pulses that resulted in activation within 5 seconds of stimulus, aligned to activation initiation frame. Shading indicates ± SEM.

For (D) and (I), asterisks refer to Kolmogorov-Smirnov test significance versus WT over full 10-s stimulus pulse. ns: not significant; **: $p < 0.01$; ***: $p < 0.001$. See Appendix C for sample sizes and test details.

For (C), (E), (F), and (H)), asterisks refer to statistical significance of an ordinary one-way ANOVA with Dunnett's multiple comparisons test versus WT. ns: not significant; **: $p < 0.01$; ***: $p < 0.001$. See Appendix D for sample sizes and test details.
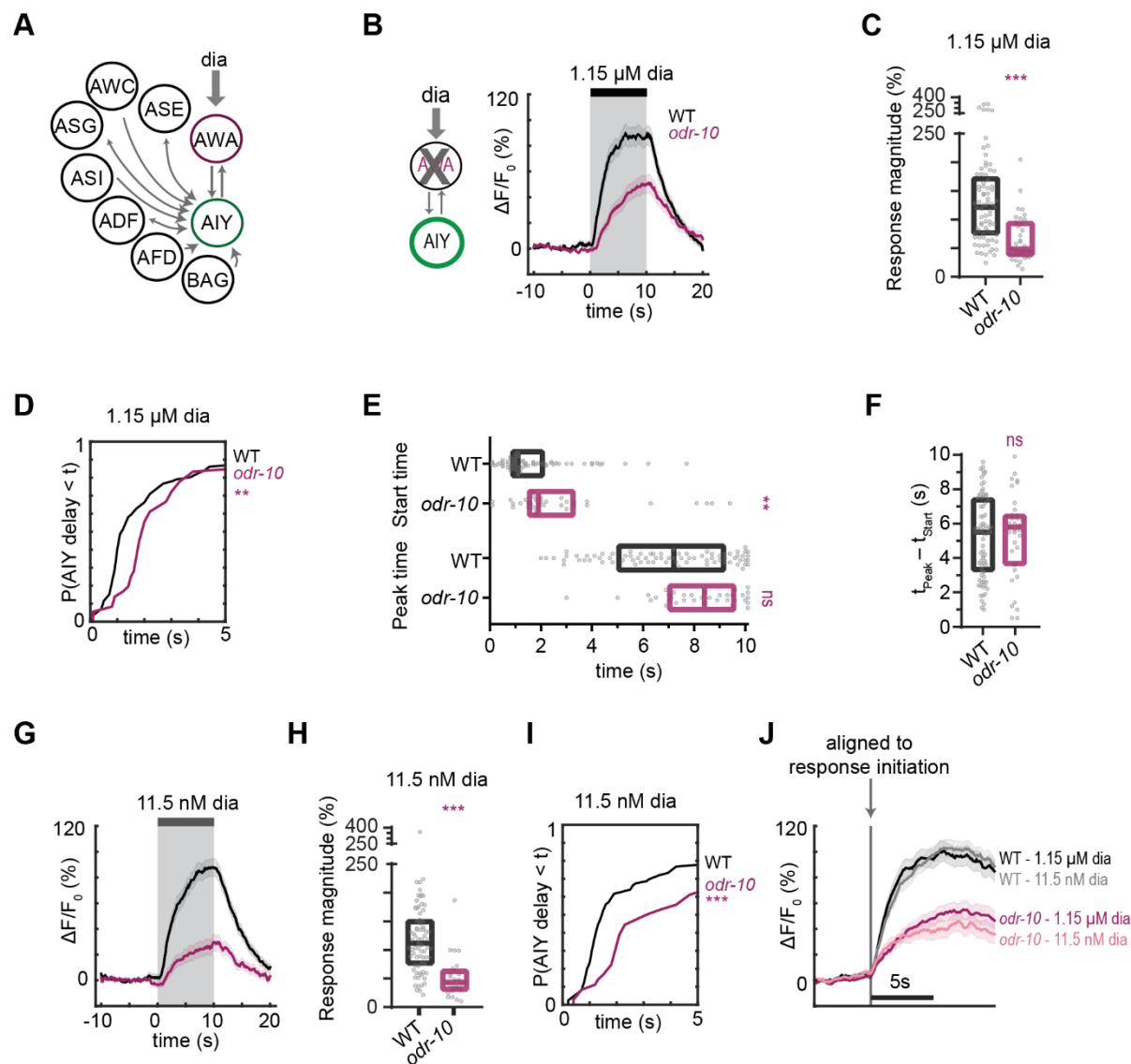
Figure Appendix A-2. Diacetyl responses in the AIY interneuron are smaller but reliable without AWA activity.

AIY responses to diacetyl are regulated by chemical synapses

Since the AWA diacetyl receptor ODR-10 was not required for reliable AIY responses to 1.15 µM diacetyl, I reasoned that other sensory neurons that respond to 1.15 µM diacetyl may trigger AIY responses. I recorded AIY responses in *unc-18* synaptic transmission mutants and compared them to wildtype (Figure Appendix A-3A, B). Unlike *odr-10* mutants, *unc-18* and another strain with defects in chemical synapses, *unc-13*, did not impact the magnitude of AIY diacetyl responses (Figure Appendix A-3C, D). Since AWA and AIY are thought to connect via chemical synapses, it is unclear why *unc-13* and *unc-18* AIY responses did not capture the *odr-10* phenotype. It is possible that AWA and AIY connect via an undetected gap junction, or that the small number of remaining chemical synapses in these mutants is sufficient for AIY to respond.

The synaptic transmission mutants did not dramatically change AIY response latencies or probabilities (Figure Appendix A-3E, F), even when I tested AIY responses to the lower concentration of 11.5 nM diacetyl (Figure Appendix A-3J). However, whereas AIY diacetyl responses in wildtype animals rose slowly, responses in the chemical synapse mutants rose sharply and peaked quickly (Figure Appendix A-3A-C, F, G). When I aligned AIA responses in wildtype and *unc-18* mutants to the frame at which each AIA response initiated, I found that the rise phase and the time derivatives of AIA responses to AWA optogenetic stimulation overlapped in the two genotypes. I did the same for AIY responses to 1.15 µM diacetyl and found that wildtype AIY responses and time derivatives did not overlap with the synaptic transmission mutants (Figure Appendix A-3H, I).

Figure Appendix A-3. **AIY responses to diacetyl are regulated by chemical synapses**.

(A) Individual AIY responses to 1.15 µM diacetyl in WT animals, down-sampled to 10 traces at random from full data set shown in Figure 3-8B.

(B) Individual AIY responses to 1.15 µM diacetyl in *unc-18(e234)* (synaptic transmission mutant) animals, down-sampled to 10 traces at random.

(C) Mean of AIY responses to 1.15 µM diacetyl in WT versus *unc-13(e51)* and *unc-18* animals, representing the full data sets sampled in (A) and (B). Shading indicates ± SEM.

(D) Magnitudes of AIY responses shown in (C), omitting traces that did not produce a detectable response. Boxes show median and interquartile range.

(E) Cumulative response time profiles of AIY responses shown in (C).

(F) Start and peak times of AIY activation responses shown in (C), omitting traces that did not produce a detectable response. Boxes show median and interquartile range.

(G) Difference between peak and start times of AIY activation responses calculated in (F). Boxes show median and interquartile range.

(H) Time derivatives of traces shown in (C), aligned to the frame of response initiation. Only responses in which activation initiated within 5 seconds of stimulus were included. Note that *unc-13* and *unc-18* do not overlap with WT.

(I) Mean of AIY traces shown in (C), including only pulses that resulted in activation within 5 seconds of stimulus, aligned to activation initiation frame. Shading indicates ± SEM.

(J) Cumulative response time profiles of AIY responses to 11.5 nM diacetyl in WT versus *unc-13* and *unc-18* mutant animals.

For (E) and (J), asterisks refer to Kolmogorov-Smirnov test significance versus WT over full 10-s stimulus pulse. ns: not significant; *: $p < 0.05$. See Appendix C for sample sizes and test details.

For (D), (F) and (G), asterisks refer to statistical significance of an ordinary one-way ANOVA with Dunnett's multiple comparisons test versus WT. ns: not significant; *: $p < 0.05$; **: $p < 0.01$; ***: $p < 0.0001$. See Appendix D for sample sizes and test details.
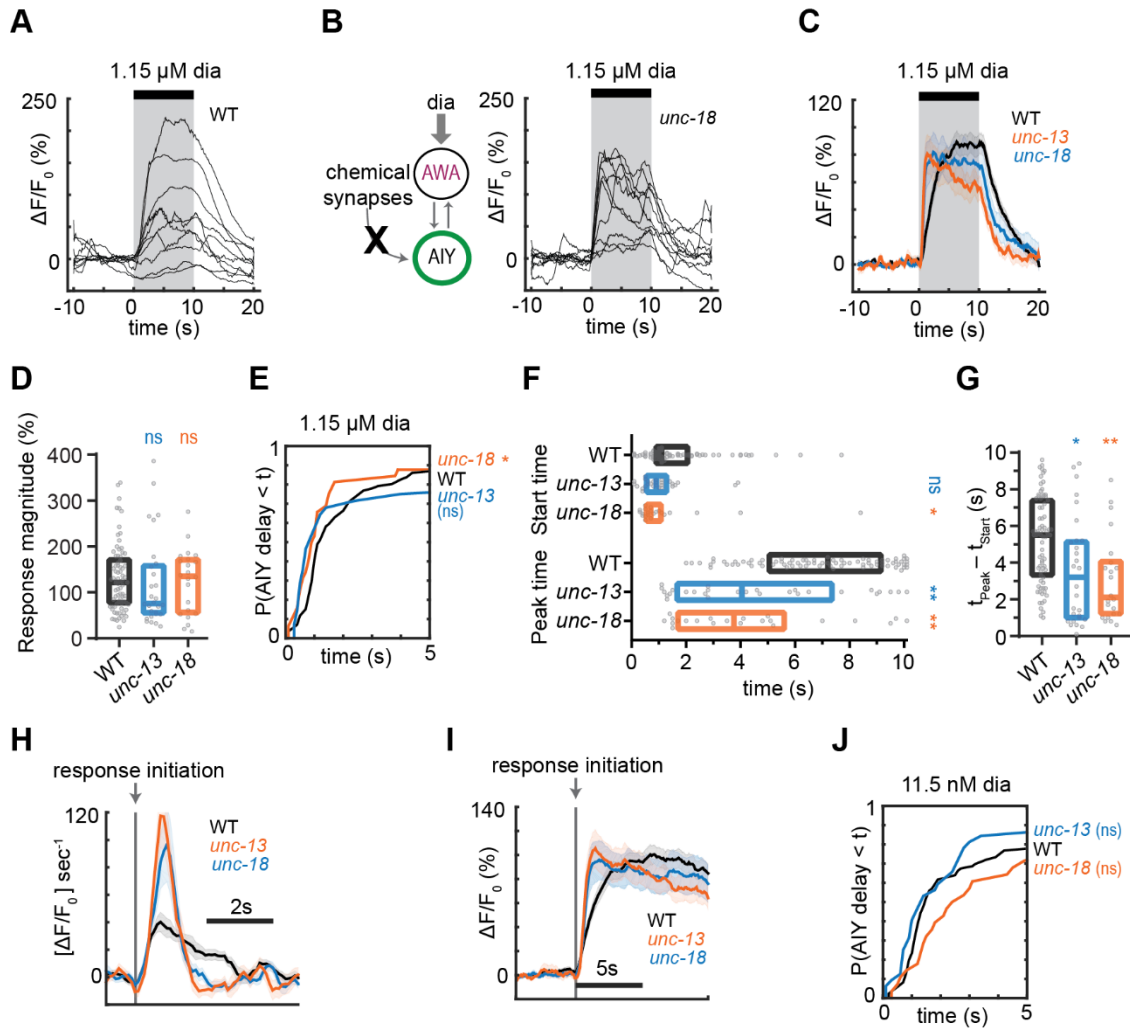
Figure Appendix A-3. **AIY responses to diacetyl are regulated by chemical synapses**.

Discussion

Chemical synapses seem to act differently on AIY odor responses than on AIA odor responses. In AIA, chemical synapses gated AIA diacetyl responses, and AIA acted as a coincidence detector for AWA and sensory input through chemical synapses. AIY responded reliably to diacetyl regardless of AWA signaling, and independent of classical synaptic transmission genes, so AIY does not function as a coincidence detector. AIA diacetyl responses had stereotyped on-dynamics in various mutants, and the main difference in the diacetyl responses was in the reliability (latency and probability). This was not the case for AIY, where the reliability did not change dramatically in *odr-10*, *unc-13* or *unc-18* mutants. Rather, AIY responses have sharper on-dynamics without chemical synapses and smaller but reliable responses without AWA signaling.

We have a lot to learn about diacetyl signaling in AIY. We do not know the source of chemical synaptic inhibition of AIY. In AIA, the inhibition was glutamatergic and sensory, but I have yet to test this in AIY. We also do not understand the nature of the AWA-AIY connection. The wiring diagram shows a chemical synapse, but the global chemical synapse mutants did not have decreased AIY response magnitudes, as *odr-10* AWA diacetyl receptor mutants did. The chemical synapse mutants I used affect only small clear vesicles; we could learn more about AIY activation by using more additional mutants such as *unc-31*, which affects dense core vesicles (Speese et al., 2007).

My thesis has focused on how AIA integrates sensory information, but AIY plays a complementary role in guiding locomotion and is known to be involved in processing sensory information. It will be very interesting to study the differences between how AIY and AIA integrate sensory information in greater detail.

Appendix B: AIA responses to non-diacetyl odors have stereotyped on-dynamics

Background

My thesis focused on responses to the odor diacetyl or to AWA optogenetic stimulation. However, diacetyl is only one bacterial metabolite. *C. elegans* responds to many volatile odorants belonging to diverse chemical classes (e.g. alcohols, pyrazines, aromatics, etc. – see Bargmann et al., 1993). I chose diacetyl because others have studied AWA dynamics to diacetyl exposure in great detail (Larsch et al., 2015), allowing me to focus on downstream responses. In Figure 2-3, I show that AIA response dynamics to AWA-dominant stimuli (AWA optogenetic stimulation and diacetyl, although diacetyl is clearly not AWA-only) had stereotyped on-dynamics. Here, I explore AIA responses to other attractive stimuli that activate subsets of the diacetyl circuit identified in Chapters 3 and 4 (AWA, ASK, AWC, ASE).

I chose the following stimuli:

(1) Isoamyl alcohol, a fermentation by-product released in abundance by at least six bacterial strains that have been isolated with *C. elegans* in natural environments (Worthy et al., 2018a). These bacterial strains are favored by *C. elegans* in laboratory choice assays, consistent with *C. elegans* reliably chemotaxing toward point sources of isoamyl alcohol in the lab. AWC is inhibited by 9, 90, and 900 µM isoamyl alcohol (Larsch et al., 2013; Yoshida et al., 2012; Gordus et al., 2015; Zaslaver et al., 2015), and AIA is activated by 9 µM (Larsch et al., 2013) and 90 µM isoamyl alcohol (Chalasani et al., 2010). Zaslaver et al. (2015) did not find any other

sensory neurons that responded to 900 µM isoamyl alcohol. I used lower

concentrations of 0.9, 9, and 90 µM isoamyl alcohol.

(2) Conditioned *Escherichia coli* OP50 medium, which includes a plethora of odorants

secreted from the bacteria. OP50 is the bacterial strain I feed animals in the lab, and

it is the only bacteria my experimental animals have been exposed to. Zaslaver et al.

(2015) found that AWA, AWC, ASE, ASK, ASJ, ASH, AFD, BAG, ASI, and ADF

sensory neurons all respond to *E. coli* OP50 conditioned medium. AWA and ASE

were activated, and AWC and ASK were inhibited by the addition of conditioned

medium, just as I found for diacetyl in Chapter 4.

(3) Ascaroside C3, also known as ascr#5, a pheromone primarily sensed by ASK. C3 is

produced by *C. elegans* (Von Reuss et al., 2012) and is weakly attractive to wildtype

animals (Macosko et al., 2009; Dal Bello et al., 2018). Cocktails of C3, C6 and C9

ascarosides inhibit ASK and activate AIA, even at low combined concentrations of

10 nM for ASK and 100 nM for AIA (Macosko et al., 2009). I used 1 µM pure C3

instead of a cocktail, and have not tested which other sensory neurons may respond

to this high level of ascaroside C3.

In Appendix B, I present results that are preliminary but interesting. First, I show that

AWA and AIA are both activated by isoamyl alcohol at concentrations spanning at least

three orders of magnitude. Unlike to diacetyl, AIA responses to isoamyl alcohol do not

lag behind AWA responses. I then show that AIA responses to isoamyl alcohol rely on

AWA in addition to AWC and/or ASE. Finally, I show that AIA responses to various

attractive stimuli have similar on-dynamics and magnitudes.

Results

AWA and AIA are activated by isoamyl alcohol without an AWA-to-AIA delay

AWC is inhibited by isoamyl alcohol addition at 9 µM (Yoshida et al., 2012; Larsch et al., 2013), but the only study I am aware of that looked at AWA and other sensory neurons did not find responses to 900 µM isoamyl alcohol (Zaslaver et al., 2015). In chemotaxis behavior assays to isoamyl alcohol, ablating AWA does not reduce the chemotaxis index (Bargmann et al., 1993). Ablating AWC reduces it somewhat; ablating both AWC and AWA diminishes it further.

I measured AWA responses to 0.9, 9, and 90 µM isoamyl alcohol and found that AWA was activated by all three concentrations, with concentration-dependent dynamics, magnitudes, latencies, and probability (Figure Appendix B-1A-C). In dynamics, AWA responses to isoamyl alcohol resembled those to diacetyl. Responses to 0.9 µM isoamyl alcohol rose smoothly during stimulation, like AWA responses to 11.5 nM diacetyl. In reliability (latency and probability), AWA responses to isoamyl alcohol increased in reliability as concentration increased, as they did to diacetyl.

AIA was activated by all three concentrations of isoamyl alcohol tested (Figure Appendix B-1D-E). AIA responses peaked at a lower magnitude at the lowest concentration of 0.9 µM isoamyl alcohol. This decreased magnitude differed from AIA responses to diacetyl, in which AIA responses to 11.5 nM had comparable magnitude to 1.15 µM diacetyl. AIA responses to isoamyl alcohol increased in reliability as concentration increased, resembling AWA (Figure Appendix B-1F).

145

Figure Appendix B-1. AWA and AIA are activated by isoamyl alcohol without an AWA-to-AIA delay.

(A and D) Mean AWA (A) and AIA (D) responses to 10-s pulses of 0.9, 9, and 90 μM isoamyl alcohol, aligned to activation initiation. Only pulses that resulted in activation within 5 seconds were included. Shading indicates ± SEM.

(B and E) Mean time derivative of AWA (B) or AIA (E) responses shown in (A) or (D), respectively. Shading indicates ± SEM.

(C and F) Cumulative response time profiles of AWA (C) or AIA (F) shown in (A) or (D), respectively. Asterisks indicate significance of Kolmogorov-Smirnov test versus buffer pulses over full 10-s stimulus pulse. **: $p < 0.01$; ***: $p < 0.001$. See Appendix C for sample sizes and test details.

(G – I) Overlaid cumulative response time profiles of AWA and AIA responses to 0.9 μM (G), 9 μM (H), and 90 μM (I) isoamyl alcohol. Time labels indicate delay between the frame at which 50% of AWA and AIA neurons have responded.
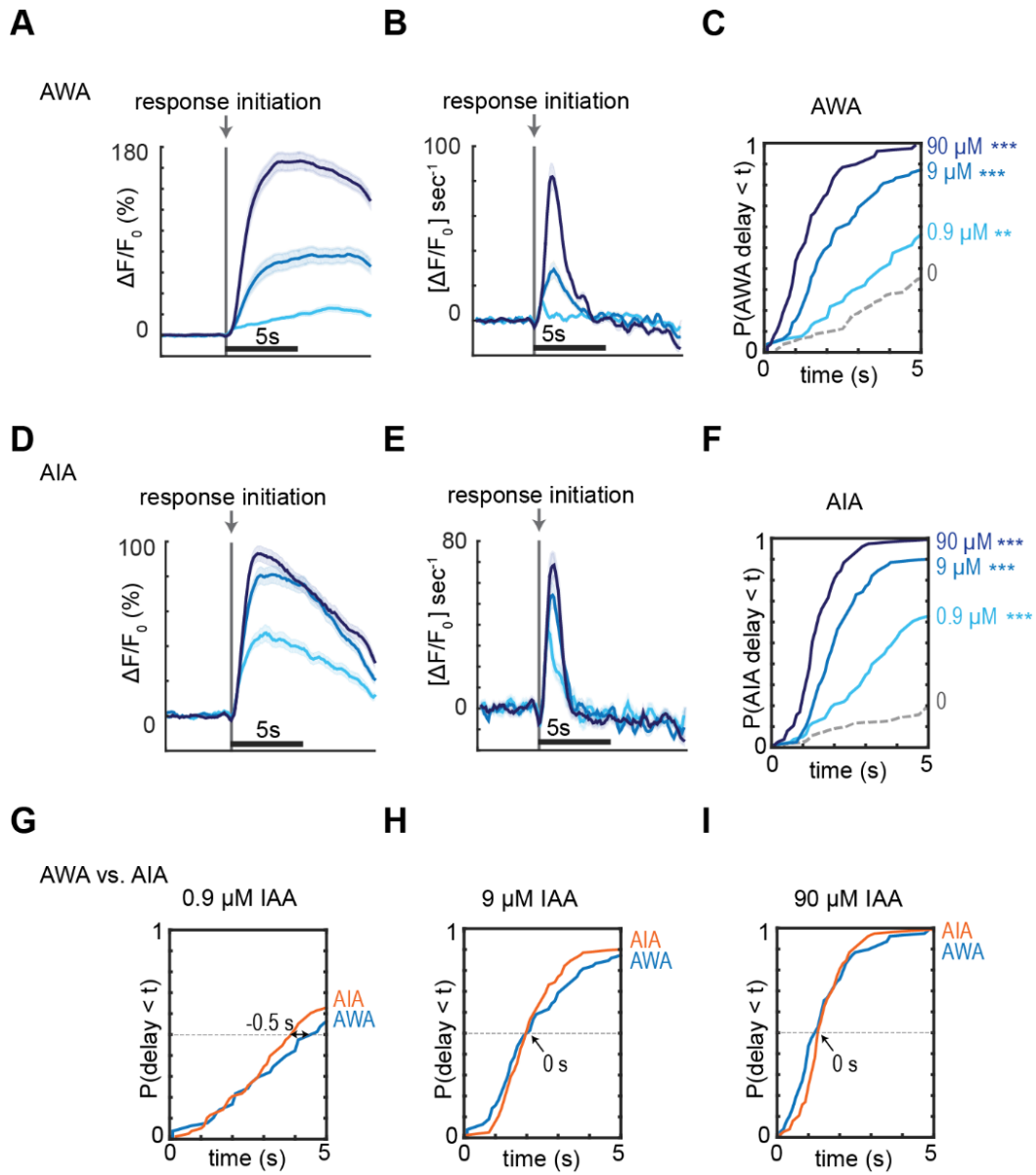
Figure Appendix B-1. AWA and AIA are activated by isoamyl alcohol without an AWA-to-AIA delay.

AIA requires AWA and AWC for reliable isoamyl alcohol responses

Since AWA was activated by isoamyl alcohol, I wanted to know whether AWA contributes to the AIA response. I recorded AIA responses to 0.9, 9, and 90 µM in *ceh-36* (AWC and ASE cell fate mutant), *odr-7* (AWA cell fate mutant), and *odr-7 ceh-36* double mutant animals. AIA responses were less reliable in *ceh-36* mutants to both 9 and 90 µM isoamyl alcohol (Figure Appendix B-2A, B). Perhaps surprisingly, the responses were even less reliable in *odr-7* mutants, indicating that reliable AIA responses to isoamyl alcohol depend more on AWA activity than on AWC, whereas chemotaxis depends more on AWC than on AWA.

odr-7 ceh-36 had very few AIA responses to any concentration of isoamyl alcohol (Figure Appendix B-2A-C). This result shows that AWA and AWC (and perhaps ASE) responses are most important for producing reliable AIA responses to isoamyl alcohol, and that each neuron can drive some AIA response on its own. However, at the lowest concentration of 0.9 µM isoamyl alcohol, neither *odr-7* nor *ceh-36* single mutants were able to produce AIA responses (Figure Appendix B-2C), suggesting that both neurons need to be recruited at low concentrations to result in an AIA response.

Consistent with all AIA responses I have compared, responses to 9 µM isoamyl alcohol had similar on-dynamics in all genotypes (Figure Appendix B-2D, E). However, the magnitude of response varied, with *odr-7* and *ceh-36* mutants producing slightly smaller AIA responses, and the double mutants producing even smaller responses (Figure Appendix B-2D).

148
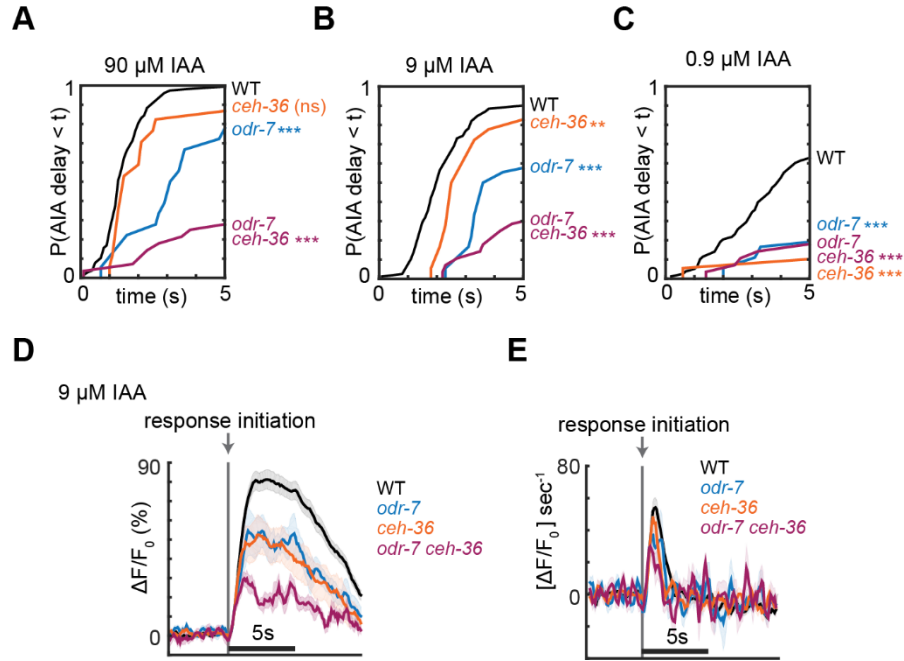
Figure Appendix B-2. AIA requires AWA and AWC for reliable isoamyl alcohol responses.

(A – C) Cumulative response time profiles to 10-s pulses of 90 μM (A), 9 μM (B), and 0.9 μM (C) isoamyl alcohol in WT versus *odr-7* AWA cell fate mutants, *ceh-36* AWC and ASE cell fate mutants, and *odr-7 ceh-36* double mutants. WT profiles are the same as shown in Figure Appendix B-1F.

(D) Mean AIA responses to 10-s pulses of 9 μM isoamyl alcohol in WT, *odr-7, ceh-36*, and *odr-7 ceh-36* mutants, aligned to the frame at which activation was initiated. Only pulses that resulted in activation within 5 seconds were included to allow for comparison of response dynamics. Shading indicates ± SEM.

(E) Mean time derivative of AIA responses shown in (D). Shading indicates ± SEM.

Asterisks refer to Kolmogorov-Smirnov test significance versus WT over full 10-s stimulus pulse. *: p<0.05; **: p<0.01; ***: p<0.001. See Appendix C for sample sizes and test details.

AIA responses to non-diacetyl odors have stereotyped on-dynamics

In addition to diacetyl and isoamyl alcohol, I recorded AIA responses to ascaroside C3 and to *E. coli* OP50-conditioned medium. I used 1 µM ascaroside C3 to inhibit ASK, and OP50-conditioned medium to modulate multiple sensory neurons (Figure Appendix B-3A). OP50-conditioned medium is a broad stimulus that includes many attractive odorants. It elicited highly reliable AIA responses (Figure Appendix B-3B). The OP50-conditioned medium reliability was similar to 1.15 diacetyl and 90 µM isoamyl alcohol. I selected 1 µM for ascaroside C3 based on previous studies showing robust ASK and AIA responses to a 1 µM ascaroside cocktail. 1 µM ascaroside C3 also produced reliable AIA responses comparable to the other stimuli.

The AIA responses with comparable reliability were also stereotyped in terms of on-dynamics (Figure Appendix B-3C, D) and magnitude (Figure Appendix B-3G). The only difference I observed was in the response decay. Responses to 1.15 µM diacetyl, 90 µM isoamyl alcohol, and 1 µM ascaroside C3 all decayed rapidly compared to OP50-conditioned media (Figure Appendix B-3F).

Figure Appendix B-3. AIA responses to non-diacetyl odors have stereotyped on-dynamics.

(A) Diagrams of which sensory neurons are known to respond to the tested stimuli. For 1.15 µM diacetyl, the arrows are drawn based on the results shown in Chapter 4. For 90 µM isoamyl alcohol, the arrow to AWA is based on the results shown in Figure Appendix B-1.

(B) Cumulative response time profiles of WT AIA responses to 1.15 µM diacetyl, 90 µM isoamyl alcohol, 1 µM ascaroside C3, and OP50 conditioned medium.

(C) Mean AIA responses to 10-s pulses of 1.15 µM diacetyl, 90 µM isoamyl alcohol, 1 µM ascaroside C3, and OP50 conditioned medium, aligned to the frame at which activation was initiated. Only pulses that resulted in activation within 2 seconds were included to allow for comparison of response dynamics. Note that we can compare response dynamics between stimuli for 8 seconds. Shading indicates $\pm$ SEM.

(D) Mean time derivative of AIA responses shown in (C). Shading indicates $\pm$ SEM.

(E) Log fit of calcium decay. $\Delta F/F_0$ traces from (C) were transformed to approximated Ca^{2+}/Ca^{2+}_0 traces, log transformed, and linearly fit from 2 to 8 seconds post-initiation.

(F) Linear fits from (E) were extrapolated to calculate the number of seconds for AIA calcium levels to decrease to 50% of the peak to find the half-time of aligned AIA responses to various stimuli.

(G) Magnitudes of AIA responses to various stimuli, omitting traces that did not produce a detectable response.

For (B), ns refers to lack of significance of Kolmogorov-Smirnov test significance versus 1.15 µM diacetyl over full 10-s stimulus pulse. See Appendix C for sample sizes and test details.

For (G), ns refers to lack of significance of one-way ANOVA with Dunnett's multiple comparisons test versus 1.15 µM diacetyl. Boxes show median and interquartile range. See Appendix D for sample sizes and test details.
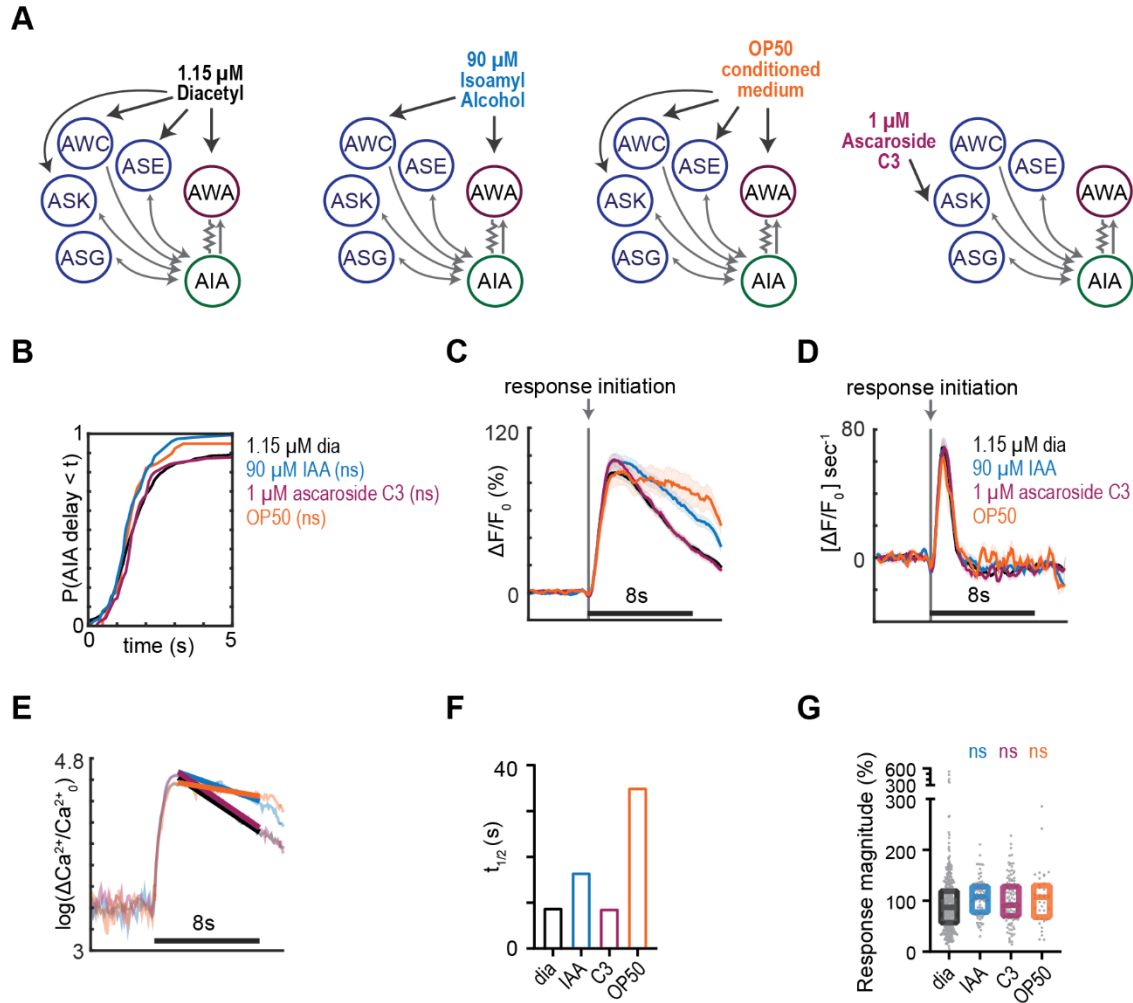
Figure Appendix B-3. AIA responses to non-diacetyl odors have stereotyped on-dynamics.

Discussion

AWA and AIA both respond to isoamyl alcohol over at least three orders of magnitude with ~one second delay, but no lag between activation of the two neurons. Previous studies showed that isoamyl alcohol rapidly and robustly inhibits AWC. Here, I found that AIA requires both AWA and AWC for its reliable response to isoamyl alcohol.

AIA gives similar calcium responses to widely varying stimuli. AIA on-dynamics, magnitude, and reliability were similar between 1.15 μM diacetyl, 90 μM isoamyl alcohol, 1 μM ascaroside C3, and OP50-conditioned medium; AIA responses are stereotyped to varied stimuli. This supports the notion that AIA is a site of integration, condensing complex upstream sensory activity into a stereotyped pattern of activity. AIA decay kinetics varied between stimuli, and in Chapter 3, I showed that this feature of AIA activity is highly sensitive to *unc-31* (dense core vesicle release; neuropeptides) as well as *unc-18* (small vesicle release; chemical synapses). I speculate that while initiation of AIA activity is driven by sensory input, termination relies upon feedback from peptides and circuit state.

Appendix C: Details of Cumulative Response Time Profiles

GT (test)	GT (control)	Neuron Recorded	Stimulus	n (test)	n (control)	D test statistic	Approximate p-value	Relevant Figure
WT + *AWA::Chr*, after *AWA::Chr* experiment	WT, no *AWA::Chr* expression or pulses	AIA	1.15 µM dia	90	438	0.1738	**0.0220**	2-4B
WT, 2nd pulse	WT, 1st pulse	AIA	AWA::Chr	282	282	0.1489	**0.0038**	2-5A
WT, 2nd pulse	WT, 1st pulse	AIA	11.5 nM dia	115	115	0.1049	0.7086	2-5D
WT, 2nd pulse	WT, 1st pulse	AIA	1.15 µM dia	217	217	0.2035	**0.0005**	2-5G
odr-7(ky4)	WT	AIA	1.15 µM dia	70	78	0.4652	**<0.0001**	2-6A
odr-10(ky32)	WT	AIA	1.15 µM dia	32	78	0.6995	**<0.0001**	2-6A
AWA::TeTx	WT	AIA	1.15 µM dia	27	20	0.2426	0.5083	2-7A
AWA::TeTx	WT	AIA	AWA::Chr	56	146	0.1580	0.2643	2-7C
unc-7(e5) unc-9(fc16)	WT	AIA	AWA::Chr	96	146	0.2042	**0.0160**	2-7D
unc-7(e5) unc-9(fc16); inx-4(ok2373)	WT	AIA	AWA::Chr	72	146	0.2040	**0.0362**	2-7D
unc-7(e5) unc-9(fc16)	WT	AIA	1.15 µM dia	86	94	0.3152	**0.0003**	2-7E
unc-7(e5) unc-9(fc16)	WT	AIA	11.5 nM dia	61	70	0.3293	**0.0017**	2-7F
unc-7(e5) unc-9(fc16)	WT	AIA	AIA::Chr	30	50	0.1600	0.7232	2-8B
unc-7(e5) unc-9(fc16)	WT	AWA	AIA::Chr	48	58	0.09626	0.9680	2-8D
unc-18(e234)	WT	AIA	AIA::Chr	46	64	0.1080	0.9137	2-8F
unc-18(e234)	WT	AWA	AIA::Chr	69	58	0.3426	**0.0012**	2-8H
unc-18(e234)	WT	AIA	AWA::Chr	57	146	0.4265	**<0.0001**	3-1C
unc-18(e81)	WT	AIA	AWA::Chr	40	146	0.4154	**<0.0001**	3-1C
unc-13(e51)	WT	AIA	AWA::Chr	45	146	0.3210	**0.0017**	3-1C
unc-13(e51)	WT	AWA	AWA::Chr	36	64	0.2448	0.1264	3-1E
unc-18(e234)	WT	AIA	1.15 µM dia	56	145	0.2895	**0.0023**	3-1I
unc-18(e81)	WT	AIA	1.15 µM dia	72	145	0.1070	0.6404	3-1I
unc-13(e51)	WT	AIA	1.15 µM dia	46	145	0.1801	0.2075	3-1I
unc-18(e234)	WT	AIA	11.5 nM dia	34	66	0.6417	**<0.0001**	3-1J
unc-13(e51)	WT	AIA	11.5 nM dia	24	66	0.5265	**0.0001**	3-1J
unc-31(e928)	WT	AIA	AWA::Chr	50	146	0.08877	0.9309	3-5A
unc-25(n2324)	WT	AIA	AWA::Chr	21	146	0.1393	0.8686	3-5B
cha-1(p1152)	WT	AIA	AWA::Chr	42	146	0.2446	**0.0403**	3-5C
eat-4(ky5)	WT	AIA	AWA::Chr	48	146	0.2080	0.0877	3-5D
eat-4(ky5)	WT	AIA	1.15 µM dia	114	67	0.2725	**0.0038**	3-5E
eat-4(ky5)	WT	AIA	11.5 µM dia	76	60	0.2860	**0.0083**	3-5F
unc-18(e234)	*eat-4-FRT*	AIA	AWA::Chr	154	214	0.2636	**<0.0001**	3-6C
eat-4-FRT; tax-4p::nFlippase	*eat-4-FRT*	AIA	AWA::Chr	64	214	0.3603	**<0.0001**	3-6C
WT	*eat-4-FRT*	AIA	AWA::Chr	149	214	0.08142	0.6053	3-6D
tax-4p::nFlippase in WT background	*eat-4-FRT*	AIA	AWA::Chr	37	214	0.1540	0.4433	3-6D
eat-4-FRT; sra-9p::nFlippase	*eat-4-FRT*	AIA	AWA::Chr	80	214	0.2244	**0.0057**	3-6E
eat-4-FRT; odr-1p::nFlippase	*eat-4-FRT*	AIA	AWA::Chr	123	214	0.1293	0.1469	3-6F
eat-4-FRT; gcy-15p::nFlippase	*eat-4-FRT*	AIA	AWA::Chr	67	214	0.06235	0.9888	3-6G
eat-4-FRT; ceh-36p::nFlippase	*eat-4-FRT*	AIA	AWA::Chr	55	214	0.1882	0.0902	3-6H
ceh-36(ky640)	WT	AIA	AWA::Chr	31	146	0.1617	0.5154	3-6I
che-1(p674)	WT	AIA	AWA::Chr	96	48	0.1875	0.2106	3-6J
unc-18(e234)	WT	AIA	AWA::Chr	70	80	0.5214	**<0.0001**	3-7
unc-18(e234); ceh-36p::unc-18(e234)	WT	AIA	AWA::Chr	72	80	0.6292	**<0.0001**	3-7

unc-18(e234); ceh-36p::unc-18(WT)#1	WT	AIA	AWA::Chr	42	80	0.1149	0.8604	3-7
unc-18(e234); ceh-36p::unc-18(WT)#2	WT	AIA	AWA::Chr	74	80	0.08784	0.9281	3-7
WT	WT	ASK	0 vs. 11.5 nM dia	82	115	0.2654	**0.0024**	4-1C
WT	WT	ASK	0 vs. 1.15 µM dia	84	115	0.5601	**<0.0001**	4-1C
WT	WT	AWC	0 vs. 11.5 nM dia	60	52	0.0615	>0.9999	4-1F
WT	WT	AWC	0 vs. 1.15 µM dia	60	52	0.2949	**0.0157**	4-1F
WT	WT	ASE	0 vs. 11.5 nM dia	54	42	0.2196	0.2196	4-1I
WT	WT	ASE	0 vs. 1.15 µM dia	53	42	0.3073	**0.0240**	4-1I
WT	WT	ASK vs. AIA	1.15 µM dia	84 (ASK)	438 (AIA)	0.1492	0.0867	5-1A
odr-10(ky32)	WT	AIY	1.15 µM dia	36	86	0.3870	**0.0010**	Appendix A-2D
odr-10(ky32)	WT	AIY	11.5 nM dia	36	86	0.4031	**0.0005**	Appendix A-2I
unc-13(e51)	WT	AIY	1.15 µM dia	32	86	0.2586	0.2093	Appendix A-2E
unc-18(e234)	WT	AIY	1.15 µM dia	28	86	0.3131	**0.0318**	Appendix A-2E
unc-13(e51)	WT	AIY	11.5 nM dia	32	86	0.1737	0.4825	Appendix A-2J
unc-18(e234)	WT	AIY	11.5 nM dia	28	86	0.2633	0.1069	Appendix A-2J
WT	WT	AWA	0 vs. 0.9 µM IAA	78	80	0.2917	**0.0024**	Appendix B-1C
WT	WT	AWA	0 vs 9 µM IAA	78	80	0.5583	**<0.0001**	Appendix B-1C
WT	WT	AWA	0 vs 90 µM IAA	78	80	0.7721	**<0.0001**	Appendix B-1C
WT	WT	AIA	0 vs. 0.9 µM IAA	78	70	0.8597	**<0.0001**	Appendix B-1F
WT	WT	AIA	0 vs 9 µM IAA	78	70	0.7575	**<0.0001**	Appendix B-1F
WT	WT	AIA	0 vs 90 µM IAA	77	70	0.5377	**<0.0001**	Appendix B-1F
odr-7(ky4)	WT	AIA	90 µM IAA	18	77	0.6869	**<0.0001**	Appendix B-2A
ceh-36(ky640)	WT	AIA	90 µM IAA	17	77	0.2368	0.4156	Appendix B-2A
odr-7(ky4) ceh-36(ky640)	WT	AIA	90 µM IAA	28	77	0.7955	**<0.0001**	Appendix B-2A
odr-7(ky4)	WT	AIA	9 µM IAA	18	78	0.6581	**<0.0001**	Appendix B-2B
ceh-36(ky640)	WT	AIA	9 µM IAA	18	78	0.4573	**0.0044**	Appendix B-2B
odr-7(ky4) ceh-36(ky640)	WT	AIA	9 µM IAA	28	78	0.7390	**<0.0001**	Appendix B-2B
odr-7(ky4)	WT	AIA	0.9 µM IAA	18	78	0.5385	**0.0004**	Appendix B-2A
ceh-36(ky640)	WT	AIA	0.9 µM IAA	18	78	0.6239	**<0.0001**	Appendix B-2A
odr-7(ky4) ceh-36(ky640)	WT	AIA	0.9 µM IAA	28	78	0.5705	**<0.0001**	Appendix B-2A
WT	WT	AIA	1.15 µM dia vs. 90 µM IAA	78	438	0.1314	0.2033	Appendix B-3B
WT	WT	AIA	1.15 µM dia vs. 1 µM ascaroside C3	125	438	0.1058	0.2260	Appendix B-3B

WT	WT	AIA	1.15 µM dia vs. OP50-conditioned medium	39	438	0.1472	0.4199	Appendix B-3B

Appendix C. Kolmogorov-Smirnov test statistics and sample sizes for all cumulative response time profiles presented, calculated for full 10-s stimulus pulse. Italics indicate non-WT genetic backgrounds. p-values below 0.05 are bolded for emphasis.

Appendix D: Details of Magnitude Comparisons

Neuron	Stimulus	All vs. Responses Only (R)	GT	Mean ± SEM	n	# compari sons	Approximate p-value	Relevant Figure
AWA	Buffer	All	WT	12.4 ± 3.4	30	N/A		2-2B
	11.5 nM dia			39.3 ± 5.1	32			
	115 nM dia			153.4 ± 9.0	31			
	1.15 µM dia			206.4 ± 8.6	32			
	AWA::Chr			125.4 ± 4.6	268			
AIA	Buffer	All	WT	32.1 ± 6.1	34	N/A		2-2D
	11.5 nM dia			70.6 ± 8.8	34			
	115 nM dia			121.2 ± 11.3	34			
	1.15 µM dia			117.5 ± 11.0	34			
	AWA::Chr			61.54 ± 2.2	569			
AIA	1.15 µM dia	R	**WT**	83.2 ± 4.4	73	3		2-6B
			odr-7(ky4)	51.7 ± 4.8	42		**<0.001**	2-6B
			odr-10(ky32)	54.3 ± 7.9	15		**0.010**	
AIA	1.15 µM dia	R	**WT**	126.7 ± 18.0	18	1*		2-7B
			AWA::TeTx	102.0 ± 12.0	26		0.240	
AIA	1.15 µM dia	R	**WT**	87.0 ± 5.0	82	1*		2-7H
			unc-7(e5) unc-9(fc16	44.2 ± 4.2	54		**<0.001**	
AIA	11.5 nM dia	R	**WT**	58.8 ± 6.0	49	1*		2-7I
			unc-7(e5) unc-9(fc16	36.4 ± 5.8	26		**0.018**	
AIA	AWA::Chr	R	**WT**	80.7 ± 6.0	88	4		2-7G
			AWA::TeTx	94.8 ± 10.9	32		0.709	2-7
			unc-7(e5) unc-9(fc16)	79.6 ± 8.4	43		>0.999	2-7G
			unc-7(e5) unc-9(fc16); inx-4(ok2373)	133.4 ± 15.2	33		**<0.001**	
AIA	AWA::Chr	R	**WT**	107.2 ± 6.8	80	10		3-2A
			unc-31(e928)	97.8 ± 8.5	28		0.996	3-5
			unc-13(e51)	106.1 ± 7.0	33		>0.999	3-2A
			unc-18(e234)	130.7 ± 8.7	50		0.248	
			unc-18(e81)	98.3 ± 7.2	35		0.996	
			eat-4(ky5)	103.2 ± 11.1	34		>0.999	3-5
			unc-25(n2324)	74.4 ± 10.1	9		0.677	3-5
			cha-1(p1152)	146.2 ± 25.2	16		0.155	3-5
			ceh-36(ky640)	127.2 ± 15.1	22		0.800	3-6
AWA	AWA::Chr	R	**WT**	136.9 ± 8.6	59	2		3-1F
			unc-13(e51)	93.1 ± 9.5	32		**0.003**	
AIA	1.15 µM dia	R	**WT**	98.9 ± 7.2	134	5		3-2B
			unc-13(e51)	82.6 ± 7.2	36		0.442	
			unc-18(e234)	87.6 ± 8.3	53		0.667	
			unc-18(e81)	97.4 ± 5.7	66		>0.999	
AIA	11.5 nM dia	R	**WT**	94.4 ± 7.4	59	2		3-2C
			unc-13(e51)	77.6 ± 6.7	21		0.366	
			unc-18(e234)	98.9 ± 9.7	32		0.901	
AIA	1.15 µM dia	R	**WT**	88.7 ± 10.0	63	1*		3-5
			eat-4(ky5)	91.3 ± 8.6	95		0.846	
AIA	11.5 nM dia	R	**WT**	57.6 ± 7.2	45	1*		3-5
			eat-4(ky5)	63.2 ± 4.8	62		0.501	
AIA	AWA::Chr	R	**eat-4-FRT**	79.9 ± 5.7	128	8		3-6C-H
			unc-18(e234)	81.3 ± 3.7	125		>0.999	3-6C
			eat-4-FRT; tax-4p::nFlippase	90.4 ± 8.2	50		0.838	3-6C
			eat-4-FRT; sra-9p::nFlippase	78.1 ± 6.1	58		>0.999	3-6E
			eat-4-FRT; ceh-36p::nFlippase	82.1 ± 8.2	31		>0.999	3-6H
			eat-4-FRT; odr-1p::nFlippase	86.3 ± 6.9	72		0.977	3-6F
			eat-4-FRT; gcy-15p::nFlippase	115.5 ± 10.0	43		**0.001**	3-6G
			WT	78.4 ± 4.2	84		>0.999	3-6D

Cell	Condition	Side	Genotype	Mean ± SEM	n	#	p	Figure
			WT *tax-4p::nFlippase*	91.4 ± 11.8	21		0.954	
AIA	AWA::Chr	R	**WT**	75.8 ± 7.7	27	2		3-6J
			che-1(p678)	69.7 ± 8.2	49		0.798	
AIA	AWA::Chr	R	**WT**	85.9 ± 9.7	42	4		3-7
			unc-18(e234)	86.4 ± 4.4	59		>0.999	
			unc-18(e234); ceh-36p::unc-18(e234)	107.2 ± 8.3	64		0.117	
			unc-18(e234); ceh-36p::unc-18(WT)#1	58.7 ± 4.7	25		0.117	
			unc-18(e234); ceh-36p::unc-18(WT)#2	66.9 ± 6.6	42		0.262	
ASK	0	All	WT	-4.0 ± 2.5	115	2		4-1B
	11.5 nM dia			-20.8 ± 2.2	82		**<0.001**	
	1.15 µM dia			-38.4 ± 2.2	84		**<0.001**	
AWC	0	All	WT	0.2 ± 2.0	52	2		4-1E
	11.5 nM dia			1.1 ± 1.9	60		0.921	
	1.15 µM dia			-7.8 ± 1.6	60		**0.005**	
ASE	0	All	WT	0.4 ± 0.7	42	2		4-1H
	11.5 nM dia			1.5 ± 0.8	54		0.743	
	1.15 µM dia			6.8 ± 1.7	53		**<0.001**	
ASE	0	All	WT	0.2 ± 0.8	38	1*		4-2B
	1.15 µM dia			17.0 ± 2.4	64		**<0.001**	
	0		*unc-18(e234)*	-1.3 ± 0.7	40	1*		
	1.15 M dia			0.9 ± 0.96	44		0.074	
	0		*odr-10(ky32)*	-0.9 ± 0.9	26	1*		
	1.15 µM dia			19.0 ± 2.5	38		**<0.001**	
	1.15 µM dia, compare to **WT**		*unc-18(e234)*			2	**<0.001**	4-2B
			odr-10(ky32)				0.777	
	+100 mM NaCl removal	All	**WT**	12.5 ± 2.2	54	2		4-2C
			unc-18(e234)	9.9 ± 1.3	44		0.508	
			odr-10(ky32)	7.0 ± 2.1	26		0.131	
ASK	0	All	WT	3.4 ± 2.5	68	1*		4-2E
	1.15 µM dia			-39.6 ± 2.2	92		**<0.001**	
	0		*unc-18(e234)*	-3.4 ± 3.2	12	1*		
	1.15 µM dia			-34.1 ± 3.7	24		**<0.001**	
	0		*odr-10(ky32)*	12.8 ± 3.9	34	1*		
	1.15 µM dia			-38.5 ± 2.9	34		**<0.001**	
	1.15 µM dia, compare to **WT**		*unc-18(e234)*			2	0.396	4-2E
			odr-10(ky32)				0.952	
AWC	0	All	WT	-4.3 ± 2.1	34	1*		4-2G
	1.15 µM dia			-13.8 ± 2.1	53		**0.002**	
	0		*unc-18(e234)*	-3.6 ± 1.2	10	1*		
	1.15 µM dia			-16.6 ± 2.1	26		**<0.001**	
	0		*odr-10(ky32)*	-5.2 ± 1.5	40	1*		
	1.15 µM dia			-18.8 ± 2.1	30		**<0.001**	
	1.15 µM dia, compare to **WT**		*unc-18(e234)*			2	0.604	4-2G
			odr-10(ky32)				0.191	
ASH	0	All	WT	-0.1 ± 0.5	78	2		4-3B
	1.15 µM dia			-0.5 ± 0.7	86		0.998	
	+100 mM NaCl			76.5 ± 7.7	86		**<0.001**	
ASK	--	All	WT	1.1 ± 3.0	24	1**		4-4E
	AWA::Chr			-1.5 ± 3.1	24		0.620	
AWC	--	All	WT	1.3 ± 1.9	44	1**		4-4E
	AWA::Chr			0.8 ± 4.4	44		0.899	
ASE	--	All	WT	0.4 ± 1.3	44	1**		4-4E
	AWA::Chr			4.0 ± 1.3	44		0.113	
AIY	1.15 µM dia	R	**WT**	130.9 ±8.3	77	4		Appendix A-2C, Appendix A-3D
			odr-10(ky32)	66.1 ± 7.0	35		**<0.001**	Appendix A-2C
			unc-13(e51)	120.0 ± 18.5	28		0.926	Appendix A-3D
			unc-18(e234)	123.7 ± 15.1	22		0.988	Appendix A-3D
AIY	11.5 nM dia	R	**WT**	118.2 ±7.0	77	4		Appendix A-2H
			odr-10(ky32)	52.5 ± 7.3	35		**<0.001**	Appendix A-2H
			unc-13(e51)	116.6 ± 14.8	28		0.999	Appendix A-3
			unc-18(e234)	111.1 ± 13.6	22		0.978	Appendix A-3
AIA	**1.15 µM dia**	R	WT	94.9 ±3.0	404	3		Appendix B-3G

90 µM IAA			107.2 ± 4.2	77		0.200	Appendix B-3G
1 µM ascaroside C3			99.8 ± 4.2	113		0.783	Appendix B-3G
OP50-conditioned medium			105.8 ± 8.9	37		0.572	Appendix B-3G

Appendix D. Magnitudes of responses to various stimuli, with ordinary one-way

ANOVA with Dunnett's multiple comparison test details (* indicates unpaired t-test

instead, ** indicates paired t-test). If Relevant Figure column does not indicate a specific

panel within a figure, the data were not shown. Bolded genotype or stimulus indicates

the control group used for comparisons. Italics indicate non-wildtype genetic

background. p-values below 0.05 are bolded for emphasis.

Appendix E: List of Strains Used

Strain Name	Description	Comments	Figure(s)
CX14887	N2; *AWA::GCaMP2.2b*	*kyIs598* [*gpa-6p::GCaMP2.2b* 50ng/µl, *unc-122p::dsRed* 15ng/µl, *pSM* 35ng/µl, integrated by UV]	2-1, 2-2, Appendix B-1
CX16573	N2; *AWA::Chrimson; AWA::GCaMP2.2b*	*kyEx5662* [*odr-7p::Chrimson::sl2::mCherry* 5ng/µl, *elt-2p::mCherry* 2ng/µl, *pSM* 93ng/µl]; *kyIs598*	2-1, 2-2, 3-1
CX15257	N2; *AIA::GCaMP5A*	*kyEx5128* [*gcy-28dp::GCaMP5A, unc-122::dsRed* 15ng/µl]	2-2, 2-3, 2-4, 2-5, 2-6, 2-7, 3-1, 3-2, 3-5, 3-9, Appendix B-1, B-2, B3
CX16561	N2; *AWA::Chrimson; AIA::GCaMP5A*	*kyEx5662, kyEx5128*	2-2, 2-3, 2-4, 2-5, 2-7, 3-1, 3-2, 3-3, 3-5, 3-6, 3-7
CX17320	*unc-7(e5) unc-9(fc16); AWA::Chrimson; AIA::GCaMP5A*	*kyEx5662, kyEx5128*	2-7
	inx-4(ok2373); unc-7(e5) unc-9(fc16); AWA::Chrimson; AIA::GCaMP5A	*kyEx5662, kyEx5128*. Cross CX17320 and RB1834 strains.	2-7
CX16979	*unc-7(e5) unc-9(fc16); AIA::GCaMP5A*	*kyEx5128*	2-7
CX16170	*odr-10(ky32); AIA::GCaMP5A*	*kyEx5128*	2-6
CX16584	*AWA::TetanusToxin; AIA::GCaMP5A*	*kyEx3848* [*gpa-6p::TeTx* 20ng/µl, *elt-2p::mCherry* 2ng/µl], *kyEx5128*	2-7
CX16171	*odr-7(ky4); AIA::GCaMP5A*	*kyEx5128*	2-6, Appendix B-2
CX17432	N2; *AIA::Chrimson; AIA::GCaMP5A*	*kyEx6105* [*ins-1(s)p::Chrimson::sl2::mCherry* 20ng/µl, *elt-2p::mCherry* 2ng/µl], *kyEx5128*	2-8, 3-3
CX17584	*unc-18(e234); AIA::Chrimson; AIA::GCaMP5A*	*kyEx6105, kyEx5128*	2-8, 3-3
CX17895	*unc-7(e5) unc-9(fc16); AIA::Chrimson; AIA::GCaMP5A*	*kyEx6105, kyEx5128*	2-8
CX17464	N2; *AIA::Chrimson; AWA::GCaMP2.2b*	*kyEx6105, kyIs598*	2-8
CX17640	*unc-18(e234); AIA::Chrimson; AWA::GCaMP2.2b*	*kyEx6105, kyIs598*	2-8
CX17897	*unc-7(e5) unc-9(fc16); AIA::Chrimson; AWA::GCaMP2.2b*	*kyEx6105, kyEx3225*	2-8
CX17519	N2; *AWA::TetanusToxin; AWA::Chrimson; AIA::GCaMP5A*	*kyEx6140* [*gpa-6p::TeTx::sl2::mCherry* 20ng/µl, *myo-2p::mCherry* 0.5ng/µl], *kyEx5662, kyEx5128*	2-7
CX16592	*unc-13(e51); AWA::Chrimson; AIA::GCaMP5A*	*kyEx5662, kyEx5128*	3-1, 3-2
CX17158	*unc-18(e234); AWA::Chrimson; AIA::GCaMP5A*	*kyEx5662, kyEx5128*	3-1, 3-2, 3-3, 3-6, 3-7
CX17640	*unc-18(e81); AWA::Chrimson; AIA::GCaMP5A*	*kyEx5662, kyEx5128*	3-1, 3-2
CX17213	*unc-13(e51); AWA::Chrimson; AWA::GCaMP2.2b*	*kyEx5662, kyIs598*	3-1, 3-2
CX16591	*unc-13(e51); AIA::GCaMP5A*	*kyEx5128*	3-1, 3-2
CX16412	*unc-18(234); AIA::GCaMP5A*	*kyEx5128*	3-1, 3-2
CX17285	*eat-4(ky5); AWA::Chrimson; AIA::GCaMP5A*	*kyEx5662, kyEx5128*	3-5
CX16410	*eat-4(ky5); AIA::GCaMP5A*	*kyEx5128*	3-5
CX17214	*ceh-36(ky640); AWA::Chrimson; AIA::GCaMP5A*	*kyEx5662, kyEx5128*	3-6, Appendix B-2
CX17678	*che-1(p674); AWA::Chrimson; AIA::GCaMP5A*	*kyEx5662, kyEx5128*	3-6
CX17319	*unc-31(e928); AWA::Chrimson; AIA::GCaMP5A*	*kyEx5662, kyEx5128*	3-5
CX17318	*unc25(n2324); AWA::Chrimson; AIA::GCaMP5A*	*kyEx5662, kyEx5128*	3-5
CX17284	*cha-1(p1152); AWA::Chrimson; AIA::GCaMP5A*	*kyEx5662, kyEx5128*	3-5
CX17714	*eat-4-FRT; coinjection marker control; AWA::Chrimson; AIA::GCaMP5A*	*kyEx6183* [*elt-2p::nlsGFP* 2ng/µl], *kySi76* [*let-85UTR::FRT::mCherry* after *eat-4* endogenous stop codon], *kySi77* [FRT before eat-4 endogenous start codon], *kyEx5662, kyEx5128*	3-6

CX17679	eat-4-FRT; AWC+ASE+ASK+ASG::nFlippase; AWA::Chrimson; AIA::GCaMP5A	kyEx6153 [tax-4p::nFlippase 40ng/µl, elt-2p::nlsGFP 2ng/µl, pSM 58ng/µl], kySi76, kySi77, kyEx5662, kyEx5128	3-6
CX17722	eat-4-FRT; ASK::nFlippase; AWA::Chrimson; AIA::GCaMP5A	kyEx6150 [sra-9p::nFlippase 40ng/µl, elt-2p::nlsGFP 2ng/µl, pSM 58 ng/µl], kySi76, kySi77, kyEx5662, kyEx5128	3-6
CX17723	eat-4-FRT; AWC+ASE::nFlippase; AWA::Chrimson; AIA::GCaMP5A	kyEx6240 [ceh-36p::nFlippase 15ng/µl, elt-2p::nlsGFP 2ng/µl, pSM 83ng/µl], kySi76, kySi77, kyEx5662, kyEx5128	3-6
CX17611	eat-4-FRT; AWC::nFlippase; AWA::Chrimson; AIA::GCaMP5A	kyEx6242 [odr-1p::nFlippase 5ng/µl, elt-2p::nlsGFP 2ng/µl, pSM 93ng/µl], kySi76, kySi77, kyEx5662, kyEx5128	3-6
CX17866	N2; AWC+ASE+ASK+ASG::nFlippase; AWA::Chrimson; AIA::GCaMP5A	kyEx6153, kySi76, kySi77, kyEx5662, kyEx5128	3-6
CX17892	eat-4-FRT; ASG::nFlippase; AWA::Chrimson; AIA::GCaMP5A	kyEx6169 [gcy-15p::nFlippase 25ng/µl, elt-2p::nlsGFP 2ng/µl, pSM 73ng/µl], kySi76, kySi77, kyEx5662, kyEx5128	3-6
CX17675	unc-18(e234); AWC+ASE::unc-18(WT)Rescue; AWA::Chrimson; AIA::GCaMP5A (line A)	kyEx6214 [ceh-36p::unc-18(WTgenomic)::sl2::mCherry 15ng/µl, unc-122p::GFP 15ng/µl, pSM 70ng/µl], kyEx5662, kyEx5128	3-7
CX17676	unc-18(e234); AWC+ASE::unc-18(WT)Rescue; AWA::Chrimson; AIA::GCaMP5A (line B)	kyEx6216 [ceh-36p::unc-18(WTgenomic)::sl2::mCherry 15ng/µl, unc-122p::GFP 15ng/µl, pSM 70ng/µl], kyEx5662, kyEx5128	3-7
CX17677	unc-18(e234); AWC+ASE::unc-18(e234)Sham; AWA::Chrimson; AIA::GCaMP5A	kyEx6218 [ceh-36p::unc-18(e234genomic)::sl2::mCherry 15ng/µl, unc-122p::GFP 15ng/µl, pSM 70ng/µl], kyEx5662, kyEx5128	3-7
CX17714 (without kyEx5128)	eat-4-FRT; coinjection marker control; AWA::Chrimson	kyEx6183, KyEx5662	3-8
CX17535	eat-4-FRT; AWC+ASE+ASK+ASG::nFlippase	kyEx6153, kySi76, kySi77	3-8
CX17679 (without kyEx5128)	eat-4-FRT; AWC+ASE+ASK+ASG::nFlippase; AWA::Chrimson	kyEx6153, kySi76, kySi77, kyEx5662	3-8
CX13914	N2; AWC::GCaMP5A	kyEx4275 [str-2p::GCaMP5A 10ng/µl, unc-122p::dsRed 10ng/µl]	3-9
CX17390	N2; AWA::Chrimson	kyEx5662	3-9
CX17903	N2; AWA::Chrimson; AIA::TetanusToxin	kyEx5662, kyEx6098 [ttx-3int7p::TetanusToxin::sl2::GFP 40ng/µl, myo-3p::mCherry 5ng/µl]	3-10, 3-11
CX17915	N2; ASK+AWC+ASE::GtACR2	kyEx6336 [sra-9p::GtACR2 50ng/µl, ceh-36p::GtACR2 20ng/µl, elt-2p::nlsGFP 2ng/µl, pSM 28ng/µl]	3-10
CX17942	N2; ASK+AWC+ASE::GtACR2; AIA::TetanusToxin	kyEx6336, kyEx6098	3-10, 3-11
CX17916	N2; AWA::Chrimson; ASK+AWC+ASE::GtACR2	kyEx5662, kyEx6336	3-10
	N2; AWA::Chrimson; ASK+AWC+ASE::GtACR2; AIA::TetanusToxin	kyEx5662, kyEx6336, kyEx6098	3-10, 3-11
CX17590	N2; ASK::GCaMP5A	kyEx6191 [sra-9p::GCaMP5A 100ng/µl, elt-2p::mCherry 2ng/µl]	4-1, 4-2
CX17724	unc-18(e234); ASK::GCaMP5A	kyEx6191	4-2
CX17867	odr-10(ky32); ASK::GCaMP5A	kyEx6191	4-2
CX17520	N2; AWC::GCaMP5A	kyEx6141 [str-2p::GCaMP5A 50ng/µl, unc-122p:dsRed 15ng/µl]	4-1, 4-2
CX17636	unc-18(e234); AWC::GCaMP5A	kyEx6141	4-2
CX17606	odr-10(ky32); AWC::GCaMP5A	kyEx6141	4-2
CX14571	N2; ASE::GCaMP3	kyEx4732 [flp-6p::GCaMP3 5ng/µl, unc-122p::dsRed 10ng/µl]	4-1, 4-2
CX17638	unc-18(e234); ASE::GCaMP3	kyEx4732	4-2
CX16497	odr-10(ky32); ASE::GCaMP3	kyEx4732	4-2
CX10979	N2; ASH::GCaMP3	kyEx2865 [sra-6p::GCaMP3 100ng/µl ofm-1p::GFP 10ng/µl]	4-3
CX17751	N2; AWA::Chrimson; ASK::GCaMP5A	kyEx5662, kyEx6191	4-4
CX17521	N2; AWA::Chrimson; AWC::GCaMP5A	kyEx5662, kyEx6141	4-4

CX17392	N2; *AWA::Chrimson; ASE::GCaMP3*	*kyEx5662, kyEx4732*	4-4
DCR2686	N2; *AIY::GCaMP6s*	*olaEx1621* [*mod-1p::GCaMP6s* 25ng/µl, *ttx-3p::mCherry* 25ng/µl, *unc-122p::dsRed* 40 ng/µl]	Appendix A-2, A-3
CX16496	*odr-10(ky32); AIY::GCaMP6s*	*olaEx1621*	Appendix A-2
CX16580	*unc-13(e51); AIY::GCaMP6s*	*olaEx1621*	Appendix A-3
CX16581	*unc-18(e234); AIY::GCaMP6s*	*olaEx1621*	Appendix A-3
	odr-7(ky4) ceh-36(ky640); AIA::GCaMP5A	*kyEx5128*	Appendix B-2

References

Abada, E. A. E. *et al. C. elegans* behavior of preference choice on bacterial food. *Mol. Cells* **28**, 209–213 (2009).

Akerboom, J. *et al.* Optimization of a GCaMP Calcium Indicator for Neural Activity Imaging. *J. Neurosci* **32**, 13819-13840 (2012).

Altun-Gultekin, Z. *et al.* A regulatory cascade of three homeobox genes, *ceh-10*, *ttx-3* and *ceh-23*, controls cell fate specification of a defined interneuron class in *C . elegans*. *Development* **128**, 1951–1969 (2001).

Altun, Z. F., Chen, B., Wang, Z. W. & Hall, D. H. High resolution map of *Caenorhabditis elegans* gap junction proteins. *Dev. Dyn.* **238**, 1936–1950 (2009).

Andersson, C., Lofstedt, R., Newcomb, R. Insect olfaction and the evolution of receptor tuning. *Front. Ecol. Evol.* **3**, 1-14 (2015).

Ayci, F., Aydinli, M., Bozdemir, O., & Mehmet, T. Gas chromatographic investigation of rose concrete, absolute and solid residue. *Flavour Fragr. J.* **20**, 481-486 (2005).

Bargmann, C. I. Chemosensation in *C. elegans*. *WormBook*, ed. The *C. elegans* Research Community, WormBook, doi/10.1895/wormbook.1.123.1. *www.wormbook.org* (2006).

Bargmann, C. I., Hartwieg, E. & Horvitz, H. R. Odorant-selective genes and neurons mediate olfaction in *C. elegan*s. *Cell* **74**, 515–527 (1993).

Bargmann, C. I. & Horvitz, H. R. Chemosensory neurons with overlapping functions direct chemotaxis to multiple chemicals in *C. elegans*. *Neuron* **7**, 729–742 (1991).

Bargmann, C., Thomas, J., & Horvitz, H. Chemosensory cell function in the behavior and development of *Caenorhabditis elegans*. *Cold Spring Harb. Symp. Quant. Biol.* **55**, 529-538 (1990).

Bathellier, B., Gschwend, O., Carleton, A. The Neurobiology of Olfaction: Temporal Coding in Olfaction. *CRC Press/Taylor & Francis* (2010).

Bear, D., Lassance, J., Hoekstra, H., & Datta, S. The Evolving Neural and Genetic Architecture of Vertebrate Olfaction. *Curr. Biol.* **26**, R1039-R1049 (2016).

Bennett, M. V. L., Aljure, E., Nakajima, Y. & Pappas, G. D. Electrotonic junctions between teleost spinal neurons: Electrophysiology and ultrastructure. *Science* **141**, 262–264 (1963).

Bhattacharya, A., Aghayeva, U., Berghoff, E. G. & Hobert, O. Plasticity of the Electrical Connectome of *C. elegans*. *Cell* **176**, 1174–1189 (2019).

Brockie, P. J., Madsen, D. M., Zheng, Y., Mellem, J. & Maricq, A. V. Differential Expression of Glutamate Receptor Subunits in the Nervous System of *Caenorhabditis elegans* and Their Regulation by the Homeodomain Protein UNC-42. *J. Neurosci.* **21**, 1510–1522 (2001).

Buck, L. & Axel, R. A Novel Multigene Family May Encode Odorant Receptors: A Molecular Basis for Odor Recognition. *Cell* **65**, 175–187 (1991).

Bushdid, C., Magnaso, M., Vosshall, L., & Keller, A. Humans Can Discriminate More than 1 Trillion Olfactory Stimuli. *Science* **343**, 1370-1373 (2014).

Bufe, B., Schumann, T., & Zufall, F. Formyl peptide receptors from immune and vomeronasal system exhibit distinct agonist properties. *J. Biol. Chem.* **287**, 33644-33655 (2012).

Cao, J. *et al.* Comprehensive single-cell transcriptional profiling of a multicellular organism. *Science,* **357**, 661–667 (2017).

Chalasani, S. H. *et al.* Neuropeptide feedback modifies odor-evoked dynamics in *Caenorhabditis elegans* olfactory neurons. *Nat. Neurosci.* **13**, 615–621 (2010).

Chalasani, S. H. *et al.* Dissecting a circuit for olfactory behaviour in *Caenorhabditis elegans*. *Nature* **450**, 63–70 (2007).

Chen, B., Liu, Q., Ge, Q., Xie, J. & Wang, Z. W. UNC-1 Regulates Gap Junctions Important to Locomotion in *C. elegans*. *Curr. Biol.* **17**, 1334–1339 (2007).

Cho, C. E., Brueggemann, C., L'Etoile, N. D. & Bargmann, C. I. Parallel encoding of sensory history and behavioral preference during *Caenorhabditis elegans* olfactory learning. *Elife* **5**, e14000 (2016).

Choi, J. I., Yoon, K. H., Subbammal Kalichamy, S., Yoon, S. S. & Lee, J. Il. A natural odor attraction between lactic acid bacteria and the nematode *Caenorhabditis elegans*. *ISME J.* **10**, 558–567 (2016).

Choi, S. *et al.* Sensory Neurons Arouse *C. elegans* Locomotion via Both Glutamate and Neuropeptide Release. *PLoS Genet.* **11**, 1–20 (2015).

Chou, J. H., Bargmann, C. I. & Sengupta, P. The *Caenorhabditis elegans odr-2* gene encodes a novel Ly-6-related protein required for olfaction. *Genetics* **157**, 211–

224 (2001).

Chuang, C. F., VanHoven, M. K., Fetter, R. D., Verselis, V. K. & Bargmann, C. I. An Innexin-Dependent Cell Network Establishes Left-Right Neuronal Asymmetry in *C. elegans*. *Cell* **129**, 787–799 (2007).

Coburn, C. M. & Bargmann, C. I. A putative cyclic nucleotide-gated channel is required for sensory development and function in *C. elegans*. *Neuron* **17**, 695–706 (1996).

Dal Bello, M., Perez-Escudero, A., Schroeder, F., & Gore, J. Attraction to pheromones in *Caenorhabditis elegans* can be reversed through associative learning. *bioRxiv* 476648 (2018).

Dalton, R. & Lomvardas, S. Chemosensory Receptor Specificity and Regulation. *Annu. Rev. Neurosci.* **38**, 331-349 (2015).

Del Punta, K. *et al*. Deficient pheromone responses in mice lacking a cluster of vomeronasal receptor genes. *Nature* **419**, 70-74 (2002).

Deng, X. *et al.* The ComP-ComA Quorum System Is Essential For 'Trojan horse' Like Pathogenesis in *Bacillus nematocida*. *PLoS One* **8**, 1–11 (2013).

Dweck, H. *et al.* Olfactory preference for egg laying on citrus substrates in *Drosophila*. *Curr. Biol.* **23**, 2472-2480 (2013).

Félix, M. A. & Braendle, C. The natural history of *Caenorhabditis elegans*. *Curr. Biol.* **20**, R965–R969 (2010).

Flanigan, S. S. *et al.* Flavoring Chemicals in E-Cigarettes: Diacetyl, 2,3-Pentanedione, and Acetoin in a Sample of 51 Products, Including Fruit-, Candy-, and Cocktail-Flavored E-Cigarettes. *Environ. Health Perspect.* **124**, 733–739 (2016).

Gerkin, R. & Castro, J. The number of olfactory stimuli that humans can discrimintae is still unknown. *Elife* **4**, e08127 (2015).

Gordus, A., Pokala, N., Levy, S., Flavell, S. W. & Bargmann, C. I. Feedback from network states generates variability in a probabilistic olfactory circuit. *Cell* **161**, 215–227 (2015).

Grabe, V. *et al.* Elucidating the Neuronal Architecture of Olfactory Glomeruli in the *Drosophila* Antennal Lobe. *Cell. Rep.* **16**, 3401-3413 (2016).

Gracheva, E. *et al.* Molecular basis of infrared detection by snakes. *Nature* **464**, 1006-1011 (2010).

Gray, J. *et al.* Oxygen sensation and social feeding mediated by a *C. elegans* guanylate cyclase homologue. *Nature* **430**, 317-322 (2004).

Greer, E. R., Pérez, C. L., Van Gilst, M. R., Lee, B. H. & Ashrafi, K. Neural and Molecular Dissection of a *C. elegans* Sensory Circuit that Regulates Fat and Feeding. *Cell Metab.* **8**, 118–131 (2008).

Greer, P. *et al.* A Family of non-GPCR Chemosensors Defines an Alternative Logic for Mammalian Olfaction. *Cell* **165**, 1734-1748 (2016).

Grewal, P. & Wright, D. Migration of *Caenorhabditis elegans* larvae towards bacteria and the nature of the bacterial stimulus. *Fundam. Appl. Nematol.* **15**, 159–166 (1992).

Grillet, M., Campagner, D., Peterson, R., McCrohan, C., & Cobb, M. The peripheral olfactory code in *Drosophila* larvae contains temporal information and is robust over multiple timescales. *Proc. R. Soc. B.* **283**, 20160665 (2016).

Hale, L. A., Lee, E. S., Pantazis, A. K., Chronis, N. & Chalasani, S. H. Altered Sensory Code Drives Juvenile-to-Adult Behavioral Maturation in *Caenorhabditis elegans*. *eNeuro* **3**, 0175-16.2016 (2016).

Hallem, E. & Sternberg, P. Acute carbon dioxide avoidance in *Caenorhabditis elegans*. *Proc. Natl. Acad. Sci.* **105**, 8038-8043 (2008).

Havercamp, A., Hansson, B., & Knaden, M. Combinatorial codes and labeled lines: How insects use olfactory cues to find and judge food, mates, and oviposition sites in complex environments. *Front. Physiol.* **9**, 1-8 (2018).

Hendricks, M., Ha, H., Maffey, N. & Zhang, Y. Compartmentalized calcium dynamics in a *C. elegans* interneuron encode head movement. *Nature* **487**, 99–103 (2012).

Hilliard, M. A. *et al.* In vivo imaging of *C. elegans* ASH neurons: Cellular response and adaptation to chemical repellents. *EMBO J.* **24**, 63–72 (2005).

Hills, T., Brockie, P. J. & Maricq, A. V. Dopamine and Glutamate Control Area-Restricted Search Behavior in *Caenorhabditis elegans*. *J. Neurosci.* **24**, 1217–1225 (2004).

Hoover, K. Smell with inspiration: The evolutionary significance of olfaction. *Am. J. Phys. Anthrop.* **53**, 63-74 (2010).

Houston, D. Scavenging Efficiency of Turkey Vultures in Tropical Forests. *The Condor*.

88, 318-323 (1986).

Hsueh, Y. P. *et al.* Nematophagous fungus *Arthrobotrys oligospora* mimics olfactory cues of sex and food to lure its nematode prey. *Elife* **6**, e20023 (2017).

Iino, Y. & Yoshida, K. Parallel Use of Two Behavioral Mechanisms for Chemotaxis in *Caenorhabditis elegans*. *J. Neurosci.* **29**, 5370–5380 (2009).

Itskovits, E., Ruach, R. & Zaslaver, A. Concerted pulsatile and graded neural dynamics enables efficient chemotaxis in *C. elegans*. *Nat. Commun.* **9**, 1-11 (2018).

Jang, H. *et al.* Neuromodulatory State and Sex Specify Alternative Behaviors through Antagonistic Synaptic Pathways in *C elegans*. *Neuron* **75**, 585-592 (2012).

Jang, H. *et al.* Dissection of neuronal gap junction circuits that regulate social behavior in *Caenorhabditis elegans*. *Proc. Natl. Acad. Sci.* **114**, E1263–E1272 (2017).

Jirovetz, L. *et al.* Solid phase microextraction/gas chromatographic and olfactory analysis of the scent and fixative properties of the essential oil of *Rosa damascena* L. from China. *Flavour Fragr. J.* **20**, 7-12 (2004).

Kadohisa, M. Effects of odor on emotion, with implications. *Front. Neurosci.* **7**, 1-6 (2013).

Kaplan, H. S., Nichols, A. L. A. & Zimmer, M. Sensorimotor integration in *Caenorhabditis elegans*: A reappraisal towards dynamic and distributed computations. *Philos. Trans. R. Soc. B* **373**, 20170371 (2018).

Kato, S. *et al.* Global Brain Dynamics Embed the Motor Command Sequence of *Caenorhabditis elegans*. *Cell* **163**, 656–669 (2015).

Kawano, T., *et al.* An imbalancing act: Gap junctions reduce the backward motor circuit activity to bias *C. elegans* for forward locomotion. *Neuron* **72**, 572-586 (2011).

Klapoetke, N. C. *et al.* Independent optical excitation of distinct neural populations. *Nat. Methods* **11**, 338–346 (2014).

Kuramochi, M. & Doi, M. An Excitatory/Inhibitory Switch From Asymmetric Sensory Neurons Defines Postsynaptic Tuning for a Rapid Response to NaCl in *Caenorhabditis elegans*. *Front. Mol. Neurosci.* **11**, 1–14 (2019).

L'Etoile, N. D. & Bargmann, C. I. Olfaction and odor discrimination are mediated by the *C. elegans* guanylyl cyclase ODR-1. *Neuron* **25**, 575–586 (2000).

Larsch, J., Ventimiglia, D., Bargmann, C. I. & Albrecht, D. R. High-throughput imaging of

neuronal activity in *Caenorhabditis elegans*. *Proc. Natl. Acad. Sci.* **110**, E4266–E4273 (2013).

Larsch, J. *et al.* A Circuit for Gradient Climbing in *C. elegans* Chemotaxis. *Cell Rep.* **12**, 1748–1760 (2015).

Laurent, P. *et al.* Decoding a neural circuit controlling global animal state in *C. elegans*. *Elife* **4**, e04241 (2015).

Leinwand, S. *et al.* Circuit mechanisms encoding odors and driving aging-associated behavioral declines in *Caenorhabditis elegans*. *Elife* **4**, e10181 (2015).

Lewis, J., Wu, C.-H., Levin, J., & Berg, H. Levamisole-Resistant Mutants of the Nematode *Caenorhabditis elegans* Appear to Lack Pharmacological Acetylcholine Receptors. *Neuroscience* **5**, 967-989 (1980).

Liberles, S. *et al.* Formyl peptide receptors are candidate chemosensory receptors in the vomeronasal organ. *Proc. Natl. Acad. Sci.* **106**, 9842-9847 (2009).

Lin, J. Y. *et al.* Optogenetic inhibition of synaptic release with chromophore-assisted light inactivation (CALI). *Neuron* **79**, 241–253 (2013).

Liu, H. *et al.* Cholinergic Sensorimotor Integration Regulates Olfactory Steering. *Neuron* **97**, 390–405 (2018).

Liu, P. *et al.* Six Innexins Contribute to Electrical Coupling of *C. elegans* Body-Wall Muscle. *PLoS One* **8**, e76877 (2013).

Liu, P., Chen, B., Mailler, R. & Wang, Z. W. Antidromic-rectifying gap junctions amplify chemical transmission at functionally mixed electrical-chemical synapses. *Nat. Commun.* **8**, 1–16 (2017).

Liu, Q., Kidd, P. B., Dobosiewicz, M. & Bargmann, C. I. *C. elegans* AWA Olfactory Neurons Fire Calcium-Mediated All-or-None Action Potentials. *Cell* **175**, 57–70 (2018).

López-Cruz, A. *et al.* Parallel Multimodal Circuits Control an Innate Foraging Behavior. *Neuron* 1–13 (2019).

Luo, L. *et al.* Dynamic encoding of perception, memory, and movement in a *C. elegans* chemotaxis circuit. *Neuron* **82**, 1115–1128 (2014).

Macosko, E. Z. *et al.* A hub-and-spoke circuit drives pheromone attraction and social behaviour in *C. elegans*. *Nature* **458**, 1171–1175 (2009).

168

Majewska, A. & Yuste, R. Topology of Gap Junction Networks in *C. elegans*. *J. Theor. Biol.* **12**, 155–167 (2001).

Malnic, B., Hirono, J., Sato, T. & Buck, L. B. Combinatorial receptor codes for odors. *Cell* **96**, 713–723 (1999).

Malnic, B. Godfrey, P., & Buck, L. The human olfactory receptor gene family. *Proc. Natl. Acad. Sci.* **101**, 2584-2589 (2004).

Marder, E. Beyond speed and synchrony to computation. *Curr. Biol.* **8**, 795-797 (1998).

McEwen, J. M. & Kaplan, J. M. UNC-18 Promotes Both the Anterograde Trafficking and Synaptic Function of Syntaxin. *Mol. Biol. Cell* **19**, 3836–3846 (2008).

Meister, M. On the dimensionality of odor space. *Elife* **4**, e07865 (2015).

Miller, A. C. *et al.* A genetic basis for molecular asymmetry at vertebrate electrical synapses. *Elife* **6**, e25364 (2017).

Mori, I. & Ohshima, Y. Neural regulation of thermotaxis in *C. elegans*. *Nature* **376**, 344–348 (1995).

Munger, S., Leinders-Zufall, T., & Zufall, F. Subsystem Organization of the Mammalian Sense of Smell. *Annu. Rev. Physiol.* **71**, 115-140 (2009).

Nara, K., Saraiva, L., Ye, X. & Buck, L. A Large-Scale Analysis of Odor Coding in the Olfactory Epithelium. *J. Neurosci*. **31**, 9179-9191 (2011).

Nguyen, J. P. *et al.* Whole-brain calcium imaging with cellular resolution in freely behaving *C. elegan*s. *Proc. Natl. Acad. Sci.* **113**, E1074–E1081 (2016).

Niu, Q. *et al.* A Trojan horse mechanism of bacterial pathogenesis against nematodes. *Proc. Natl. Acad. Sci.* **107**, 16631–16636 (2010).

Oshima, A., Matsuzawa, T., Murata, K., Tani, K., & Fujiyoshi, Y. Hexadecameric structure of an invertebrate gap junction channel. *J. Mol. Biol.* **428**, 1227-1236 (2016).

Ouellette, M.-H., Desrochers, M. J., Gheta, I., Ramos, R. & Hendricks, M. A Gate-and-Switch Model for Head Orientation Behaviors in *Caenorhabditis elegans. eNeuro* **5**, e0121 (2018).

Peracchia, C. Low resistance junctions in crayfish. *J. Cell Biol.* **57**, 66-76 (1973).

Pereda, A. E. Electrical synapses and their functional interactions with chemical synapses. *Nat. Rev. Neurosci.* **15**, 250–263 (2014).

Pereda, A. E. *et al.* Gap junction-mediated electrical transmission: Regulatory mechanisms and plasticity. *Biochim. Biophys. Acta* **1828**, 134–146 (2013).

Pereira, L. *et al.* A cellular and regulatory map of the cholinergic nervous system of *C. elegans*. *Elife* **4**, e12432 (2015).

Phelan, P. Innexins: Members of an evolutionarily conserved family of gap-junction proteins *Biochim. Biophys. Acta* **1711**, 225-245 (2005).

Phelan, P. *et al.* Molecular Mechanism of Rectification at Identified Electrical Synapses in the *Drosophila* Giant Fiber System. *Curr. Biol.* **18**, 1955–1960 (2008).

Piatkevich, K. D. *et al.* A robotic multidimensional directed evolution approach applied to fluorescent voltage reporters. *Nat. Chem. Biol.* **14**, 352-360 (2018).

Pierce-Shimomura, J. T., Morse, T. M. & Lockery, S. R. The fundamental role of pirouettes in *Caenorhabditis elegans* chemotaxis. *J. Neurosci.* **19**, 9557–69 (1999).

Qiao, M. & Sanes, J. R. Genetic Method for Labeling Electrically Coupled Cells: Application to Retina. *Front. Mol. Neurosci.* **8**, 1–15 (2016).

Riffell, J., Lei, H., Christensen, T., & Hildebrand, J. Characterization and Coding of Behaviorally Significant Odor Mixtures. *Curr. Biol*. **19**, 335-340 (2009).

Riviere, S., Challet, L., Fluegge, D., Spehr, M., & Rodriguez, I. Formyl peptide recepter-like proteins are a novel family of vomeronasal chemosensors. *Nature* **459**, 574-577 (2009).

Robertson, H. & Thomas, J. The putative chemoreceptor families of *C. elegans*. *Wormbook* ed. The *C. elegans* Research Community, WormBook, doi/10.1895/wormbook.1.66.1, http://www.wormbook.org (2006).

Samuel, B. S., Rowedder, H., Braendle, C., Félix, M.-A. & Ruvkun, G. *Caenorhabditis elegans* responses to bacteria from its natural habitats. *Proc. Natl. Acad. Sci.* **113**, E3941–E3949 (2016).

Schumacher, J. A. *et al.* Intercellular calcium signaling in a gap junction-coupled cell network establishes asymmetric neuronal fates in *C. elegans*. *Development* **139**, 4191–4201 (2012).

Sengupta, P., Chou, J. H. & Bargmann, C. I. *odr-10* Encodes a seven transmembrane domain olfactory receptor required for responses to the odorant diacetyl. *Cell* **84**,

899–909 (1996).

Serrano-Saiz, E. *et al.* Modular control of glutamatergic neuronal identity in *C. elegans* by distinct homeodomain proteins. *Cell* **155**, 659-673 (2013).

Shinkai, Y. *et al.* Behavioral Choice between Conflicting Alternatives Is Regulated by a Receptor Guanylyl Cyclase, GCY-28, and a Receptor Tyrosine Kinase, SCD-2, in AIA Interneurons of *Caenorhabditis elegans*. *J. Neurosci.* **31**, 3007-3015 (2011).

Si, G. *et al.* Structured Odorant Response Patterns across a Complete Olfactory Receptor Neuron Population. *Neuron* **101**, 950-962 (2019).

Silva, L. & Antunes, A. Vomeronasal Receptors in Vertebrates and the Evolution of Pheromone Detection. *Annu. Rev. Anim. Biosci.* **5**, 353-370 (2017).

Skora, S., Mende, F. & Zimmer, M. Energy Scarcity Promotes a Brain-wide Sleep State Modulated by Insulin Signaling in *C. elegans*. *Cell Rep.* **22**, 953–966 (2018).

Song, J., Ampatzis, K., Björnfors, E. R. & El Manira, A. Motor neurons control locomotor circuit function retrogradely via gap junctions. *Nature* **529**, 399–402 (2016).

Speese, S. *et al.* UNC-31 (CAPS) Is Required for Dense-Core Vesicle But Not Synaptic Vesicle Exocytosis in *Caenorhabditis elegan*s. *J. Neurosci* **27**, 6150–6162 (2007).

Starich, T. A., Hall, D. H. & Greenstein, D. Two classes of gap junction channels mediate soma-germline interactions essential for germline proliferation and gametogenesis in *Caenorhabditis elegans*. *Genetics* **198**, 1127–1153 (2014).

Starich, T. A., Miller, A., Nguyen, R. L., Hall, D. H. & Shaw, J. E. The *Caenorhabditis elegans* innexin INX-3 is localized to gap junctions and is essential for embryonic development. *Dev. Biol.* **256**, 403–417 (2003).

"Size of the global fragrance, deodorant and antiperspirant market from 2012 to 2024 (in billion U.S. dollars). *Statista*, accessed 36 March 2019. www.statista.com/statistics/259221/global-fragrance-market-size/.

Stein, B., Sanford, T., & Rowland, B. The Neural Basis of Multisensory Integration in the Midbrain: Its Organization and Maturation. *Hearing Research* **258**, 4-15 (2009).

Suzuki, H. *et al.* Functional asymmetry in *Caenorhabditis elegans* taste neurons and its computational role in chemotaxis. *Nature* **454**, 114–117 (2008).

Taniguchi, G., Uozumi, T., Kiriyama, K., Kamizaki, T. & Hirotsu, T. Screening of Odor-Receptor Pairs in *Caenorhabditis elegans* Reveals Different Receptors for High

and Low Odor Concentrations. *Sci. Signal.* **7**, ra39 (2014).

Thiele, T. R., Faumont, S. & Lockery, S. R. The Neural Network for Chemotaxis to Tastants in *Caenorhabditis elegans* Is Specialized for Temporal Differentiation. *J. Neurosci.* **29**, 11904–11911 (2009).

Tomioka, M. *et al.* The Insulin/PI 3-Kinase Pathway Regulates Salt Chemotaxis Learning in *Caenorhabditis elegans*. *Neuron* **51**, 613–625 (2006).

Troemel, E. R., Chou, J. H., Dwyer, N. D., Colbert, H. A. & Bargmann, C. I. Divergent seven transmembrane receptors are candidate chemosensory receptors in *C. elegans*. *Cell* **83**, 207–218 (1995).

Troemel, E. R., Kimmel, B. E. & Bargmann, C. I. Reprogramming chemotaxis responses: Sensory neurons define olfactory preferences in *C. elegans*. *Cell* **91**, 161–169 (1997).

Tsalik, E. L. & Hobert, O. Functional mapping of neurons that control locomotory behavior in *Caenorhabditis elegans*. *J. Neurobiol.* **56**, 178–197 (2003).

Tumkaya, T., Stewart, J., Burhanudin, S. & Claridge-Chang, A. Optogenetic olfactory behavior depends on illumination characteristics. *bioRxiv* 559674 (2019).

Ventimiglia, D. & Bargmann, C. I. Diverse modes of synaptic signaling, regulation, and plasticity distinguish two classes of *C. elegans* glutamatergic neurons. *Elife* **6**, e31234 (2017).

Vidal, B. *et al.* An atlas of *Caenorhabditis elegans* chemoreceptor expression. *PLoS Biol.* **16**, 1–34 (2018).

Von Reuss, S. *et al*. Comparative metabolomics reveals biogenesis of ascarosides, a modular library of small-molecule signals in *C. elegans*. *J. Am. Chem. Soc.* **134**, 1817-1824 (2012).

Wakabayashi, T., Kitagawa, I. & Shingai, R. Neurons regulating the duration of forward locomotion in *Caenorhabditis elegans*. *Neurosci. Res.* **50**, 103–111 (2004).

Wang, L. *et al.* A Gustatory Neural Circuit of *Caenorhabditis elegans* Generates Memory-Dependent Behaviors in Na$^+$ Chemotaxis. *J. Neurosci.* **37**, 2097–2111 (2017).

Ward, S., Thomson, N., White, J., & Brenner, S. Electron microscopical reconstruction of the anterior sensory anatomy of the nematode *Caenorhabditis elegans*. *J.*

Comp. Neurol. **160**, 313-337 (1975).

Weimer, R. *et al.* Defects in synaptic vesicle docking in *unc-18* mutants. *Nat. Neurosci.* **6**, 1023–1030 (2003).

Weiss, T. *et al.* Perceptual convergence of multi-component mixtures in olfaction implies an olfactory white. *Proc. Natl. Acad. Sci.* **109**, 19959-19964 (2012).

Werblin, F. S. Six different roles for crossover inhibition in the retina: Correcting the nonlinearities of synaptic transmission. *Vis. Neurosci.* **27**, 1–8 (2010).

Wes, P. & Bargmann, C. *C. elegans* odour discrimination requires asymmetric diversity in olfactory neurons. *Nature* **410**, 698–701 (2001).

White, J. G., Southgate, E., Thomson, J. & Brenner, S. The structure of the nervous system of the nematode *Caenorhabditis elegans*. *Philos. Trans. R. Soc. B* **314**, 1–340 (1986).

Worthy, S. *et al.* Identification of attractive odorants released by preferred bacterial food found in the natural habitats of *C. elegans*. *PLoS One* **13**, 1–14 (2018).

Worthy, S., Rojas, G., Taylor, C. & Glater, E. Identification of odor blend used by *Caenorhabditis elegans* for pathogen recognition. *Chem. Senses* **43**, 169–180 (2018).

Wu, L., Dong, A., Dong, L., Wang, S.-Q. & Li, Y. PARIS, an optogenetic method for functionally mapping gap junctions. *Elife* **8**, e43366 (2019).

Yoshida, K. *et al.* Odour concentration-dependent olfactory preference change in *C. elegans*. *Nat. Commun.* **3**, 711–739 (2012).

Yu, S., Avery, L., Baude, E., & Garbers, D. L. Guanylyl cyclas expression in specific sensory neurons: A new family of chemosensory receptors. *Proc. Natl. Acad. Sci.* **94**, 3384-3387 (1997).

Zaslaver, A. *et al.* Hierarchical sparse coding in the sensory system of *Caenorhabditis elegans*. *Proc. Natl. Acad. Sci.* **112**, E1688–E1689 (2015).

Zhang, C. *et al.* The Signaling Pathway of *Caenorhabditis elegans* Mediates Chemotaxis Response to the Attractant 2-Heptanone in a Trojan Horse-like Pathogenesis. *J. Biol. Chem.* **291**, 23618–23627 (2016).

Zufall, F. & Leinders-Zufall, T. Mammalian pheromone sensing. *Curr. Opin. Neurobiol.* **17**, 483–489 (2007).